Quantitative analysis of astrocyte properties in a Syrian hamster model of COVID-19

by

Mohammadreza Rahmani Manesh

B.Sc., University of Isfahan, 2022

A Thesis Submitted in Partial Fulfillment

of the Requirements for the Degree of

MASTER OF SCIENCE

in the Division of Medical Sciences

Supervisory committee

Quantitative analysis of astrocyte properties in a Syrian hamster model of COVID-19

by

Mohammadreza Rahmani Manesh

B.Sc., University of Isfahan, 2022

Supervisory Committee

Dr. Leigh Anne Swayne (Division of Medical Sciences)
Supervisor

Dr. Craig Brown (Division of Medical Sciences)
Departmental Member

Dr. Bob Chow (Department of Biology)
Outside Member

Abstract

Supervisory Committee

Dr. Leigh Anne Swayne (Division of Medical Sciences)
Supervisor

Dr. Craig Brown (Division of Medical Sciences)
Departmental Member

Dr. Bob Chow (Department of Biology)
Outside Member

COVID-19 (Coronavirus disease 2019), caused by infection with SARS-CoV-2 (severe acute respiratory syndrome coronavirus 2), is primarily a respiratory disease, but it can cause a spectrum of acute and long-term neurological symptoms, like fatigue and impaired cognition. Although there is some debate regarding the underlying mechanisms, there is mounting evidence of neuroinflammation in both animal and human models of COVID-19. Neuroinflammation is commonly associated with astrogliosis, which includes changes in astrocytes, such as increased proliferation and increased distribution of the astrocyte-enriched intermediate filament protein, glial fibrillary acidic protein (GFAP); however, this remains relatively unexplored in the context of COVID-19. To this end, my thesis investigated whether mild COVID-19 respiratory infection induces astrogliosis. I created an unbiased imaging and analysis pipeline to quantify astrocyte changes associated with astrogliosis. My pipeline for astrogliosis quantification involves two measures that are increased in the context of astrogliosis: (1) the distribution of GFAP (i.e., the density of GFAP-positive pixels) and (2) the density of astrocytes (with the astrocyte-specific nuclear marker, SOX9). To implement this pipeline within the context of COVID-19, I collaborated with the Kobasa Lab at the National Microbiology Laboratory. The Kobasa Lab modeled mild, peripheral COVID-19 by intranasal inoculation of Syrian hamsters with SARS-

CoV-2. They collected brains at 1, 3, 5, 7, and 31 days post-inoculation (DPI). Following extensive fixation (30 days), they shipped the brains to the University of Victoria. In collaboration with a team of UVic researchers, I sectioned the brains coronally. I then performed immunolabelling with SOX9, GFAP, NeuN, and Hoechst and generated tiled confocal micrographs of entire coronal sections. I then digitally isolated key brain regions involved in cognition and susceptibility to inflammation, including the cortex, the corpus callosum, the dorsal striatum, the hippocampus, and the third ventricle. I then subjected these images to my pipeline for astrogliosis quantification. My analysis revealed a significant increase in GFAP distribution in the cortex of female hamsters at 3 DPI. Similarly, I observed increases in GFAP distribution within the hippocampus and corpus callosum of female hamsters at 3 DPI, although these were not statistically significant. In contrast, SOX9+ cell numbers remained unchanged across DPI in both sexes and across brain regions. These findings suggest that mild peripheral COVID-19 may induce partial and transient astrogliosis, specifically in female hamsters. Additionally, minor fluctuations in Hoechst and NeuN staining across various brain regions and time points suggest possible COVID-19-associated changes in marker expression and/or cell/neuronal density, which require further validation. In conclusion, my findings suggest partial and transient, female-specific astrogliosis response to mild peripheral COVID-19, emphasizing the need to consider regional and temporal factors to understand the neurological impacts of COVID-19.

Table of contents

List of abbreviations

ACE2	angiotensin-converting enzyme 2
AMPA	α-amino-3-hydroxy-5-methyl-4-isoxazolepropionic acid
ANLS	astrocyte-neuron lactate shuttle
BBB	blood-brain barrier
CC	corpus callosum
CNS	central nervous system
COVID-19	coronavirus disease 2019
CVD	cardiovascular disease
DM	diabetes mellitus
DPI	days post-inoculation
GFAP	glial fibrillary acidic protein
ICU	intensive care unit
iGluRs	ionotropic glutamate receptors
IL	interleukin
NMDA	N-methyl-D-aspartate

RA	rheumatoid arthritis
ROS	reactive oxygen species
SARS-CoV-2	severe acute respiratory syndrome coronavirus 2
TNF	tumor necrosis factor

Acknowledgments

The completion of this dissertation would not have been possible without the contributions of many people. First, Dr. Leigh Anne Swayne gave me the opportunity to pursue this research, and was always available for advice, encouragement, and training. My committee members, Dr. Craig Brown and Dr. Bob Chow also gave support and advice throughout my project.

The Canadian Institute for Health Research (CIHR: grant# GA4-177766) awarded to Dr. Swayne, Dr. Tremblay, and Dr. Kobasa provided funding for this work. I was supported by Dr. Swayne's CIHR grant, UVic Graduate and donor awards, and a UVic fellowship for master's students.

Thank you to the Swayne Lab members for their help and support, especially Leigh Wicki-Stordeur and Nicole York. Leigh taught me the basics of immunohistochemistry and confocal imaging, and I could not write this thesis without her valuable feedback. Nicole helped me a lot during my analysis because I was blinded. Her kindness and support helped me during tough times.

Thank you to the Tremblay lab, especially Dr. Tremblay, for her helpful and valuable insights during the project. Also, my dear friend Parsa was always there for me whenever I needed him. Finally, I want to express my deepest gratitude to my mother and father. Their unwavering love and constant support have shaped me into who I am today. I could not have achieved any of this without them by my side.

Dedication

To my dear uncle, Masoud Samaraweera,
I am deeply grateful for your unwavering financial and emotional support throughout this journey.

Without your belief in me, this achievement would not have been possible.

Chapter one

1. Introduction

1.1. Overview

COVID-19 (Coronavirus disease 2019), caused by the Severe Acute Respiratory Syndrome Coronavirus 2 (SARS-CoV-2), is not only a primary respiratory illness but also triggers a range of neurological symptoms such as impaired cognition and fatigue (reviewed in Nittas et al. 2022; and Xu, Xie, and Al-Aly 2022). The mechanisms underlying neurological effects of COVID-19 are mainly categorized into direct viral invasion and indirect effects due to peripheral inflammation compromising blood-brain barrier (BBB) integrity (reviewed in Ahmad et al. 2020; Oxley et al. 2020). Regardless of the mechanism, both animal and human studies have shown significant neuroinflammation (reviewed in Booz et al. 2020; Srivastava et al. 2021). Neuroinflammation is often associated with astrogliosis (Kwon and Koh 2020), which is marked by increases in the expression levels and distribution of the astrocyte-enriched intermediate filament protein, glial fibrillary acidic protein (GFAP) (reviewed in Nourbakhsh et al. 2021) and the proliferation of astrocytes (Kwon and Koh 2020; reviewed in Nourbakhsh et al. 2021). Despite some recent advances (Dey 2024; Haverty et al. 2024; reviewed in Proust et al. 2023), we currently have limited understanding of the extent of astrogliosis in the context of mild, peripheral COVID-19. To this end, my thesis developed an imaging pipeline to investigate astrogliosis within the context of mild, peripheral COVID-19.

I optimized this pipeline to measure the distribution of GFAP (labels astrocytes by targeting the glial fibrillary acidic protein (Balouch et al. 2021)), and to measure the density of astrocytes, via the astrocyte-specific nuclear marker SOX9 (a marker almost exclusively expressed by astrocytes in the adult brain and upregulated in reactive astrocytes (Sun et al. 2017)). I employed this pipeline on a mild, peripheral animal model of COVID-19, in collaboration with the Kobasa Lab at the National Microbiology Laboratory. Members of the Kobasa Lab intranasally infected Syrian hamsters with a 10^5 TCID50 dose of SARS-CoV-2. They collected the brains at 1-, 3-, 5-, 7-, and 31-days post-inoculation (DPI). Following prolonged fixation (30 days) they shipped the fixed brains to the University of Victoria. Together with a team of researchers, I coronally sectioned the brains and then processed them for immunofluorescence microscopy with antibodies against SOX9 (astrocyte nucleus; (Sun et al. 2017)), GFAP (astrocyte-enriched intermediate filament), NeuN, and Hoechst. I used a confocal microscope (Leica TCS SP8) equipped with tile-scan and stitching capacity to produce micrographs of entire coronal brain sections. Subsequently, I digitally extracted critical brain regions associated with cognitive functions and inflammation susceptibility, such as the cortex, corpus callosum, dorsal striatum, hippocampus, and third ventricle. I analyzed the images by designing a critical coding step using MATLAB to handle and quantify the positive cells of each staining efficiently. My analysis showed a clear increase in GFAP in the cortex of female hamsters 3 DPI. I also noted rises in GFAP levels in the hippocampus and corpus callosum at 3 DPI in female hamsters, but these were not statistically significant. In contrast, the numbers of SOX9+ cells did not significantly change with DPI, sex, or brain region. These results indicate that mild peripheral COVID-19 might cause a temporary and localized increase in astrogliosis in female hamsters only. Additionally, slight variations in Hoechst and NeuN staining across different brain areas and times point to potential COVID-19-related changes in cell markers and

density, although these findings need further confirmation. Overall, my results highlight a temporary and female-specific response in the brain to mild peripheral COVID-19, underlining the importance of considering both regional and temporal aspects to grasp the neurological effects of COVID-19 fully.

In Chapter 1, I present the background and aim of my research. I provide an overview of COVID-19 and highlight its multisystemic nature and associated neurological symptoms and dysfunction. I made major contributions to a recently published review paper on this topic (reviewed in Volk et al. 2024), and touch on several of the topics discussed in that review here as well. I discuss the potential mechanisms behind these neurological effects, including direct and indirect central nervous system (CNS) infection, with a focus on the latter as it relates directly to my thesis work. I then discuss the role of astrocytes in a healthy brain and in the context of neuroinflammation. Then, I explain the current evidence of COVID-19 induced neuroinflammation and its effects on astrocytes. Finally, I describe my rationale for choosing my animal model, markers, and specific brain regions.

In Chapter 2, I detail my study's hypothesis, methods and results. I describe the infection protocol of the Syrian hamster model. I outline the development and implementation of my imaging and analysis pipeline and present the results from my immunohistochemical staining paradigm (GFAP, SOX9, Hoechst, and NeuN) for 6 brain regions: cortex, corpus callosum, third ventricle, hippocampus and dorsal striatum.

In Chapter 3, I include relevant discussion, conclusions, and future paths. I summarize my findings, including the impact of mild, peripheral COVID-19 on astrocyte density and GFAP coverage in addition to NeuN and Hoechst analysis results. Finally, I address the limitations and considerations of the study.

1.2. COVID-19

In this section, I discuss COVID-19 as a respiratory and multisystemic infection, beginning with the mechanism of SARS-CoV-2 entry into cells via the ACE2 (angiotensin- converting enzyme 2) receptor (Azizan and Brown 2020; reviewed in Mehta et al. 2020). The discussion progresses to cellular reactions, emphasizing how rapid viral replication triggers extensive peripheral inflammatory reactions, including leukocyte activation and cytokine storms (a systemic release of cytokines and other inflammatory mediators), exacerbating systemic inflammation and physiological disruptions (reviewed in Booz et al. 2020; Sriwastava et al. 2021). Additionally, I discuss the virus's neurological impacts, exploring theories of (1) heightened peripheral inflammation and (2) direct CNS infection, which leads to neuroinflammation (Oxley et al. 2020; Patel et al. 2020). Finally, I provide an overview of its symptomatology—from acute neurological conditions to chronic multisystemic manifestations (reviewed in Nittas et al. 2022; and Xu, Xie, and Al-Aly 2022). Note that several of these topics were also covered in a recent review paper published by the Swayne Lab (reviewed in Volk et al. 2024), to which I made major contributions.

COVID-19 is an infectious disease caused by the SARS-CoV-2 virus. It was first identified in Wuhan, China, in late 2019 (Alberca et al. 2020). The virus has since spread globally, leading to a pandemic (reviewed in Ahmad et al. 2020). Common symptoms include fever, cough, and shortness of breath, with less frequent occurrences of muscle pain and sore throat (reviewed in Jain et al. 2020). The virus spreads primarily through respiratory droplets during coughing and sneezing, with an incubation period of 2-14 days (Alberca et al. 2020). While most cases are mild, some can progress to severe pneumonia and multi-organ failure,

particularly in older adults and those with prior health conditions (Kishor and Ramhari 2020).

1.2.1. COVID-19, a respiratory and multisystemic infection

The SARS-CoV-2 virus primarily enters cells by binding to the ACE2 receptor (reviewed in Mehta et al. 2020). ACE2 is a transmembrane glycoprotein and a type 1 zinc mono-carboxypeptidase that plays a critical role in the cardiovascular system by converting angiotensin II, a pro-inflammatory molecule, into the vasodilator angiotensin 1-7, an anti-inflammatory heptapeptide (Azizan and Brown 2020; Donoghue et al. 2000, and Tipnis et al. 2000). In humans, ACE2 is differentially expressed across tissues and organs, and the observed pattern of SARS-CoV-2 infection aligns with this expression (reviewed in Beyerstedt, Casaro, and Rangel 2021). The expression is enriched in the respiratory tract cells, but its expression levels vary across other organs (reviewed in Beyerstedt, Casaro, and Rangel 2021). Within the respiratory system, ACE2 is predominantly expressed in type 2 pneumocytes, which are alveolar cells responsible for producing pulmonary surfactants and serve as stem cells enabling lung tissue repair (Azizan and Brown 2020). Adipose tissue, heart, kidneys, small intestine, testis, and thyroid express high levels of ACE2. Medium expression levels are observed in the adrenal gland, bladder, colon, liver, and lungs, while lower levels are noted in the blood, blood vessels, bone marrow, brain, muscle, and spleen (Bilinska et al. 2020; Hamming et al. 2004; Haverty et al. 2024; M.-Y. Li et al. 2020). The virus's spike protein binds to the ACE2 receptor, facilitating viral entry into the host cell (Zhang, Li, and Niu 2020). This binding is followed by the cleavage of the spike protein by proteases such as TMPRSS2, which further aids in the fusion of the viral and cellular membranes, allowing the virus to enter the cell (Abassi et al. 2020). When SARS-CoV-2 enters the cell, it rapidly multiplies and disrupts the balance between ACE and ACE2.

This imbalance leads to the overactivation of the renin-angiotensin system, which can cause inflammation, increased vascular permeability, and fibrosis (reviewed in Beyerstedt, Casaro, and Rangel 2021; Zhang, Li, and Niu 2020). This damage results in an inflammatory reaction by releasing pro-inflammatory cytokines and chemokines from the immune cells (reviewed in Mehta et al. 2020). Moreover, the infection by SARS-CoV-2 causes a strong immune response in the body by affecting the number and behavior of leukocytes. Leukopenia (a decrease in leukocyte count) is common, especially in the early stages of the disease (Nurprilinda and Simanjuntak 2023; Zhao et al. 2020). However, leukocytosis (an increase in leukocyte count) can also occur, particularly in older patients with underlying chronic diseases and severe cases (Zhao et al. 2020). COVID-19 significantly disrupts the innate immune system by altering monocytes and macrophages: it reduces monocyte numbers—particularly CD16- monocytes—while increasing CD16+ pro-inflammatory monocytes in critical patients (reviewed in Knoll, Schultze, and Schulte-Schrepping 2021; Qin et al. 2021). Monocytes exhibit altered phenotypes with impaired antigen presentation due to decreased HLA-DR (a molecule on antigen-presenting immune cells that presents antigens to T helper cells, crucial for activating the adaptive immune response) expression, leading to immunosuppression and affecting the adaptive immune system (reviewed in Knoll, Schultze, and Schulte-Schrepping 2021; Qin et al. 2021). Infected monocytes and macrophages become hyperactivated, producing excessive pro-inflammatory cytokines and chemokines, contributing to cytokine storms and hypercytokinemia—a hallmark of macrophage activation syndrome—which can lead to acute respiratory distress syndrome and multi-organ failure (Jafarzadeh et al. 2020; Kosyreva et al. 2021).

In summary, SARS-CoV-2 primarily enters cells by binding to ACE2 receptors—especially abundant in respiratory tract cells like type 2 pneumocytes—disrupting the balance

between ACE and ACE2, which over activates the renin-angiotensin system leading to inflammation and vascular damage; this triggers a strong immune response characterized by altered leukocyte counts, impaired antigen presentation due to decreased Human Leukocyte Antigen – DR isotype expression on monocytes (affecting the adaptive immune system), and hyperactivated monocytes and macrophages producing excessive pro-inflammatory cytokines and chemokines, contributing to cytokine storms and severe complications like acute respiratory distress syndrome and multi- organ failure (Abassi et al. 2020; Azizan and Brown 2020; reviewed in Beyerstedt, Casaro, and Rangel 2021; Jafarzadeh et al. 2020; reviewed in Knoll, Schultze, and Schulte-Schrepping 2021; Kosyreva et al. 2021; reviewed in Mehta et al. 2020; Nurprilinda and Simanjuntak 2023; Qin et al. 2021; Zhang, Li, and Niu 2020; Zhao et al. 2020)

1.2.2. Symptomology – peripheral inflammation and nervous system inflammation

COVID-19 can lead to both acute and long-term symptoms (reviewed in Crook et al. 2021). Common acute symptoms include fever, cough, and breathing difficulties (Roy et al. 2023). Long COVID usually involves fatigue, breathlessness, cognitive impairment, and cardiovascular issues and persists beyond four weeks (reviewed in Crook et al. 2021; Shah et al. 2021). First, I will explain some common acute symptoms; then, I will explain long-term symptoms in detail, focusing on neuroinflammation.

1.2.3. Acute symptoms

In this paragraph, I discuss the mild to moderate symptoms experienced during the acute phase (<4 weeks) of COVID-19. The prevalence of respiratory symptoms in survivors of hospital admission after COVID-19 infection is as follows: fatigue (52%), dyspnoea (37%), chest pain (16%), and cough (14%) (reviewed in Cares-Marambio et al. 2021). A persistent cough is frequently reported among COVID-19 patients. This symptom can last for weeks or months after the initial infection and may be dry or productive (Chudzik et al. 2022; reviewed in Healey et al. 2022; and Nguyen et al. 2022; Salamanna et al. 2021; reviewed in Yong 2021). Many COVID patients experience difficulty breathing, or shortness of breath. This can occur even with minimal exertion and may be related to lung damage or other respiratory issues (Chudzik et al. 2022; reviewed in Healey et al. 2022; reviewed in Nguyen et al. 2022; Salamanna et al. 2021; reviewed in Yong 2021). Some patients report ongoing chest pain, which can be sharp or dull and may be associated with heart or lung issues. (Chudzik et al. 2022; reviewed in Nguyen et al. 2022; and Yong 2021).

1.2.4. Long-COVID symptoms

COVID-19 not only causes immediate and short-term health issues but also leads to a range of long-term symptoms—including neurological complications—that present significant public health and socioeconomic challenges (reviewed in Xu, Xie, and Al-Aly 2022). This condition, commonly referred to as "long-COVID," is typically defined as symptoms that persist or emerge 4 to 12 weeks after the initial SARS-CoV-2 infection, although definitions vary (reviewed in Nittas et al. 2022; and Volk et al. 2023). The World Health Organization (WHO) labels this collection of symptoms as post-COVID-19 condition, though "long-COVID" is the

more prevalent term (Soriano et al. 2022; reviewed in Volk et al. 2023). Due to the broad scope of this classification, estimates of its prevalence and severity vary widely. For example, a recent umbrella review found adult prevalence rates ranging from 2.3% to 53%, with a significantly higher rate of 36.7% among hospitalized patients (COVID-19 cases | WHO COVID-19 dashboard n.d.; reviewed in Nittas et al. 2022; and Volk et al. 2023).

Neuroinflammation could potentially contribute to neurological symptoms observed in some COVID-19 patients (Sarubbo et al. 2022). These symptoms have been categorized into five main groups: cerebrovascular, motor, sensorial, cognitive, and miscellaneous (Mao et al. 2020; Sarubbo et al. 2022). Among the most common neurological symptoms of long-COVID are cognitive impairment (often referred to as "brain fog"), fatigue, depression, and anxiety (Graham et al. 2021; Groff et al. 2021; reviewed in Xu, Xie, and Al-Aly 2022). These symptoms can vary in severity and often lead to mild to severe disruptions in daily life, contributing to the broader public health and socioeconomic burdens associated with the condition (reviewed in Nittas et al. 2022).

Brain fog, a term frequently associated with post-acute sequelae of COVID-19 (long-term symptoms and health complications that persist or appear after the initial recovery from a COVID-19 infection), refers to a collection of cognitive dysfunctions that include difficulties with concentration, executive function deficits, and memory impairments. Brain fog is characterized by symptoms such as the inability to concentrate, anterograde and retrograde amnesia, and deficits in processing speed and attention (reviewed in Araújo et al. 2023; and Krishnan et al. 2022). These cognitive impairments can significantly impact daily functioning, making it challenging for individuals to perform routine tasks or return to their professional roles effectively (Nouraeinejad 2023). The prevalence of brain fog among COVID-19 survivors

varies, with studies indicating that 18-36% of hospitalized patients with neurological symptoms experience brain fog in the post-acute phase (reviewed in Araújo et al. 2023). The impact of brain fog extends beyond cognitive impairments to include profound psychosocial consequences. Individuals often experience reduced functionality in everyday activities and may struggle with professional and personal identity, leading to feelings of guilt, shame, and stigma (Callan et al. 2022). The fluctuating nature of the symptoms, which can vary daily, weekly, and monthly, adds to the difficulty of experience (Callan et al. 2022). Depression has been identified as a significant predictor of persistent brain fog, further complicating its proper diagnosis (Cristillo et al. 2022). Brain fog can also lead to long-term neurodegenerative diseases or advance the progression of existing neurodegenerative conditions (reviewed in Chakrabarti 2022). The complexity of post-COVID sequelae, including brain fog, make its diagnosis challenging, as symptoms can overlap with other health-related issues (reviewed in Chakrabarti 2022).

Encephalopathy and encephalitis represent severe neurological conditions observed in COVID-19 patients. These conditions range from mild confusion to severe impairment and coma, with varied manifestations such as fever, headache, and brain dysfunction symptoms (Sarubbo et al. 2022). Encephalopathy has been reported in as high as one fifth individuals affected by COVID-19 (Abenza Abildúa et al. 2021). Brain MRI and EEG studies in these patients have shown some brain alterations (Abenza Abildúa et al. 2021). Confusion, including delirium and acute brain failure, are experienced by roughly a third of individuals affected by COVID-19 (Abenza Abildúa et al. 2021; reviewed in Pranata et al. 2021; Sarubbo et al. 2022). Dizziness and seizures are also reported, although less frequently, but highlight the indirect effects of COVID-19, such as fever-induced hyperthermia affecting the BBB (Nikbakht, Mohammadkhanizadeh, and Mohammadi 2020).

Cerebrovascular symptoms are among the most serious neurological complications, with acute events being more common in severely ill or ICU patients (reviewed in Bridwell, Long, and Gottlieb 2020). The prevalence of acute cerebrovascular diseases in COVID-19 patients is relatively low but significantly impacts those affected, with ischemic stroke being the most common type. The comorbidities, such as hypertension and diabetes, along with sepsis-induced coagulopathy, are considered major factors contributing to these ischemic events (Garcia et al. 2021; Mishra et al. 2021). Motor symptoms, including neuropathic pain and myopathic changes have been identified, particularly in critically ill patients, highlighting the long-term recovery challenges in the ICU (M. Liu et al. 2020; Mao et al. 2020). The association of COVID-19 with Guillain-Barre Syndrome suggests post-viral deregulation of the immune system as a trigger for GBS in COVID-19 patients (Ellul et al. 2020). There have also been reports of Parkinson's disease following COVID-19 (Calculli et al. 2023).

1.2.5. Sex-specific neurological symptoms

There is notable evidence of sex-specific differences in neurological symptoms of COVID-19. For example, women are more likely to experience anosmia (loss of smell) and facial pain (Biadsee et al. 2020). Women also reported a higher frequency of symptoms such as cough, weakness, myalgia, fever, headache, impaired sense of smell, impaired sense of taste, sore throat, runny nose, and nasal congestion, although only the runny nose was statistically significant (Biadsee et al. 2020). In terms of COVID-19 sequelae, females are more likely to experience psychiatric/mood disorders, ear, nose, and throat issues, musculoskeletal problems, and respiratory sequelae, while males are more likely to experience renal sequelae

(reviewed in Sylvester et al. 2022). For long COVID symptoms, females have a higher likelihood of experiencing ear, nose, and throat, gastrointestinal, psychiatric/mood, neurological, and dermatological disorders, whereas males have higher odds of endocrine and renal disorders (reviewed in Sylvester et al. 2022). Additionally, male patients have higher plasma levels of innate immune cytokines (e.g., IL-8, IL-18) and more non-classical monocytes (reviewed in Takahashi et al. 2020).

1.2.6. Neurological sequelae: potential mechanisms

There are two main, non-mutually exclusive theories for neurological symptoms observed in COVID-19; one involves the heightened peripheral inflammation (this includes vascular system effects), which is the most relevant to my work, and the other involves direct infection of the CNS (Oxley et al. 2020; Patel et al. 2020; reviewed in Tremblay et al. 2020), which will be covered only briefly below.

The indirect inflammatory response occurs when the peripheral inflammation is initiated by a cytokine storm (reviewed in Nagu et al. 2021; Najjar et al. 2020). Elevated levels of pro-inflammatory cytokines such as IL-6, IL-1β, and TNF-α characterize this excessive immune response (reviewed in Nagu et al. 2021; Najjar et al. 2020). Systemic inflammation not only exacerbates the primary respiratory symptoms of COVID- 19 but also sets the stage for potential neurological complications (Najjar et al. 2020; reviewed in Volk et al. 2023). One of the critical impacts of this peripheral inflammation is the disruption of theBBB. The systemic release of cytokines and other inflammatory mediators can compromise the integrity of the BBB, making it more permeable (Almutairi 2021; reviewed in Nagu 2020). This increased permeability allows immune cells and inflammatory mediators to infiltrate the CNS, which would otherwise be

protected from such systemic inflammatory responses. Once the BBB is disrupted, the infiltrating immune cells and inflammatory mediators activate resident glial cells within the CNS, particularly astrocytes and microglia (Almutairi 2021; Zamani 2021). Astrocytes, which are crucial for maintaining the homeostasis of the CNS, respond to this activation by releasing additional cytokines and chemokines, further exacerbating the neuroinflammatory response (Almutairi 2021; Zamani 2021). Simultaneously, there is an upsurge in reactive oxygen species (ROS), exacerbating the oxidative state and contributing to systemic inflammation (Spindler and Hsu 2012; reviewed in Volk et al. 2023). This activation of astrocytes and microglia creates a feedback loop of inflammation, leading to sustained neuroinflammation and contributing to neuronal damage. The neuroinflammation and subsequent neuronal damage have significant implications for cognitive function, as the inflammatory environment within the CNS can disrupt normal neuronal signaling and synaptic function, leading to cognitive impairments.

Direct brain infection by SARS-CoV-2 involves the virus invading and replicating within CNS cells through multiple pathways, including olfactory, hematogenous, and neuronal transport routes, as well as direct viral invasion and the Trojan horse mechanism (Liu et al. 2021), but there is limited evidence for this in most cases (reviewed in Volk et al. 2024). One common route is via the olfactory nerve, where the virus moves from the nasal cavity to the brain and cerebrospinal fluid within a week (Liu et al. 2021; reviewed in Nagu et al. 2021). This is supported by studies showing that blocking this pathway in mice limits the virus's entry into the CNS (reviewed in Nagu et al. 2021). Another pathway is the hematogenous route. The virus enters the bloodstream, infects the blood-brain barrier (BBB) cells, and increases their permeability, allowing the virus to infiltrate the CNS (J. Liu et al. 2021; reviewed in Nagu et al. 2021). Other viruses, like hepatitis and herpes, show similar mechanisms (J. Liu et al. 2021).

Additionally, neuronal transport allows the virus to travel along the gustatory and trigeminal nerves into the CNS, facilitated by binding to ACE2 receptors (Martinez et al. 2024; reviewed in Nagu et al. 2021). This pathway shows correlation with neurological symptoms, such as loss of taste and smell (Huang et al. 2020). Lastly, the "Trojan horse" mechanism involves the virus hijacking immune cells to cross the BBB and infect the CNS, a strategy similar to HIV and Zika virus (reviewed in Gasmi et al. 2021; Martinez et al. 2024; reviewed in Nagu et al. 2021; Najjar et al. 2020).

1.3. Astrocytes properties and role in naïve brain

Astrocytes, the most abundant glial cells in the CNS, play a crucial role in regulating neurotransmitters in the brain which is very important for neural signaling (reviewed in Cekanaviciute and Buckwalter 2016; Gao et al. 2022; reviewed in Pang et al. 2022). They regulate the uptake and recycling of neurotransmitters to control their level in the synaptic cleft (Gao et al. 2022; reviewed in Pang et al. 2022; and Saikarthik et al. 2022). Additionally, astrocytes can release gliotransmitters such as glutamate, ATP, & D-serine in response to neurotransmitters for modulating synaptic transmission and plasticity (reviewed in Cekanaviciute and Buckwalter 2016; Gao et al. 2022). Astrocytes also help maintain the balance of ions in the extracellular space, which is crucial for neuronal signaling. Furthermore, astrocytes maintain the BBB, a controlling gate for the circulating substances, including neurotransmitters, cytokines, and chemokines traffic into the brain (reviewed in Cekanaviciute and Buckwalter 2016; Gao et al. 2022; J. Li et al. 2022; reviewed in Pang et al. 2022; reviewed in Saikarthik et al. 2022).

Astrocytes provide both physical and metabolic support for BBB. Physically, astrocytes extend their end-feet processes to envelop the majority of the brain's vasculature, aiding in the formation and maintenance of the BBB. Functionally, they regulate the passage of molecules from the blood to the brain and vice versa. By this mechanism, only necessary substances with the right concentration can reach the brain (Andrews et al. 2022; Beckman et al. 2022). In addition to their physical roles, astrocytes control the BBB's 'tightness'. They release factors that control the expression and localization of tight junction proteins in endothelial cells (Chen and Li 2021; reviewed in Lawrence et al. 2023). These tight junctions are crucial for preventing the uncontrolled passage of substances into the brain. Hence, astrocytes play a significant role in maintaining the selective permeability of the BBB (Chen and Li 2021; reviewed in Lawrence et al. 2023). Astrocytes also have an immunological role at the BBB. They regulate the invasion of peripheral immune cells to prevent unnecessary immune responses in the brain (reviewed in Tremblay et al. 2020). Furthermore, astrocytes can communicate with other cells in the BBB, such as pericytes (reviewed in Tremblay et al. 2020).

Astrocytes are fundamental in regulating the homeostasis of key ions—K^+, Na^+, Ca^{2+}, and Cl^- in the central nervous system (CNS), directly influencing neuronal excitability and the processes of rhythmogenesis. Here I will explain the role of astrocytes in regulating extracellular K^+ levels around neurons, especially when there is a lot of brain activity. K^+ is essential for maintaining the resting membrane potential, action potential repolarization, and extracellular fluid balance (Akyuz et al. 2020; Somjen 2002). The concentration of extracellular K^+ ($[K^+]_{ex}$) is lower in the brain compared to other parts of the body. This lower $[K^+]_{ex}$ helps maintain the stability of cerebral function because high $[K^+]_{ex}$ enhances neuron excitability (Somjen 2002). Increased brain activity results in more frequent action potentials, leading to

more K^+ exiting neurons and accumulating outside the cells (Akyuz et al. 2020). Astrocytes, by regulating $[K^+]_{ex}$, prevent the neurons from becoming overactive and causing seizures, which can happen when too much K^+ accumulates around them. A process known as spatial buffering absorbs excessive K^+ via the gap junctions, which prevents excitotoxicity (Bellot-Saez et al. 2017; Enkvist and McCarthy 1994, 1994; Kadala et al. 2015; Orkand, Nicholls, and Kuffler 1966).

1.4. Neuroinflammation

Neuroinflammation is an inflammatory response within the CNS involving the production of cytokines, chemokines, ROS, and secondary messengers, primarily mediated by microglia and astrocytes (reviewed in DiSabato, Quan, and Godbout 2016). While acute neuroinflammation can aid in clearing pathogens and repairing tissue, chronic neuroinflammation causes a cycle of inflammation that results in neuronal damage and plays an important role in neurodegenerative diseases such as Alzheimer's disease (reviewed in DiSabato, Quan, and Godbout 2016; and Frank-Cannon et al. 2009). Some of the events involved in neuroinflammation are depicted in Figure 1.

In this section, I will explain how neuroinflammation involves astrocytes and microglia. Then, I will discuss several conditions associated with peripheral inflammation that can lead to neuroinflammation. Finally, I will focus on COVID-19's effects on astrocytes and microglia and highlight the current gaps in our knowledge.

1.4.1. Astrogliosis

When the CNS is injured or invaded, astrocytes react by altering their gene expression, cellular structure, and function, a process collectively termed astrogliosis (reviewed in Sofroniew and Vinters 2010). Astrogliosis can range from mild changes, such as upregulation or increased distribution of GFAP and cellular hypertrophy, to critical changes like astrocyte proliferation and scar formation (reviewed in Sofroniew 2015; Sofroniew and Vinters 2010). These changes can include alterations in oxidative stress defense, cholesterol metabolism, and gene transcription (reviewed in Osborn et al. 2016). One key signaling pathway in astrogliosis is the Janus kinase/signal transducer and activator of transcription pathway. Activation of this pathway, particularly through STAT3, regulates the expression of genes associated with astrogliosis, such as GFAP and vimentin (reviewed in Sofroniew 2015; Sofroniew and Vinters 2010). Deletion of STAT3 in astrocytes leads to increased inflammation and tissue damage, proving its role in modulating the astrocytic response (reviewed in Sofroniew 2015; Sofroniew and Vinters 2010).

Another important pathway is the nuclear factor kappa-light-chain-enhancer of activated B cells (NF-κB) pathway, which is activated by IL-1 and TNF-α. This pathway regulates the expression of various inflammatory mediators and contributes to the reactive phenotype of astrocytes (reviewed in Correa-Cerro and Mandell 2007). Astrocytes also respond to CNS damage by upregulating the expression of intermediate filament proteins, such as GFAP and vimentin, which contribute to the structural changes observed during astrogliosis (reviewed in Correa-Cerro and Mandell 2007). These changes include cellular hypertrophy and the formation of astrocytic processes that can encapsulate and isolate damaged tissue (reviewed in Sofroniew 2015; Sofroniew and Vinters 2010). The results of astrogliosis can be both beneficial and detrimental. On the beneficial side, astrogliosis aims to restore homeostasis, limit tissue

damage, and protect neural cells (reviewed in Sofroniew 2015; Sofroniew and Vinters 2010). For example, reactive astrocytes can help repair the blood-brain barrier, regulate inflammation, and provide neuroprotection (reviewed in Sofroniew 2015). However, under certain circumstances, astrogliosis can become dysfunctional and inhibit adaptive neural plasticity mechanisms needed for functional recovery. This can lead to detrimental effects such as the inhibition of axon regeneration by astrocyte scars, which can restrict inflammation but also prevent neural repair (reviewed in Pekny and Pekna 2016; Sofroniew 2015; Sofroniew and Vinters 2010).

Astrogliosis is also associated with various CNS disorders. In Alzheimer's disease, for instance, the presence of misfolded amyloid-beta protein triggers reactive gliosis, leading to changes in glutamate and GABA signaling, K^+ buffering, and other signaling pathways (reviewed in Osborn et al. 2016). This dysregulation can destabilize microcircuits within key brain regions, contributing to cognitive decline (reviewed in Osborn et al. 2016). Additionally, genetic mutations that cause astrocyte dysfunctions can lead to neurological diseases such as Alexander disease and amyotrophic lateral sclerosis, where abnormal astrocytes contribute to neuronal dysfunction and degeneration (reviewed in Sofroniew 2015; Sofroniew and Vinters 2010).

1.4.2. Microgliosis

Microglia, the resident macrophages of the CNS, become activated in response to various stimuli, which can lead to neurodegeneration if chronic (reviewed in DiSabato, Quan, and Godbout 2016; Kwon and Koh 2020). Microgliosis refers to the activation and proliferation of microglia. Under normal conditions, microglia play a crucial role in maintaining CNS

homeostasis by constantly survey the CNS environment for signs of damage or pathogens (reviewed in Subhramanyam et al. 2019). Microgliosis can be triggered by a variety of stimuli, including pathogens, toxins, injury, and abnormal protein accumulation, such as amyloid-beta plaques in Alzheimer's disease (reviewed in Krause and Müller 2010). Microglia amoeboid shape in their natural state shows they are ready for phagocytosis and cytokine release in neuroinflammation (Davalos et al. 2005; Nimmerjahn, Kirchhoff, and Helmchen 2005; Takagi et al. 2019). Activated microglia can adopt different phenotypes, traditionally categorized as M1 (pro-inflammatory and neurotoxic) or M2 (anti-inflammatory and neuroprotective), although this dichotomy may not fully capture the complexity of microglial responses (Kwon and Koh 2020). In the situation of microgliosis, microglia release a wide range of inflammatory mediators, including cytokines, chemokines, ROS, and reactive nitrogen species, which can attract other immune cells, promote inflammation, and contribute to the clearance of pathogens and debris through phagocytosis (reviewed in Subhramanyam et al. 2019). Limited injury spread can trigger a beneficial activation of microglia, known as microgliosis. For example, microglia can degrade amyloid-beta plaques and remove neurotoxic substances like glutamate, which can otherwise lead to neuronal death (reviewed in Krause and Müller 2010).

However, prolonged or excessive activation of microglia can lead to chronic neuroinflammation, which is associated with progressive neuronal damage and neurodegenerative diseases such as Alzheimer's disease, Parkinson's disease, and amyotrophic lateral sclerosis (reviewed in Frank-Cannon et al. 2009; and Minghetti 2005). Moreover, chronic microgliosis creates a self- perpetuating cycle of inflammation, where the sustained release of inflammatory mediators leads to further activation of microglia and additional neuronal damage (reviewed in Frank-Cannon et al. 2009; and Subhramanyam et al. 2019). Microgliosis also involves complex interactions with other glial cells, particularly astrocytes. Activated microglia

can release signaling molecules that influence astrocyte activation, leading to neuroprotective or neurotoxic outcomes (Kwon and Koh 2020). This bidirectional communication between microglia and astrocytes is crucial for regulating the inflammatory response and determining the overall impact of microgliosis on CNS health (Kwon and Koh 2020).

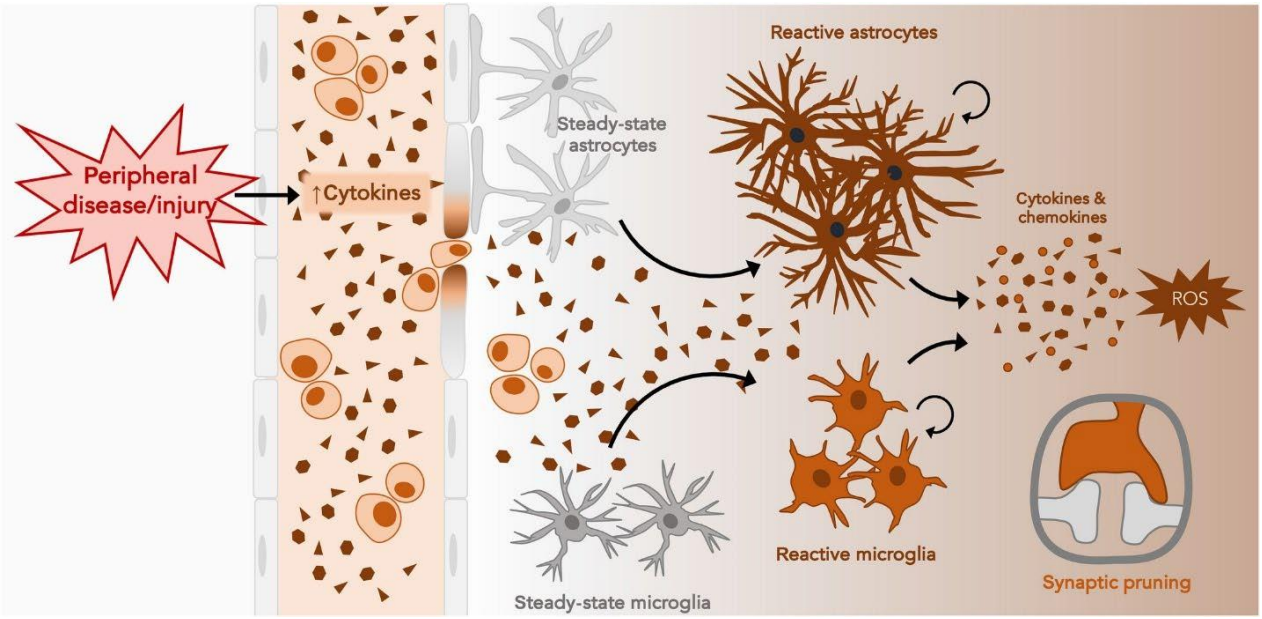

Figure 1. Peripheral inflammation leads to CNS dysfunction.

COVID-19 increases peripheral inflammation. This involves the release of cytokines and chemokines into the circulation, as well as immune cell modulation. These peripheral events culminate in blood-brain–barrier dysfunction, characterized by "leaky" vasculature, enabling invasion of inflammatory molecules and cells into the central nervous system. These inflammatory stimuli modulate astrocytes and microglia, thus changing their morphology and function, in a process known as gliosis. These modulated glial cells can further exacerbate the immune response by releasing cytokines, chemokines, and reactive oxygen species (ROS), which together may result in the loss or dysfunction of neurons and/or synapses, leading to cognitive impairment and other forms of neurological dysfunction. Reproduced from Volk et al., *Journal of Neurochemistry* (2024), under the Creative Commons Attribution 4.0 International License (CC BY 4.0). Original work available at https://onlinelibrary.wiley.com/doi/abs/10.1111/jnc.16016.

1.4.3. Examples of other peripheral conditions causing neuroinflammation

COVID-19 begins as peripheral inflammation, and neurological symptoms and their associated neuroinflammation occur afterward (reviewed in Crook et al. 2021; Shah et al. 2021). Therefore, it is crucial to compare COVID-19 with other inflammatory diseases that cause neuroinflammation. In this section, I will mention a couple of important inflammatory diseases and some evidence of their neurological impacts.

1.4.3.1. Influenza

Influenza can cause neuroinflammation by increasing proinflammatory cytokines and microglial activation and reducing neurotrophic factors in the hippocampus (Hosseini et al. 2018; Jurgens, Amancherla, and Johnson 2012). These changes are associated with altered hippocampal neuron morphology, impaired long-term potentiation, and deficits in spatial memory formation (Hosseini et al. 2018). Some of these effects can persist long after the acute infection phase (Hosseini et al. 2018). Even non-neurotropic strains like H1N1 can induce sustained microglial activation in brain regions such as the substantia nigra and hippocampus (Sadasivan et al. 2015). Highly pathogenic strains like H5N1 can directly infect the central nervous system, potentially initiating neurodegenerative processes through protein aggregation and dopaminergic neuron loss (Jang et al. 2009). Note that this topic was also covered in a recent review paper published by the Swayne Lab (reviewed in Volk et al. 2024), to which I made major contributions.

1.4.3.2.Diabetes mellitus (DM)

Hyperglycemia-driven neuroinflammation has been shown to compromise the BBB, leading to memory loss in both type 1 and type 2 DM mouse models (Rom et al. 2019). Neuroinflammation plays a critical role in diabetic neuropathy, contributing to neuropathic pain and chronic itch (reviewed in Fang et al. 2022). Mitochondrial dysfunction and oxidative stress may initiate neuroinflammation by upregulating heat shock protein 60, which activates pattern recognition receptors and potentially spreads inflammation to neighboring astrocytes via exosomes (Liyanagamage and Martinus 2020). These findings suggest that targeting neuroinflammation may provide potential therapies for DM-related cognitive decline and neuropathic symptoms.

1.4.3.3. Arthritis

In rheumatoid arthritis (RA), systemic inflammation is characterized by elevated levels of pro-inflammatory cytokines, which can cross the BBB and induce neuroinflammation (reviewed in Sun, Koyama, and Shimada 2022; and Süß et al. 2020). This process activates microglia and astrocytes, which release additional pro-inflammatory mediators, exacerbating the inflammatory response within the brain (reviewed in Sun, Koyama, and Shimada 2022; and Süß et al. 2020). Additionally, chronic pain and stress associated with RA can activate the hypothalamic-pituitary-adrenal axis, leading to the release of stress hormones that can modulate immune responses and contribute to neuroinflammation (Sun, Koyama, and Shimada 2022).

1.4.3.4. Cardiovascular disease (CVD)

Cardiovascular disease (CVD) can trigger neuroinflammation by activating autonomic afferent nerves and disrupting BBB, allowing proinflammatory mediators and immune cells to infiltrate the CNS (reviewed in Moyse et al. 2022). Additionally, chronic conditions like atherosclerosis, a major CVD, are associated with increased neuroinflammatory markers and microglial activation (reviewed in Moyse et al. 2022). The interplay between peripheral and neuronal inflammation is also evident in the shared risk factors and pathological processes between CVD and neurodegenerative diseases, such as Alzheimer's disease, where neuroinflammation is a common feature (Zarate et al. 2024).

1.5. Study design and rationale

1.5.1. Hypothesis

My research question is whether mild COVID-19 respiratory infection induces transient astrogliosis in Syrian hamsters. Specifically, I aimed to determine if changes occur in astrocyte GFAP distribution and astrocyte density—measured by SOX9 expression—in various brain regions at different time points post-inoculation. I hypothesized that mild peripheral COVID-19 infection might lead to region-specific, time-dependent, sex-dependent astrogliosis.

1.5.2. Choice of animal model

We chose Syrian hamsters *(Mesocricetus auratus)* as they have emerged as an excellent model for studying SARS-CoV-2 infection and COVID-19. They are highly susceptible to the virus, with an infectious dose 50 of just five particles (an "infectious dose 50" (ID50) of just five particles meaning that it takes only five viral particles to infect 50% of the exposed population) (Rosenke et al. 2020). Upon infection, hamsters develop moderate broncho-interstitial

pneumonia, high viral loads, and extensive shedding, mirroring many aspects of human infections (Braxton et al. 2021; Miao et al. 2019). Furthermore, unlike K18-hACE2 mice, which experience fatal and severe outcomes, Syrian hamsters exhibit transient infection and mild to moderate disease without mortality (Jeong et al. 2022). Despite limited diagnostic tools, anatomy atlases and molecular pathways information compared to mice, the Syrian hamster has become an important non-transgenic model for COVID-19 research (reviewed in Gruber et al. 2022). Other hamster species, such as the Roborovsky dwarf hamster and the Chinese hamster, can be used to study COVID-19. However, the Syrian hamster shows a moderate, self-limiting course, which makes it ideal for studying various aspects of COVID-19, especially neuroinflammation (reviewed in Gruber et al. 2022).

SARS-CoV-2 infection in Syrian hamsters results in a systemic immune response, including the activation of peripheral blood mononuclear cells (Castellan et al. 2022, 2023). The activation of immune responses was evident in both sexes at multiple time points, with enriched gene ontology related to cytokine/chemokine-mediated signaling pathways, regulation of lymphocyte activation, and inflammatory responses (Castellan et al. 2022, 2023). Moreover, BBB disruption was a significant finding in the context of SARS-CoV-2 infection. This was shown by elevated levels of extravasated serum IgG in the olfactory bulb, cortex, hippocampus, and medulla oblongata of infected hamsters, with the hippocampus showing the most significant changes (Castellan et al. 2022, 2023; Soung et al. 2022). Moreover, there is weak evidence for neurological tropism, with minimal host response and absence of lesions in the brains of infected hamsters (Castellan et al. 2023; Sia et al. 2020). Notably, SARS-CoV-2 infection in hamsters leads to microglial activation and cytokine expression in the brain, particularly in the hippocampus, which may explain neuropsychiatric symptoms observed in

COVID-19 patients (Käufer et al. 2022; Soung et al. 2022).

1.5.3. Brain region selection

Now, I will explain why I chose cortex, corpus callosum, hippocampus, dorsal striatum, and third ventricle for my study, summarizing how each is linked to the changes seen in COVID-19. First, the cerebral cortex, essential for memory and learning, shows significant alterations in COVID-19 patients. Patients with COVID-19 exhibit lower cortical volume in orbitofrontal, frontal, and cingulate regions compared to healthy controls (Sanabria-Diaz et al. 2022). Post-mortem examinations reveal increased reactive astrocytes, activated microglia, and upregulated inflammation-related genes, highlighting the cortex's vulnerability to COVID-19-induced neuroinflammatory processes (Bayat et al. 2022).

Second, the corpus callosum (CC), a part of the brain's circumventricular organs with a permeable BBB, is a critical frontier for neuroinflammation. This indicates CC susceptibility during cytokine storms and neuroinflammation (Arıkan et al. 2022; Garcia Castro, Utrilla Contreras, and Martín Montes 2022; reviewed in Rasmussen et al. 2020).

Third, the hippocampus is critical in processing spatial and contextual information. COVID-19 significantly affects the hippocampus. Evidence of neuronal degeneration altered glial cell morphology, and increased expression of pro-inflammatory cytokines in the hippocampus associates with long-term cognitive deficits in COVID-19 (Bayat et al. 2022; reviewed in Klein 2022). Advanced imaging studies shows structural and functional changes, which emphasize the hippocampus's role in the neuropsychiatric and cognitive sequelae observed in patients post-infection (Nouraeinejad 2023; Vints et al. 2024; reviewed in Zorzo et al. 2023).

Fourth, the third ventricle, critical for blood-brain barrier function and cerebrospinal fluid

homeostasis, exhibits changes during neuroinflammatory responses. The width of the third ventricle correlates with cognitive impairments in neurological disorders like multiple sclerosis (Benedict et al. 2004). Imaging studies in COVID-19 patients show increased ventricle size and associated white matter changes, suggesting its involvement in the broader spectrum of COVID-19 (Agarwal et al. 2021).

Fifth, the striatum integrates crucial aspects of behavior and cognitive function and is particularly relevant in Parkinson's disease and other neurodegenerative disorders (reviewed in Haber 2016; Jeong et al. 2022). Neuroinflammation in the striatum, characterized by increased expression of inflammatory mediators and microglial activation, contributes to neuronal degeneration (Choi et al. 2009; reviewed in Haber 2016; Hald and Lotharius 2005; Jeong et al. 2022; Kaur et al. 2017; Pott Godoy, Ferrari, and Pitossi 2010; Silvestroni et al. 2009).

1.6. Summary

In summary, I explained the significant neurological implications of long-COVID, focusing on how SARS-CoV-2 infection triggers long-term symptoms like cognitive impairment, fatigue, and depression. This inflammation makes the BBB permeable and causes neuroinflammation, which may contribute to neurological symptoms like brain fog. Then, I talked about the importance of studying astrocytes, which play a crucial role in maintaining neural homeostasis and are deeply involved in neuroinflammatory responses. Their dysfunction in COVID-19 could worsen neuroinflammation and contribute to cognitive deficits and other neurological complications. Then, I discussed my rationale and methodology, including the choice of Syrian hamsters as a model, choosing specific time points, and the selection of specific brain regions—cortex, corpus callosum, hippocampus, dorsal striatum, and third ventricle. Now, I am going to explain my pipeline and the method I used to answer my research questions.

Chapter two

2. Overview

In this chapter, I will explain how I selected and used the Syrian hamster to investigate the effect of mild COVID-19 on astrocytes. I will then discuss how I collected tissue samples and processed them through immunohistochemistry, focusing on the critical steps in imaging and analysis. This overview includes my approach to examining different thresholding techniques to find the best one for my studies, which is Kapur's entropy. Finally, I will present the results of my pipeline, which include the quantification of GFAP, SOX9, Hoechst, and NeuN staining, along with the associated statistical analyses. I was blinded to the identity of the experimental groups throughout all stages of this research to ensure unbiased analysis and interpretation.

2.1. Pipeline development

2.1.1. Syrian hamster infection protocol

We selected the Syrian hamster (*Mesocricetus auratus*; obtained from Charles River Laboratories, Wilmington, Massachusetts, USA; also known as Golden Syrian hamster) as the model organism for its notable susceptibility to SARS-CoV-2. Syrian hamsters endogenously express the ACE2 receptor, enabling infection with SARS-CoV-2 without the need for genetic manipulations (as is the case with mice) (Castellan et al. 2022, 2023; Fomin et al. 2022). Moreover, infected Syrian hamsters present with mild to moderate disease severity, mimicking the majority of human COVID-19 cases (Castellan et al. 2022, 2023; Fomin et al. 2022; Frere et

al. 2022; reviewed in Gruber et al. 2022; Israelow et al. 2020; Knight et al. 2021; Moreau et al. 2020; Oliveira 2020; Patil, Mohandas, and Yadav 2021; Rosenke et al. 2020; Shou et al. 2021; Sia et al. 2020).

The Kobasa lab (National Microbiology Laboratory; Public Health Agency of Canada, Winnipeg, Manitoba, Canada) housed the hamsters (weighing between 61 and 70 grams) under standardized laboratory conditions: 12-hour light/dark cycle, 21-22°C, and humidity levels 30-40%. The Kobasa lab provided food and water *ad libitum* and closely monitored animal well-being through daily health checks. Hamsters were housed five per cage with provisions in place to separate individuals if aggression occurred. Equal numbers of male and female animals were used for each experimental group. Experiments were approved by the Animal Care Committee at the Canadian Science Center for Human and Animal Health per the guidelines provided by the Canadian Council on Animal Care under animal use document H-20-027. Hamsters were monitored by registered Animal Health Technicians throughout the experiment and were provided food and water ad libitum. Animals were acclimatized for 5-7 days before the beginning of all experiments. All animals were monitored and weighed daily throughout all experiments and were provided food and water ad libitum. All manipulations such as blood collection and infection were performed under isoflurane anesthesia. Animals meeting euthanasia criteria or at the end point of the experiment were anesthetized with isoflurane and exsanguinated via cardiac puncture.

To initiate the SARS-CoV-2 infection, the Kobasa lab intranasally inoculated hamsters with a 10^5 TCID50 dose of SARS-CoV-2 (original Wuhan strain) under isoflurane anesthesia delivering 100 µL of the viral inoculum equally between the nostrils to ensure thorough inhalation. Uninfected controls received no treatment. The Kobasa lab noted any changes in

animal weight to assess the impact and progression of the infection. They euthanized animals under deep isoflurane anesthesia, followed by exsanguination via cardiac puncture with cervical dislocation. The Kobasa lab collected the brain tissues at 1-, 3-, 5-, 7-, and 31-days post-inoculation. Finally, brains were fixed in 10% formalin for at least 30 days and subsequently shipped to the University of Victoria, where they were immediately transferred into phosphate buffered saline (the mM PBS solution was prepared using NaCl, KCl, Na_2HPO_4, and KH_2PO_4 in a molar ratio of 136,893:2,683:10,144:1,764) and stored at 4°C until sectioning.

2.1.2. Immunohistochemistry

To ensure safety, I handled all samples in designated containment areas, such as fume hoods. Using a vibratome (Leica VT1000, Leica Camera, Wetzlar, Germany), I sectioned the brains in Dulbecco's PBS (DPBS; catalogue #14190250, Thermo Fisher Scientific, Waltham, Massachusetts, USA) into 50 µm coronal slices and stored them in cryoprotectant (DPBS, ethylene glycol, glycerol in 4:3:3 volume ratio) at -20°C. For immunohistochemistry, I selected brain slices based on anatomical landmarks from the Allen mouse brain atlas (https://mouse.brain- map.org/experiment/thumbnails/100142143) and golden hamster atlas (Smith Jr., Bodemer, and Halsey 1963) within two regions: 1) the dorsal hippocampus (hamster equivalent of mouse bregma -1.255 mm to -2.355 mm) and 2) the lateral ventricles (hamster equivalent of mouse bregma 1.145 mm to 0.020 mm) (Smith Jr., Bodemer, and Halsey 1963). I washed the tissue sections stored in cryoprotectant solution three times for 5 minutes each in DPBS. I then permeabilized them with 1% Triton-X in DPBS at room temperature for 30 minutes in a designated fume hood. After permeabilization, I blocked the tissue with 10% normal donkey serum (017-000-121 catalogue number, Jackson ImmunoResearch Labs,

Pennsylvania, USA) and 0.5% Triton-X in DPBS at room temperature for 1 hour. I incubated slices with primary antibodies in 5% normal donkey serum and 0.5% Triton-X in DPBS for two nights at 4°C on a shaker. Primary antibodies used were SOX9 (82630S catalogue number, 1:200; Cell Signaling Technology, Danvers, Massachusetts, USA), GFAP (13-0300 catalogue number, 1:200; Invitrogen, Waltham, Massachusetts, USA), and NeuN (MAB377 catalogue number, 1:500; Millipore Sigma, Burlington, Massachusetts, USA). After primary antibody incubation, I washed the tissue three times for 5 minutes each in DPBS. I then incubated samples with secondary antibody in 5% normal donkey serum and 0.1% Triton-X in DPBS for 1 hour at room temperature. Secondary antibodies were donkey anti-Rat IgG (H+L) Alexa Fluor 488 conjugate (A-21208 catalogue number), donkey anti-Mouse IgG Alexa Fluor 568 conjugate (A10037 catalogue number), donkey anti-Rabbit IgG (A-31573 catalogue number) Alexa Fluor 647 conjugate (all 1:300; Thermo Fisher Scientific), and Hoechst 33342 nuclear counter-stain (H1399 catalogue number, 1:1000; Thermo Fisher Scientific). Before use, I centrifuged the secondary antibodies at 4°C for 5 minutes. I washed the tissue four times for 5 minutes each in DPBS. I then mounted the tissue onto glass slides with ProLong Gold anti-fade reagent (P36934 catalogue number, Thermo Fisher Scientific), let the mounting media harden at room temperature for at least 24 hours, protected from light, and stored the slides at - 20°C until imaging. Figure 2 shows a confocal micrograph taken from deep cortical layers depicting staining with Hoechst, GFAP, SOX9, and NeuN, which confirms the expected distribution profile of each marker.

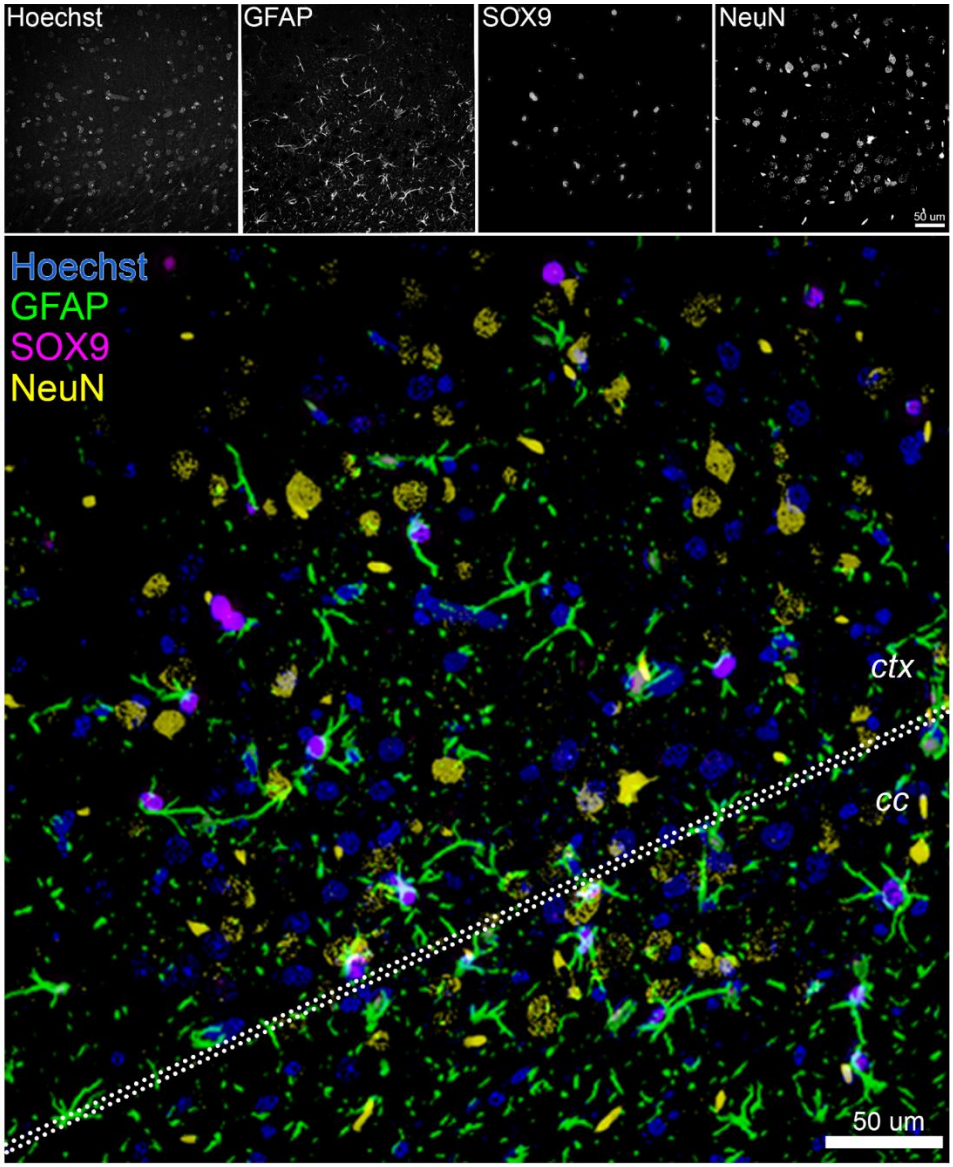

Figure 2. Confocal immunofluorescence labeling of Hoechst, GFAP, SOX9, and NeuN demonstrating the proper distribution profiles.

Representative high magnification confocal micrograph of 5 DPI hamster brain tissue. Individual single channels are shown in greyscale in the upper panels, and the merged image in the bottom panel, with Hoechst in blue, GFAP in green, SOX9 in magenta, and NeuN in yellow. The dotted line denotes the boundary between the cortex (ctx) and corpus callosum (cc).

2.1.3 Confocal microscopy imaging for the pipeline

I conducted imaging using a Leica confocal microscope (Leica TCS SP8) with Leica Application Suite Software version 3.1.3.16308. I employed a tiling method to capture comprehensive images of the entire brain slice from the middle Z plane of the tissue, as shown in Figure 3. This method involved tile scanning to precisely map the outermost points of the slice, ensuring accuracy and minimizing biases. For a detailed protocol on tiling, refer to the link: https://bbic.nsm.uh.edu/protocols/leica-tile-scans-a-brief-overview. I optimized the confocal settings to enhance the signal to noise ratio. The settings I used are in Table 1. Resulting images were processed and analyzed by my newly-developed pipeline, outlined below.

Category	Details
Objective Name	HC PL APO
Magnification	20x Dry
Numerical Aperture	0.7
Immersion Medium	Dry
Resolution	512 x 512 pixels
Zoom	1.0
Frame Average	1
Line Average	1
Frame Accumulation	2
Line Accumulation	4
Pinhole size	1-1.5 AU

Table 1. Confocal microscope settings used in the imaging pipeline

2.1.4 Analysis pipeline

The critical steps in my analysis are consistent across all staining procedures, each associated with specific MATLAB codes available on the lab's GitHub page [https://github.com/SwayneLab/Quantitative-analysis-of-astrocyte-properties-in-a-Syrian-hamster-model-of-COVID-19]. The pipeline steps for GFAP and SOX9 are visualized in Figure 4, and the pipeline steps for Hoechst and NeuN are shown in Figure 5. Note that pixel densities were used for GFAP and Hoechst, and cell densities were used for SOX9 and NeuN.

First, I performed background subtraction using the morphological opening function to enhance the visibility of the SOX9, GFAP, Hoechst and NeuN signals (Benraya and Benblidia 2018; Webb et al. 2019). Next, I applied a Gaussian filter to reduce image noise (Hamad, Muhamad, and Yaba 2015; Webb et al. 2019). I used entropy thresholding for binary conversion to isolate signal-positive cells (Kapur, Sahoo, and Wong 1985; Nie et al. 2017). Thresholding, a fundamental method in image segmentation, was essential for differentiating between objects and backgrounds in my image analysis. This process, also known as binarization, simplifies grayscale images into binary ones by categorizing pixels based on intensity thresholds (Ali et al., 2017). I will provide more details on this method in the next section (Thresholding). In object counting, I excluded objects smaller than 5 pixels (5 μm) for SOX9 and 7 pixels (7 μm) for NeuN, based on manual counts of 100 cells in various regions using Cell Profiler software (1 pixel is equivalent to 1 μm). Finally, I calculated the area of the region of interest (ROI) using MATLAB's "*numel"* function, which counts total elements in an array or matrix. This helped me to determine the total pixel count in images (Webb et al. 2019). In the following section I will discuss the concept of thresholding in detail and provide evidence supporting my choice of specific thresholding method in the development of my image analysis pipeline.

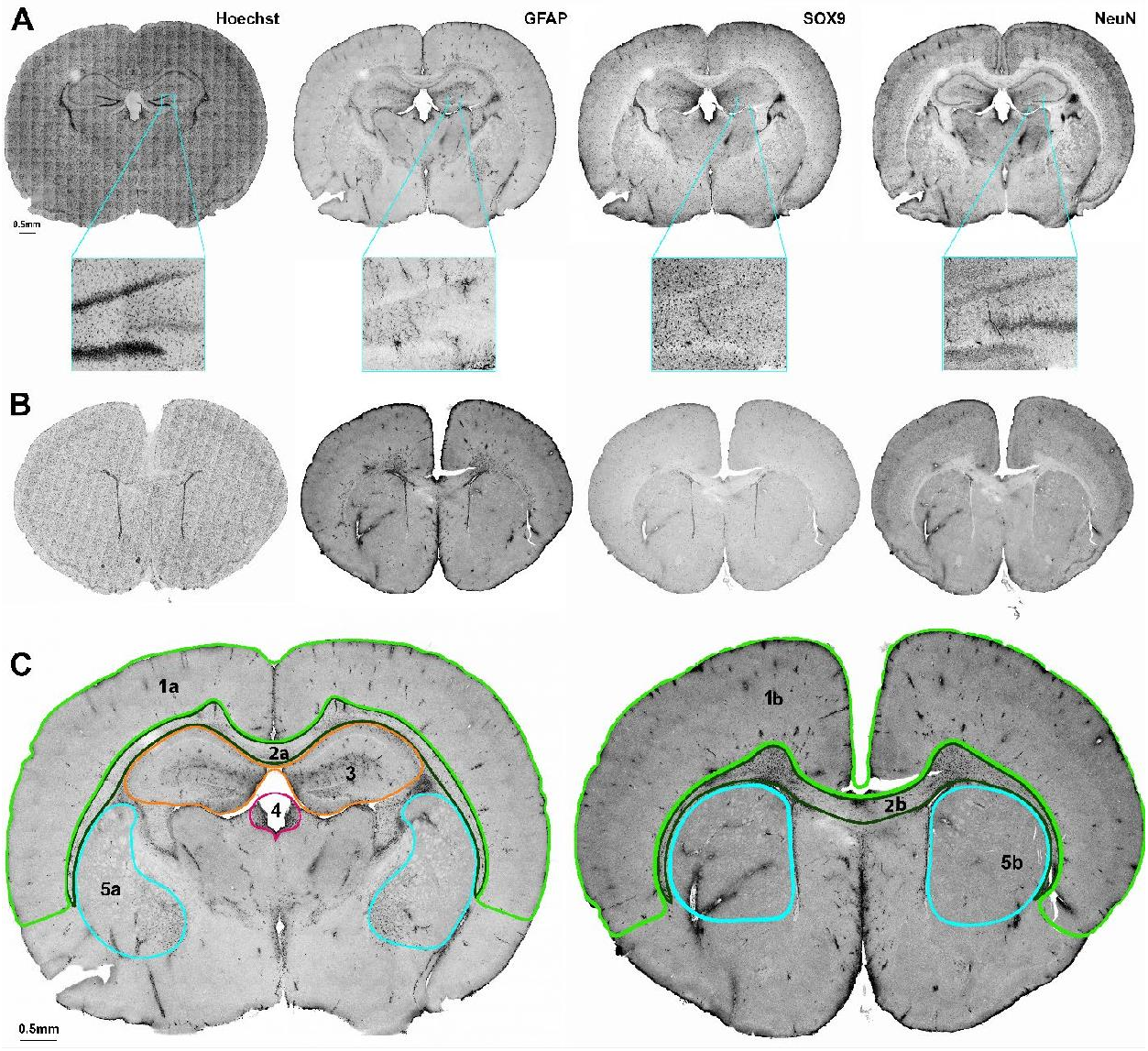

Figure 3. Distribution of SOX9-positive astrocytes, GFAP, and NeuN-positive neurons in full hamster brain sections.

Tiled and stitched confocal immunofluorescence micrographs of coronal Syrian hamster brain sections taken at the level of the dorsal hippocampus (A) and lateral ventricles (B) labeled with Hoechst nuclear dye and SOX9, GFAP, and NeuN antibodies. (C) Representative brain sections immunolabelled for GFAP with my regions of interest outlined and numbered as follows: cortex (1a, 1b), corpus callosum (2a, 2b), hippocampus (3), third ventricle (4), and dorsal striatum (5a, 5b).

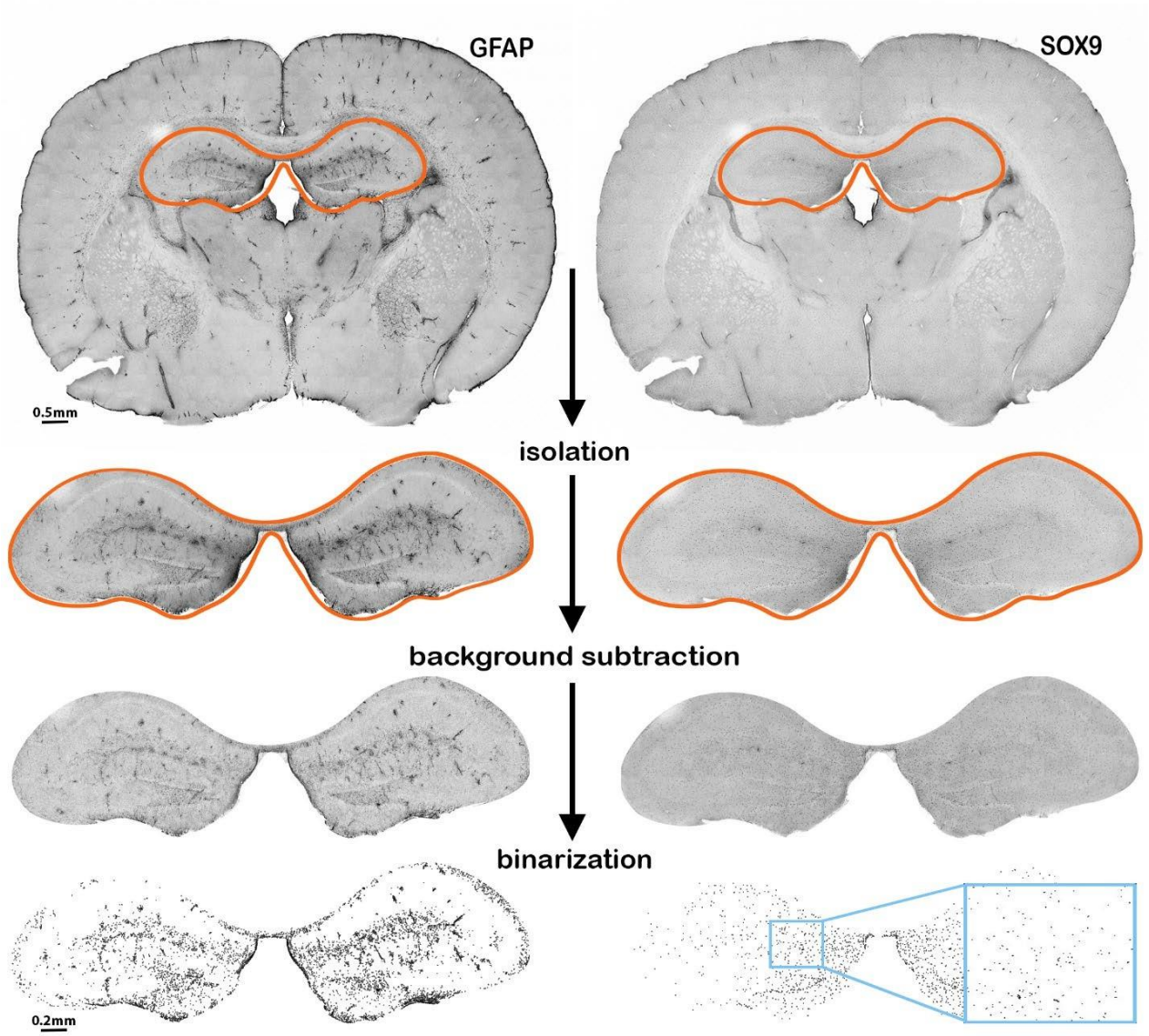

metrics	value
Sum of GFAP positive pixels	1.22e+05
GFAP area (mm^2)	1.22e-01
total area of sample (mm^2)	9.41
percentage GFAP coverage	1.30%

metrics	value
Sox9 positive cells number	3.583e+03
Sox9 area (mm^2)	3.583e-02
total area of sample (mm^2)	9.41
Number of Sox9 positives averaged by area coverage	3.7e-03

Figure 4. Quantitative astrocyte analysis workflow in hamster brain sections: from staining to binarization.

Top row: Example tiled and stitched raw confocal immunofluorescence micrographs of GFAP (left) and SOX9 (right) signals. **Isolation:** This step exclusively selects the precise region of interest for quantitative analysis. **Background Subtraction:** This step reduces noise and improves the visibility of the specific signal for both GFAP and SOX9. **Binarization:** The images are binarized, where the GFAP and SOX9 signals are converted to a binary format—black on white.

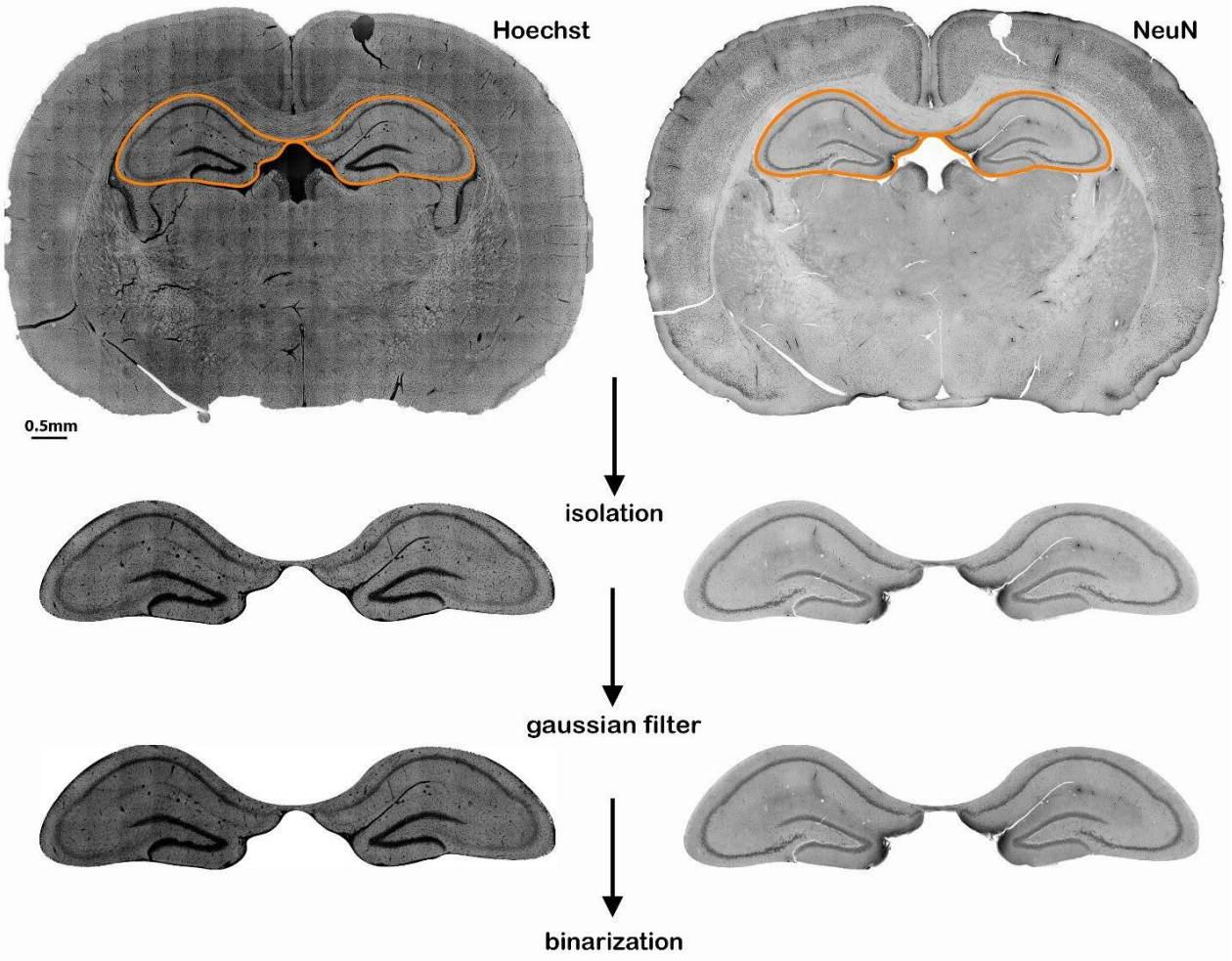

metrics	value
Sum of Hoechst positive pixels	6.53e+05
Hoechst area (mm^2)	6.53e-01
total area of sample (mm^2)	11.12
Percentage of Hoechst coverage	5.86%

metrics	value
Sum of NeuN positive pixels	3.88e+05
NeuN area (mm^2)	0.38
total area of sample (mm^2)	11.12
percentage NeuN coverage	3.49%

Figure 5. Quantitative cellular nuclei analysis workflow in brain sections: Hoechst and NeuN staining to binarization.

Top row: Micrographs of brain sections stained with Hoechst (left) and NeuN (right). **Isolation:** This step involves selective extraction of the highlighted areas from the entire brain section. **Gaussian Filter:** This step enhances the clarity by reducing noise and improving the contrast of the staining. **Binarization:** This step converts the grayscale staining into binary format. Note that pixel densities were used for Hoechst, as we were unable to reliably segment individual Hoechst-positive nuclei in areas of high cell density.

2.1.5. Thresholding

The methodological core of my thesis, thresholding, involves assigning a binary value to each pixel in an image based on a predefined threshold value ţ. This value is determined by whether the pixel's brightness or gray level exceeds ţ (Ali, Siarry, and Pant 2017; Kapur, Sahoo, and Wong 1985; reviewed in Sahoo, Soltani, and Wong 1988). The objective of thresholding in my project was to segment an image to maximize different antibodies' signals to the background or noises.

Thresholding techniques are broadly categorized into two types: global threshold and local threshold. Global thresholding uses a single threshold value for the entire image. The threshold is typically derived from global image properties, such as the overall histogram. The local or adaptive threshold approach assigns a unique threshold value to each pixel based on the local information surrounding that pixel (Baghel 2020; Khurana 2015). This method is more flexible and can adapt to variations in lighting and texture (Khurana 2015). However, since my imaging techniques provide steady light and a clear background, local thresholding was not the best

option for my samples (Khurana 2015). Next, I will provide an overview of each thresholding technique relevant to my analysis, followed by a comparison. This discussion will conclude with a justification of why Kapur's entropy thresholding method was the optimal choice for this project.

2.1.5.1. Otsu Method

Developed by Otsu (reviewed in Bangare et al. 2015), this method minimizes the variance within two classes: those below (objects) and those above the threshold (background). The process involves classifying pixels into two groups: C1 (pixels darker than the threshold ţ) and C2 (pixels lighter than ţ). It seeks to find the threshold ţ that minimizes within-class variance or maximizes between-class variance, effectively enhancing the contrast between objects and background. The optimal threshold ţ is computed by minimizing the function η(t), representing the weighted sum of within-class variances for C1 and C2. Most image-analyzing software has a built-in Otsu thresholding function, so I will not explain its formula and mathematical basis in detail (Khurana 2015; reviewed in Sahoo, Soltani, and Wong 1988; Webb et al. 2019).

2.1.5.2 Minimum Error Thresholding Method

The Minimum Error Threshold method treats the gray-level histogram as an estimation of a probability density function for the image's pixels (Long, Shen, and Chen 2012). This method assumes that the pixels belonging to the object and the background are components of a mixed population, each normally distributed with specific statistical properties (Khurana 2015; reviewed in Sahoo, Soltani, and Wong 1988).

The pixel intensity distribution, P(g), is modeled as a mixture of two normal distributions for the object and the background. Each component, p (g | i), is assumed to be normally distributed with a mean μ_i, standard deviation σ_i, and a prior probability P_i, where i indicates the component (object or background). The formula for the probability density function of each element is expressed as:

$$p(g|i) = \frac{1}{\sigma_i\sqrt{2\pi}} \exp\left(-\frac{(g-\mu_i)^2}{2\sigma_i^2}\right)$$

Traditionally, this process involves setting up a criterion function based on the parameters of the mixed distribution model. The criterion function, J(t), is designed to minimize the sum of the probabilities of misclassifying pixels. It is defined as:

$$J(t) = \sigma_1(t)P_1(t) + \sigma_2(t)P_2(t)$$

Here, σ1(t) and σ2(t) are the standard deviations of the gray levels for each distribution below and above the threshold ţ, respectively. P1(t) and P2(t) are the summed probabilities for each distribution separated by ţ. The optimal threshold, t*, is determined by minimizing J(t), using: $t^* = \arg\min_t J(t)$

This optimization ensures that the threshold maximizes the likelihood of correct classification based on the mixture model, reducing errors due to variance within each class. However, one of the main challenges with this method is estimating the parameters μ_i , σ_i, and P_i of the distribution, as they are not usually known in advance. Estimation techniques or additional assumptions might be necessary to approximate these values before applying the thresholding method (Khurana 2015; reviewed in Sahoo, Soltani, and Wong 1988).

2.1.5.2. Moment-Preserving Thresholding Method

The Moment-Preserving Threshold method calculates threshold values so that the statistical moments of the original image's gray-level distribution are preserved in the resultant binary image (Khurana 2015; reviewed in Sahoo, Soltani, and Wong 1988). The calculation of the moment m_i is based on the pixel intensities and their frequencies across the image:

$$m_i = \sum_{g=0}^{L-1} g^i \cdot h(g)$$

where g represents the gray level, h(g) is the histogram count for gray level g, and L is the total number of distinct gray levels in the image. The threshold ţ is derived from the image histogram, guided by a specific measure referred to as the PO-tile. The PO-tile is determined through the following formula that incorporates the calculated moments:

$$p_0 = \frac{c_1 - \sqrt{c_1^2 - 4 \cdot c_0 \cdot c_2}}{2 \cdot c_0}$$

in which, c_0, c_1, and c_2 are coefficients derived from the moments of the gray level distribution, such that:

$$c_0 = m_2^2 - m_1^2, \quad c_1 = m_1 \cdot m_3 - m_2^2, \quad c_2 = m_0 \cdot m_3 - m_2^2$$

and these coefficients relate to the central moments of the distribution, providing a statistical basis for selecting the threshold that maintains the moment properties in the thresholded image. Coefficients preserve the underlying statistical properties of the image and improves reproducibility in analysis workflows. However, achieving coefficients requires accurate calculation of image moments, which can be sensitive to noise and outliers in the image data. Moreover, this method assumes that the moments can adequately represent the essential

characteristics of the image, which might not hold for all types of images, particularly those with complex or multimodal distributions.

2.1.5.3. Kapur's entropy thresholding

In this method, the entropy of the histogram is used to maximize the information content between segmented parts of an image. This method is grounded in information theory, which considers entropy as a measure of uncertainty or randomness (Kapur, Sahoo, and Wong 1985; Nie et al. 2017). By maximizing entropy, the algorithm aims to find a threshold that divides the image into parts (foreground and background) with the highest degree of randomness or unpredictability, thereby ensuring that the division contains the most distinctive features of the image (Kapur, Sahoo, and Wong 1985; reviewed in Sahoo, Soltani, and Wong 1988).

The detailed step-by-step description involves initially defining the probability distributions for image thresholding. For each potential threshold, the histogram is divided into two segments: Segment A, covering gray levels from 1 to s, and Segment B, extending from s+1 to the maximum gray level, n. I recalculated the probabilities for each gray level relative to the segment size within these segments. Following this, I calculated the entropy for each segment to measure the randomness or unpredictability within that segment. This calculation helps quantify how effectively the threshold separates the histogram into meaningful groups.

The entropy for each segment is calculated using the formula:

$$H = -\sum_{i=\text{start}}^{\text{end}} p_i \log(p_i)$$

where p_i is the probability of gray level i occurring within the segment, the sum is over all gray

levels.

I computed the combined entropy for each threshold, representing the total entropy when the image was divided at gray level s. My goal was to maximize q(s), theoretically, the threshold where the sum of the entropies of the two segments was greatest. During the maximization process, I iterated through all possible values of s from 1 to n-1 (since s=n would not split the histogram) and calculated q(s) for each value. I chose the s value that yielded the maximum q(s) as the optimal threshold. This method's reliance on the histogram's global properties makes it robust against local variations in pixel intensity, which can often lead to errors in local and other global thresholding methods. Table 2 summarizes all thresholding methods discussed in this chapter.

Thresholding Technique	Key Characteristics	Main Approach
Otsu Method	Minimizes within-class variance or maximizes between-class variance to enhance contrast between objects and background.	Classifies pixels into two groups (darker or lighter than threshold) and finds the threshold that minimizes the sum of the within-class variances for these groups. It computes the optimal threshold by minimizing the function representing the weighted sum of variances.
Minimum Error Thresholding	Treats the gray-level histogram as a probability density function assuming two normally distributed mixed populations.	Sets a criterion function based on parameters of the mixed distribution model to minimize the probability of misclassification of pixels. The optimal threshold maximizes the likelihood of correct classification by minimizing the criterion function involving the standard deviations and probabilities of the distributions separated by the threshold.
Moment-Preserving Thresholding	Calculates threshold values to preserve the statistical moments of the original image's gray-level distribution in the resultant binary image.	Threshold values are derived from the image histogram using coefficients related to the moments of the gray level distribution. The process involves calculating moments from pixel intensities and frequencies, and the threshold is determined using a formula that incorporates these moments to maintain the underlying statistical properties of the image.
Kapur's Entropy Thresholding	Uses entropy of the histogram to maximize the information content between segmented parts of an image, based on information theory principles.	Initially defines the probability distributions for image thresholding at each potential threshold, splitting the histogram into two segments. The entropy for each segment is calculated to measure the randomness or unpredictability within those segments. The combined entropy for each threshold is computed, and the optimal threshold is the one that maximizes the sum of the entropies of the two segments, reflecting maximum information separation.

Table 2. Summary of the key characteristics and main approaches of the discussed thresholding techniques

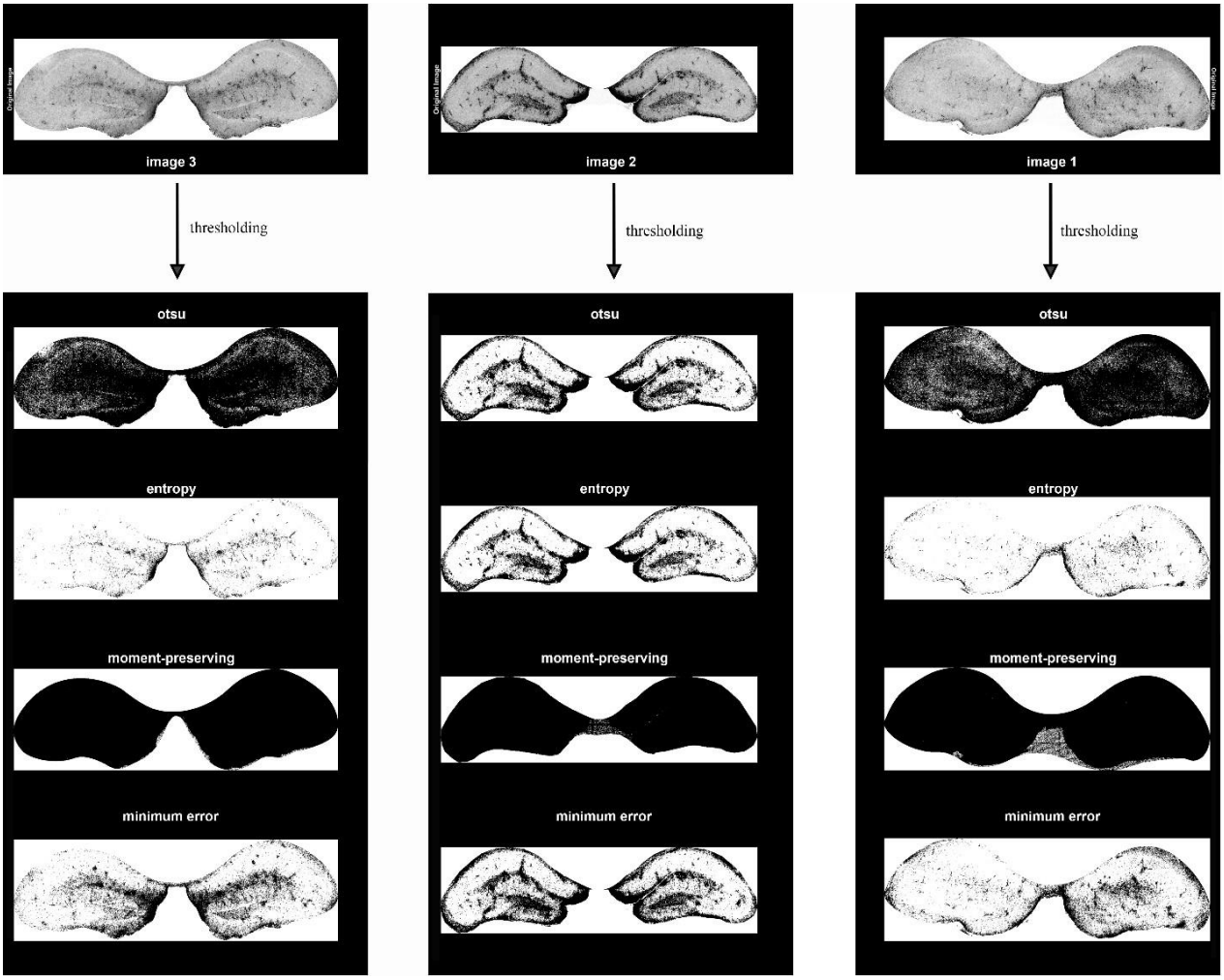

Figure 6. Multiple dorsal hippocampus visualizations with different thresholding methods using MATLAB

This figure shows the application of different thresholding methods to three hippocampus images. Each column corresponds to a separate image (Image 3, Image 2, Image 1, from left to right). The process involves four thresholding methods applied sequentially. The rows represent, from top to bottom: the original grayscale images, binary images after Otsu's, Kapur's entropy,

moment preserving and minimum error thresholding methods. As this figure shows, the entropy method is more effective in keeping the most signal compared to the noise in GFAP staining.

To demonstrate that entropy-based thresholding surpasses other methods visually and mathematically, I used the PSNR (Peak Signal-to-Noise Ratio) metric. PSNR provides a quantitative measure by comparing the quality of thresholded images against a predefined ground truth.

$$\mathrm{PSNR} = 20 \cdot \log_{10}\left(\frac{\mathrm{MAX}_I}{\sqrt{\mathrm{MSE}}}\right)$$

Ground truth represents the ideal outcome of the thresholding process. I began by establishing a "ground truth" image for each of the three cases where I provided figures, manually adjusting the threshold levels until my team and I agreed on the optimal representation. The next step involved calculating the Mean Squared Error (MSE) between the ground truth image and the image produced by each thresholding method, forming the basis for PSNR calculation.

$$\mathrm{MSE} = \frac{1}{MN}\sum_{i=1}^{M}\sum_{j=1}^{N}\big(I(i,j) - K(i,j)\big)^2$$

In my analysis, where I(i,j) represents the pixel value in the ground truth image and K(i,j) the pixel value in the thresholded image, with M and N being the dimensions of the images, I calculated the Mean Squared Error (MSE). I first identified the maximum possible pixel value in the image, denoted as $\mathrm{MAX_I}$ (for instance, 255 for an 8-bit image). Using the MSE and this peak signal value, I then calculated the PSNR to quantitatively assess the efficiency of the thresholding method compared to the established ground truth. This approach allowed me to measure the performance of entropy-based thresholding mathematically. This formula gives the PSNR in decibels (dB) (Khurana 2015; N and S 2016).

We can examine comparative graphs displaying each technique's performance metrics to determine which thresholding method performs best. In these graphs, each method is represented by a bar, with the height of the bar indicating the method's performance level. A higher bar signifies better performance, indicating that the method's results are closer to the established ground truth as shown in Figure 7. Table 3 shows a Comparison of different thresholding method values and their associated PSNRs.

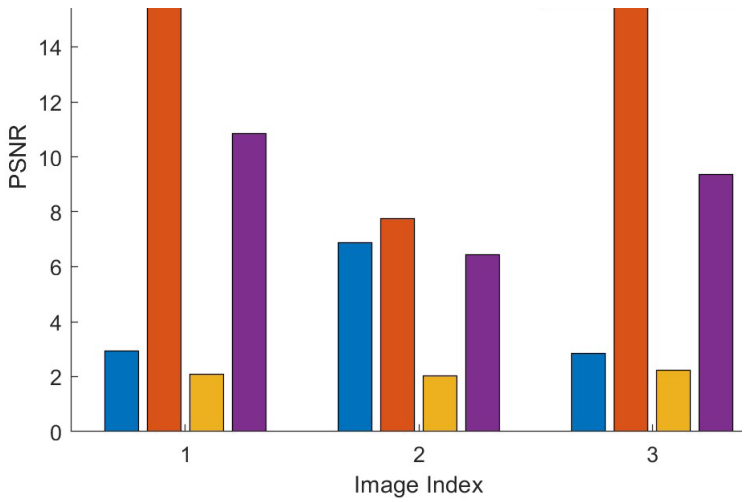

Figure 7. PSNR comparison of each thresholding method

As shown here, Kapur's entropy thresholding outperforms other methods. Blue is Otsu, red is Kapur, yellow is Moment and purple is Minimum Error thresholding. Image index refers to the image numbers mentioned in the figure 6.

	Otsu	*Kapur*	*Moment*	*Minimum Error*	*Otsu_PSNR*	*Kapur_PSNR*	*Moment_PSNR*	*Minimum Error_PSNR*
Image1	0.17	0.54	0.0007263	0.39	2.93	19.82	2.10	10.86
Image2	0.41	0.47	0.0010056	0.39	6.86	7.73	2.04	6.44
Image3	0.18	0.58	0.0007899	0.39	2.85	19.59	2.22	9.35

Table 3. Comparison of different thresholding method values and their associated PSNRs

2.1.6 Statistical analysis rationale

I analyzed data from multiple time points post-infection: 1-, 3-, 5-, 7-, and 31-DPI. Given that I had more than two groups to compare, one-way ANOVA was used as the statistical test of choice. One-way ANOVA is effective for determining if there are statistically significant differences between the means of three or more independent groups, which is particularly useful for my setup involving several time points. The rationale behind using one-way ANOVA, rather than multiple t-tests, is to avoid an increase in Type I error (the probability of incorrectly rejecting a true null hypothesis) that comes with multiple comparisons. One-way ANOVA provides a comprehensive view by assessing the overall effect of time post-infection on the measured variables across all groups simultaneously.

Following the one-way ANOVA, I used Dunnett's post hoc test. This choice is optimal for experiments like mine, where comparisons are primarily made between each experimental group and a common control. Moreover, Dunnett's test is specifically designed to compare multiple treatment groups against a single control group without the increased risk of Type I errors associated with multiple comparisons (Greenwood, M. C. 2021).

2.1.7 Data management plan

As for the data management plan, I ensured comprehensive documentation of experiment details, data collection methods, and analysis techniques to facilitate future interpretation and replication. I organized data using specific naming conventions and version control, supported by README files and adherence to the DataCite metadata standard. I stored all relevant scripts and codes on GitHub for source code management, enabling version tracking. My storage strategy included local and cloud-based solutions, such as UVic Microsoft 365 OneDrive and the Federated Research Data Repository, to secure data backup and accessibility. For long-term preservation, I used open-standard file formats and maintained detailed documentation to enable straightforward access and reuse of the data.

2.2 Pipeline outcomes

2.2.1. Early transient increase in GFAP distribution in the cortex of female hamsters following peripheral SARS-CoV-2 infection

To probe the astrocytic response to peripheral SARS-CoV-2 infection, I performed

immunolabelling for astrocyte markers, on all experimental groups, including control uninfected (CTL), as well as 1-, 3-, 5-, 7-, and 31-days post-infection and employed the analysis pipeline described above. As explained earlier, I immunostained for GFAP to quantify GFAP distribution, which is normally restricted, but can increase in the context of neuroinflammation (reviewed in Nourbakhsh et al. 2021). Additionally, I immunostained for SOX9, a nuclear-localized transcription factor expressed by astrocytes in the adult brain (Sun et al. 2017), to assay for astrocyte proliferation. I also used NeuN, a marker for neurons (Wolf et al. 1996), . I analyzed the outcomes with the imaging pipeline I developed in the previous section. The data for GFAP are shown in Figure 8, and the statistical analyses are reported in Table 4. My analysis revealed a significant increase in GFAP expression in the female cortex at 3 DPI relative to uninfected controls (Figure 8). A similar, non-significant increase at 3 DPI was observed in the hippocampus of female animals. These changes were not observed in males. Important, I observed no baseline differences in raw GFAP distribution between males and females. Notably, a two-way ANOVA exploring for effects of DPI and sex, revealed no significant main effect of DPI ($F(5,26)=0.814$, $p=0.551$) or Sex ($F(1,26)=3.565$, $p=0.070$), but there was a significant interaction between DPI and Sex ($F(5,26)=3.350$, $p=0.018$). post hoc Dunnett's test revealed significant differences in females between DPI 3 and DPI 5 ($p = 0.0297$) and between DPI 3 and DPI 7 ($p=0.0155$). No significant differences were found between DPI levels in males by two way ANOVA. Additionally, there were no statistically significant changes in SOX9-positive cell density, as shown in Figure 9, and Table 5. No changes were observed in overall cell density, quantified by Hoechst pixel density, as shown in Figure 10, and summarized in Table 6 (note that pixel density was used for Hoechst as we were unable to segment it in some brain areas of high cell density). Similarly, no significant changes were observed in NeuN, as shown in Figure 11, and summarized in Table 7, suggesting there were no changes in neuron viability. In summary, our

findings suggest there is an early, partial astrogliosis in female animals consisting of a transient increase in GFAP at 3 DPI, in the context of the Syrian hamster model of mild peripheral COVID-19.

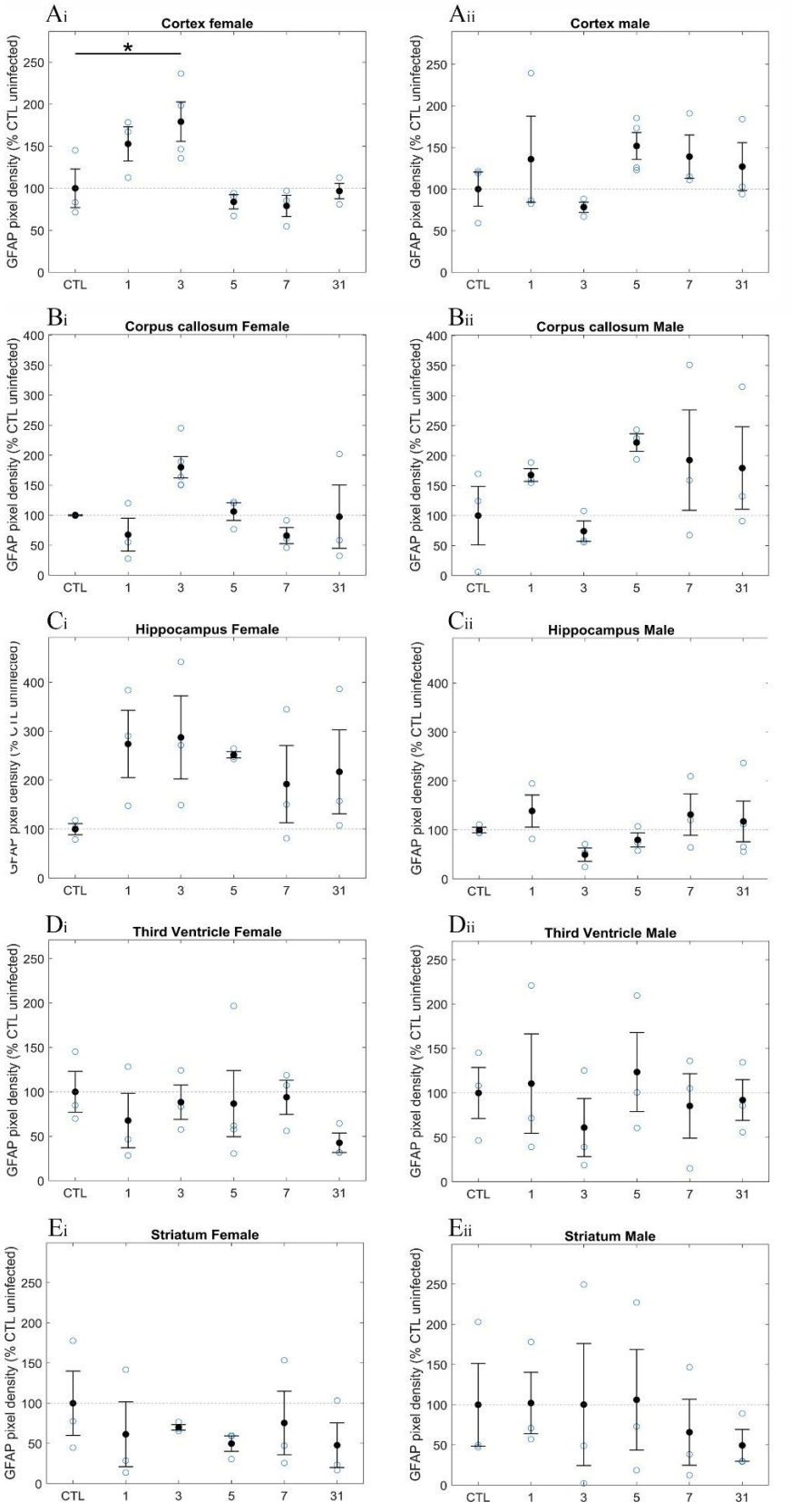
Ai
Cortex female
*
Aii
Cortex male
Bi
Corpus callosum Female
Bii
Corpus callosum Male
Ci
Hippocampus Female
Cii
Hippocampus Male
Di
Third Ventricle Female
Dii
Third Ventricle Male
Ei
Striatum Female
Eii
Striatum Male
GFAP pixel density (% CTL uninfected)
CTL
1
3
5
7
31

Figure 8. Transient early increase in GFAP in female animals in the context of mild peripheral COVID-19

Scatter plots displaying the relative pixel density of Glial Fibrillary Acidic Protein (GFAP) in male and female Syrian hamsters over several days post-inoculation (CTL, 1 DPI, 3 DPI, 5 DPI, 7 DPI, 31 DPI) in (A) the cortex of (i) females, and (ii) males, (B) the corpus callosum of (i) females, and (ii) males, (C) the hippocampus of (i) females, and (ii) males, (D) the third ventricle of (i) females and (ii) males and (E) the striatum of (i) females and (ii) males expressed as percent control based on CTL values . Each blue point represents one biological replicate, with sample sizes (N) varying from 3 to 5. Black points represent the average values, with horizontal lines indicating the standard error of the mean (SEM). A significant increase in GFAP expression was observed in the cortex of female animals at 3 DPI ($p = 0.00694$ by one-way ANOVA, (**)$p = 0.029708$ by post-hoc Dunnet's test; N = 3-4).

Fig. Name	Comparison	Lowerdiff	ESTdiff	Upperdiff	pValue
A_i	1 vs. CTL	-24.2033	52.80717	129.8176	0.232258
	3 vs. CTL	7.179696	79.2164	151.2531	0.029708
	5 vs. CTL	-93.1272	-16.1167	60.89376	0.958148
	7 vs. CTL	-97.9645	-20.9541	56.05642	0.891997
	31 vs. CTL	-80.2764	-3.26594	73.74453	0.999974
	ANOVA (Overall)	NaN	NaN	NaN	0.00694
A_{ii}	1 vs. CTL	-77.8539	35.96827	149.7905	0.827138
	3 vs. CTL	-135.603	-21.7811	92.04107	0.970617
	5 vs. CTL	-54.653	51.81791	158.2888	0.516241
	7 vs. CTL	-74.7606	39.06162	152.8838	0.781183
	31 vs. CTL	-86.8006	27.02156	140.8438	0.932858
	ANOVA (Overall)	NaN	NaN	NaN	0.439092
B_i	1 vs. CTL	-139.194	-32.4706	74.25315	0.84853
	3 vs. CTL	-15.4898	79.96686	175.4235	0.114704
	5 vs. CTL	-100.507	6.216468	112.9403	0.99988
	7 vs. CTL	-140.668	-33.9442	72.77955	0.826834
	31 vs. CTL	-109.136	-2.4126	104.3112	0.999999
	ANOVA (Overall)	NaN	NaN	NaN	0.031609
B_{ii}	1 vs. CTL	-135.392	67.70174	270.7959	0.794499
	3 vs. CTL	-229.018	-25.9242	177.1699	0.994655
	5 vs. CTL	-81.34	121.7541	324.8482	0.332303
	7 vs. CTL	-110.607	92.4868	295.5809	0.56805
	31 vs. CTL	-123.844	79.24966	282.3438	0.690884
	ANOVA (Overall)	NaN	NaN	NaN	0.319427
C_i	1 vs. CTL	-94.2007	174.044	442.2887	0.269693
	3 vs. CTL	-80.8504	187.3943	455.639	0.21641
	5 vs. CTL	-116.252	151.9929	420.2375	0.37937
	7 vs. CTL	-176.112	92.13245	360.3771	0.776739
	31 vs. CTL	-151.13	117.1152	385.3598	0.603123
	ANOVA (Overall)	NaN	NaN	NaN	0.406092
C_{ii}	1 vs. CTL	-91.8552	38.57245	169.0001	0.858792
	3 vs. CTL	-180.968	-50.5401	79.88762	0.700545
	5 vs. CTL	-150.804	-20.3768	110.0509	0.987422
	7 vs. CTL	-99.0206	31.40713	161.8348	0.92932
	31 vs. CTL	-104.577	17.42644	139.4304	0.991481
	ANOVA (Overall)	NaN	NaN	NaN	0.401102
D_i	1 vs. CTL	-145.896	-32.2874	81.32078	0.875397
	3 vs. CTL	-125.217	-11.6093	101.9989	0.998145
	5 vs. CTL	-119.553	-13.282	92.98869	0.9953
	7 vs. CTL	-119.623	-6.01486	107.5933	0.999922
	31 vs. CTL	-170.939	-57.3306	56.27763	0.484439
	ANOVA (Overall)	NaN	NaN	NaN	0.717452
D_{ii}	1 vs. CTL	-146.98	10.59432	168.1682	0.99974
	3 vs. CTL	-196.513	-38.9395	118.6345	0.920619
	5 vs. CTL	-133.996	23.57785	181.1518	0.989187
	7 vs. CTL	-172.144	-14.5697	143.0042	0.998801
	31 vs. CTL	-165.543	-7.96947	149.6044	0.999936
	ANOVA (Overall)	NaN	NaN	NaN	0.893451
E_i	1 vs. CTL	-164.773	-38.6221	87.52885	0.839693
	3 vs. CTL	-156.101	-29.9503	96.20067	0.93114
	5 vs. CTL	-176.368	-50.2166	75.93438	0.676119
	7 vs. CTL	-150.676	-24.5254	101.6256	0.967845
	31 vs. CTL	-178.399	-52.2484	73.90257	0.645692
	ANOVA (Overall)	NaN	NaN	NaN	0.842983
E_{ii}	1 vs. CTL	-146.965	10.59432	168.154	0.999741
	3 vs. CTL	-196.499	-38.9395	118.6202	0.920588
	5 vs. CTL	-133.982	23.57785	181.1375	0.989219
	7 vs. CTL	-172.129	-14.5697	142.99	0.998798
	31 vs. CTL	-165.529	-7.96947	149.5902	0.999935
	ANOVA (Overall)	NaN	NaN	NaN	0.893451

Table 4. Statistical analyses for GFAP distribution

This table provides the outcomes of statistical tests comparing each DPI against the control (CTL) for each brain region using ANOVA and the post hoc Dunnett's test. It is organized according to figure labels from Ai to Eii. Each row, except those labeled "ANOVA (Overall)", corresponds to a Dunnett's post hoc test, comparing specific conditions labeled as "1 vs. CTL" and so on, against the control group. The columns in the table are defined as follows:

Figure Name: Identifier for the specific graph in Figure 8

Comparison: Specifies the experimental condition compared against the control.

Lowerdiff: The lower bound of the 95% confidence interval for the estimated difference between the experimental condition and the control.

ESTdiff: The point estimate of the difference between the experimental condition and the control.

Upperdiff: The upper bound of the 95% confidence interval for the estimated difference.

pValue: The p-value from Dunnett's test, indicating the probability that any observed difference is due to chance, with a lower value suggesting more significant differences.

The rows labeled "ANOVA (Overall)" present the results of an ANOVA test assessing overall differences among all conditions and the control.

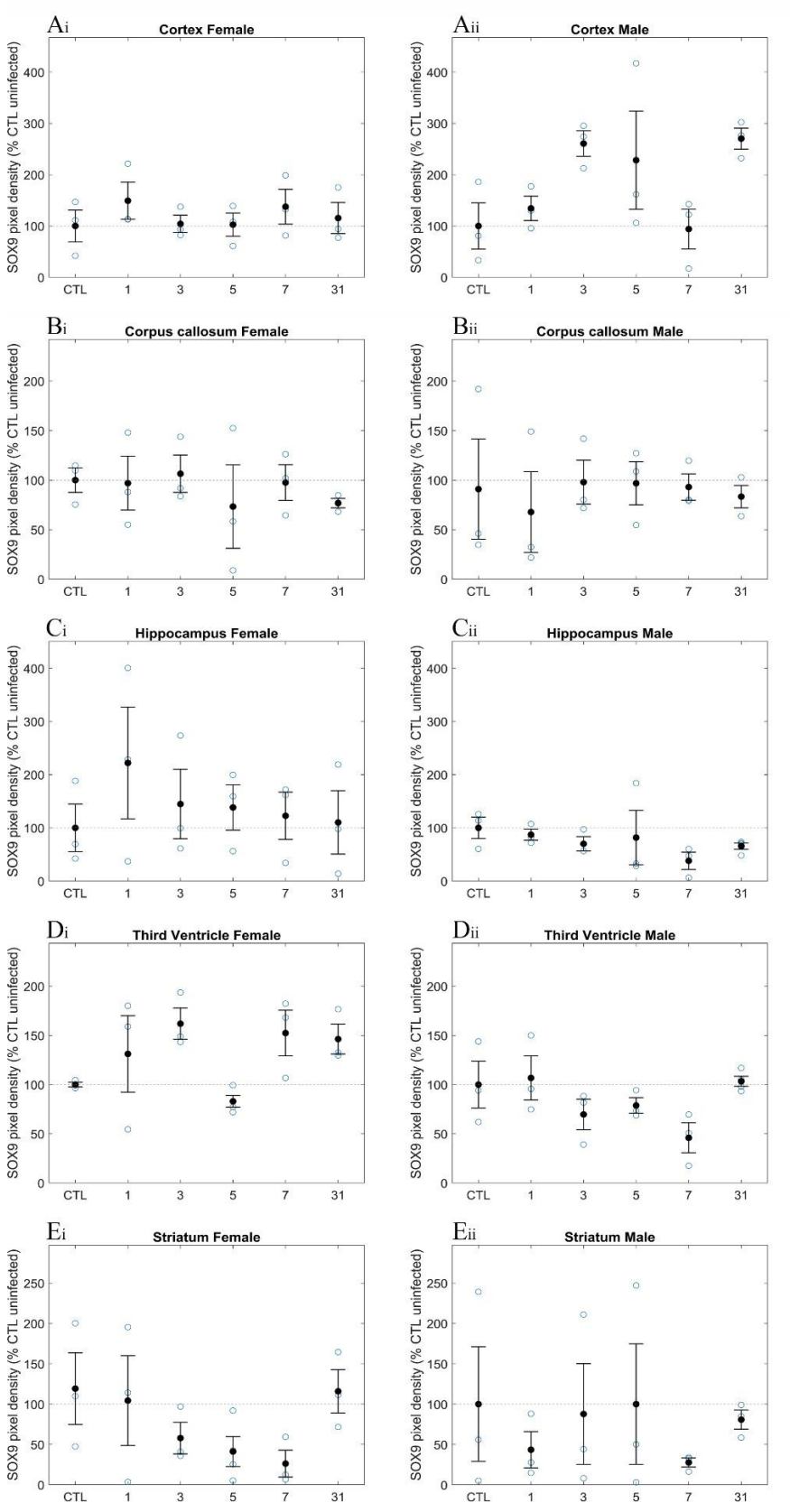
Ai
Cortex Female
Aii
Cortex Male
Bi
Corpus callosum Female
Bii
Corpus callosum Male
Ci
Hippocampus Female
Cii
Hippocampus Male
Di
Third Ventricle Female
Dii
Third Ventricle Male
Ei
Striatum Female
Eii
Striatum Male
SOX9 pixel density (% CTL uninfected)
CTL
1
3
5
7
31

Figure 9. No changes in SOX9-positive cell density in the context of mild peripheral COVID-19

Scatter plots displaying the relative pixel density of SOX9 in male and female Syrian hamsters over several days post-inoculation (CTL, 1 DPI, 3 DPI, 5 DPI, 7 DPI, 31 DPI) in (A) the cortex of (i) females, and (ii) males, (B) the corpus callosum of (i) females, and (ii) males, (C) the hippocampus of (i) females, and (ii) males, (D) the third ventricle of (i) females and (ii) males and (E) the striatum of (i) females and (ii) males expressed as percent control based on CTL values . Each blue point represents one biological replicate, with sample sizes (N) varying from 3 to 5. Black points represent the average values, with horizontal lines indicating the standard error of the mean (SEM). The data indicate no significant changes in SOX9 staining (analyzed by one-way ANOVA).

Fig. name	Comparison	Lowerdiff	ESTdiff	Upperdiff	pValue
	1 vs. CTL	-70.5913	49.25124	169.0937	0.651765
	3 vs. CTL	-115.603	4.239926	124.0824	0.999989
	5 vs. CTL	-117.257	2.585935	122.4284	0.999999
	7 vs. CTL	-82.2135	37.62897	157.4715	0.827129
	31 vs. CTL	-104.373	15.46998	135.3125	0.994361
A_i	ANOVA (Overall)	NaN	NaN	NaN	0.773145
	1 vs. CTL	-166.239	34.32842	234.8954	0.980903
	3 vs. CTL	-39.9175	160.6495	361.2164	0.134388
	5 vs. CTL	-72.3487	128.2183	328.7852	0.281117
	7 vs. CTL	-206.537	-5.97004	194.5969	0.999995
	31 vs. CTL	-30.2235	170.3435	370.9104	0.106353
A_{ii}	ANOVA (Overall)	NaN	NaN	NaN	0.070154
	1 vs. CTL	-100.273	-3.03035	94.21241	0.999994
	3 vs. CTL	-90.7761	6.466652	103.7094	0.999753
	5 vs. CTL	-123.958	-26.715	70.52778	0.886081
	7 vs. CTL	-99.6706	-2.42787	94.81489	0.999998
	31 vs. CTL	-120.47	-23.2271	74.01562	0.929672
B_i	ANOVA (Overall)	NaN	NaN	NaN	0.888742
	1 vs. CTL	-147.27	-23.1509	100.9681	0.972784
	3 vs. CTL	-117.111	7.00838	131.1274	0.999889
	5 vs. CTL	-118.179	5.940183	130.0592	0.999951
	7 vs. CTL	-122.035	2.084162	126.2032	1
	31 vs. CTL	-131.701	-7.58248	116.5365	0.999837
B_{ii}	ANOVA (Overall)	NaN	NaN	NaN	0.979416
	1 vs. CTL	-140.899	121.9894	384.8779	0.552176
	3 vs. CTL	-218.167	44.72163	307.6101	0.981332
	5 vs. CTL	-224.541	38.34775	301.2362	0.990346
	7 vs. CTL	-240.251	22.63714	285.5256	0.999146
	31 vs. CTL	-252.662	10.22692	273.1154	0.999982
C_i	ANOVA (Overall)	NaN	NaN	NaN	0.795472
	1 vs. CTL	-108.686	-12.771	83.14356	0.993774
	3 vs. CTL	-125.886	-29.9712	65.94339	0.832768
	5 vs. CTL	-114.224	-18.3091	77.60548	0.970865
	7 vs. CTL	-157.856	-61.9412	33.97338	0.27683
	31 vs. CTL	-124.134	-34.4139	55.30599	0.707794
C_{ii}	ANOVA (Overall)	NaN	NaN	NaN	0.55528
	1 vs. CTL	-49.8653	31.18495	112.2352	0.705524
	3 vs. CTL	-19.1345	61.91574	142.966	0.162127
	5 vs. CTL	-92.8662	-17.0507	58.76486	0.944977
	7 vs. CTL	-28.6687	52.3815	133.4317	0.276231
	31 vs. CTL	-34.7688	46.28138	127.3316	0.377202
D_i	ANOVA (Overall)	NaN	NaN	NaN	0.063968
	1 vs. CTL	-57.7902	6.768602	71.32739	0.997914
	3 vs. CTL	-94.8943	-30.3356	34.22322	0.546388
	5 vs. CTL	-85.7777	-21.2189	43.33984	0.806057
	7 vs. CTL	-118.694	-54.1353	10.42347	0.113174
	31 vs. CTL	-57.0638	3.325399	63.71461	0.999906
D_{ii}	ANOVA (Overall)	NaN	NaN	NaN	0.102804
	1 vs. CTL	-148.975	-14.8159	119.3437	0.99734
	3 vs. CTL	-195.489	-61.329	72.83055	0.569701
	5 vs. CTL	-203.498	-78.003	47.49171	0.306894
	7 vs. CTL	-227.161	-93.0019	41.15767	0.224641
	31 vs. CTL	-137.486	-3.32636	130.8332	0.999998
E_i	ANOVA (Overall)	NaN	NaN	NaN	0.233497
	1 vs. CTL	-57.7841	6.768602	71.32132	0.997914
	3 vs. CTL	-94.8883	-30.3356	34.21715	0.546387
	5 vs. CTL	-85.7717	-21.2189	43.33377	0.806133
	7 vs. CTL	-118.688	-54.1353	10.4174	0.113126
	31 vs. CTL	-57.0581	3.325399	63.70893	0.999905
E_{ii}	ANOVA (Overall)	NaN	NaN	NaN	0.102804

Table 5. Statistical analyses for SOX9 distribution

This table provides the outcomes of statistical tests comparing each DPI against the control (CTL) for each brain region using ANOVA and the post hoc Dunnett's test. It is organized according to figure labels from Ai to Eii. Each row, except those labeled "ANOVA (Overall)", corresponds to a Dunnett's post hoc test, comparing specific conditions labeled as "1 vs. CTL" and so on, against the control group. The columns in the table are defined as follows:

Figure Name: Identifier for the specific graph in Figure 9.

Comparison: Specifies the experimental condition compared against the control.

Lowerdiff: The lower 95% confidence interval bound for the estimated difference between the experimental condition and the control.

ESTdiff: The point estimate of the difference between the experimental condition and the control.

Upperdiff: The upper bound of the 95% confidence interval for the estimated difference.

pValue: The p-value from Dunnett's test indicates the probability that any observed difference is due to chance, with a lower value suggesting more significant differences.

The rows labeled "ANOVA (Overall)" present the results of an ANOVA test assessing overall differences among all conditions and the control.

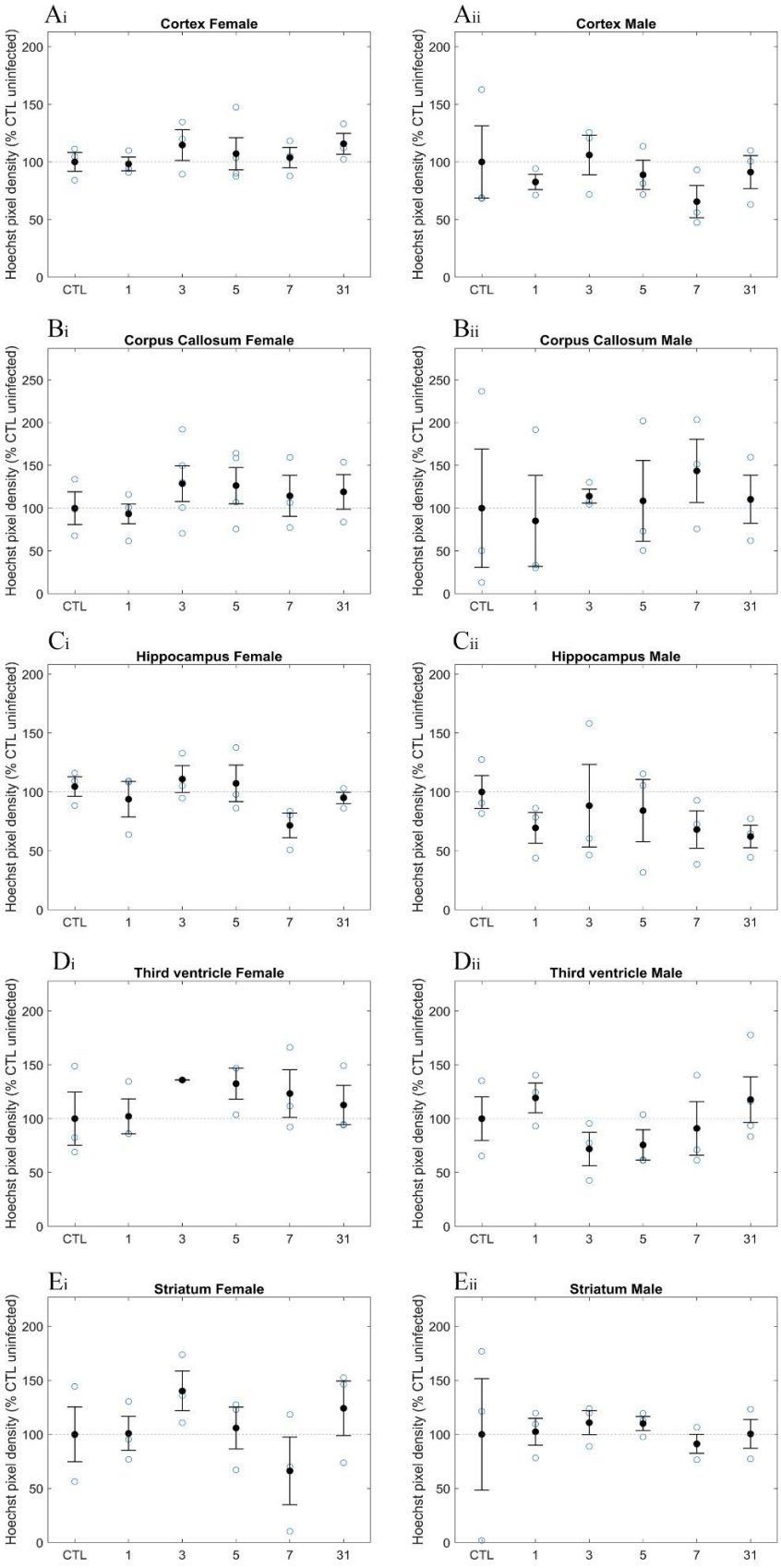
Ai
Cortex Female
Aii
Cortex Male
Bi
Corpus Callosum Female
Bii
Corpus Callosum Male
Ci
Hippocampus Female
Cii
Hippocampus Male
Di
Third ventricle Female
Dii
Third ventricle Male
Ei
Striatum Female
Eii
Striatum Male
Hoechst pixel density (% CTL uninfected)
CTL
1
3
5
7
31

Figure 10. No changes in Hoechst-positive cell density in the context of mild peripheral COVID-19

Scatter plots displaying the relative pixel density of Hoechst in male and female Syrian hamsters over several days post-inoculation (CTL, 1 DPI, 3 DPI, 5 DPI, 7 DPI, 31 DPI) in (A) the cortex of (i) females, and (ii) males, (B) the corpus callosum of (i) females, and (ii) males, (C) the hippocampus of (i) females, and (ii) males, (D) the third ventricle of (i) females and (ii) males and (E) the striatum of (i) females and (ii) males expressed as percent control based on CTL values. Each blue point represents one biological replicate, with sample sizes (N) varying from 3 to 5. Black points represent the average values, with horizontal lines indicating the standard error of the mean (SEM). The data indicate no significant changes in Hoechst staining (analyzed by one-way ANOVA).

Fig. name	Comparison	Lowerdiff	ESTdiff	Upperdiff	pValue
A_i	1 vs. CTL	-47.3539	-1.74022	43.87342	0.999985
	3 vs. CTL	-30.9495	14.66411	60.27776	0.818227
	5 vs. CTL	-35.5731	7.094524	49.76218	0.983578
	7 vs. CTL	-41.8972	3.716449	49.33009	0.999368
	31 vs. CTL	-29.8607	15.75293	61.36657	0.777386
	ANOVA (Overall)	NaN	NaN	NaN	0.822598
A_{ii}	1 vs. CTL	-90.1911	-17.4247	55.34166	0.928934
	3 vs. CTL	-66.7887	5.977622	78.74399	0.999315
	5 vs. CTL	-83.9781	-11.2117	61.55462	0.98772
	7 vs. CTL	-107.228	-34.4616	38.30475	0.53456
	31 vs. CTL	-81.5946	-8.82829	63.93808	0.995765
	ANOVA (Overall)	NaN	NaN	NaN	0.674199
B_i	1 vs. CTL	-88.3789	-6.72971	74.91953	0.999364
	3 vs. CTL	-49.3931	28.67846	106.7501	0.74437
	5 vs. CTL	-55.2574	26.39187	108.0411	0.820439
	7 vs. CTL	-72.9156	14.37109	101.6578	0.984919
	31 vs. CTL	-68.3105	18.97616	106.2629	0.95344
	ANOVA (Overall)	NaN	NaN	NaN	0.738395
B_{ii}	1 vs. CTL	-199.088	-14.9074	169.2733	0.999364
	3 vs. CTL	-170.083	14.09756	198.2783	0.999513
	5 vs. CTL	-175.701	8.479449	192.6602	0.999959
	7 vs. CTL	-140.587	43.59335	227.7741	0.931924
	31 vs. CTL	-173.776	10.40462	194.5853	0.999889
	ANOVA (Overall)	NaN	NaN	NaN	0.962653
C_i	1 vs. CTL	-58.0263	-10.7134	36.59954	0.942164
	3 vs. CTL	-40.9428	6.370156	53.68309	0.993218
	5 vs. CTL	-44.6082	2.704775	50.01771	0.999883
	7 vs. CTL	-80.2707	-32.9578	14.35514	0.21853
	31 vs. CTL	-56.9244	-9.61144	37.70149	0.961747
	ANOVA (Overall)	NaN	NaN	NaN	0.253331
C_{ii}	1 vs. CTL	-116.537	-30.4905	55.55641	0.757354
	3 vs. CTL	-97.7161	-11.6692	74.37768	0.993004
	5 vs. CTL	-101.853	-15.8056	70.24127	0.974381
	7 vs. CTL	-117.959	-31.9123	54.1346	0.727097
	31 vs. CTL	-123.826	-37.7788	48.26806	0.598604
	ANOVA (Overall)	NaN	NaN	NaN	0.788002
D_i	1 vs. CTL	-70.8458	2.131234	75.10824	0.999996
	3 vs. CTL	-37.137	35.83999	108.817	0.503391
	5 vs. CTL	-40.5456	32.43139	105.4084	0.588578
	7 vs. CTL	-49.6746	23.30239	96.27939	0.818333
	31 vs. CTL	-60.3278	12.6492	85.62621	0.979823
	ANOVA (Overall)	NaN	NaN	NaN	0.612916
D_{ii}	1 vs. CTL	-60.8942	19.27264	99.43951	0.929767
	3 vs. CTL	-108.328	-28.1614	52.00551	0.766853
	5 vs. CTL	-104.59	-24.4235	55.74336	0.845128
	7 vs. CTL	-89.2202	-9.05337	71.11351	0.99705
	31 vs. CTL	-57.3293	17.65997	92.64922	0.934806
	ANOVA (Overall)	NaN	NaN	NaN	0.395779
E_i	1 vs. CTL	-94.1671	0.875533	95.91818	1
	3 vs. CTL	-54.9041	40.13857	135.1812	0.630234
	5 vs. CTL	-89.1641	5.87858	100.9212	0.999827
	7 vs. CTL	-128.83	-33.7871	61.25555	0.755364
	31 vs. CTL	-70.9013	24.14133	119.184	0.912611
	ANOVA (Overall)	NaN	NaN	NaN	0.378648
E_{ii}	1 vs. CTL	-92.8249	2.442552	97.71002	0.999998
	3 vs. CTL	-84.461	10.80646	106.0739	0.996886
	5 vs. CTL	-85.264	10.00342	105.2709	0.997825
	7 vs. CTL	-104.034	-8.76688	86.50059	0.998825
	31 vs. CTL	-94.8591	0.408384	95.67585	1
	ANOVA (Overall)	NaN	NaN	NaN	0.990786

Table 6. Statistical analyses for Hoechst distribution

This table provides the outcomes of statistical tests comparing each DPI against the control (CTL) for each brain region using ANOVA and the post hoc Dunnett's test. It is organized according to figure labels from Ai to Eii. Each row, except those labeled "ANOVA (Overall)", corresponds to a Dunnett's post hoc test, comparing specific conditions labeled as "1 vs. CTL" and so on, against the control group. The columns in the table are defined as follows:

Figure Name: Identifier for the specific graph in Figure 10.

Comparison: Specifies the experimental condition compared against the control.

Lowerdiff: The lower bound of the 95% confidence interval for the estimated difference between the experimental condition and the control.

ESTdiff: The point estimate of the difference between the experimental condition and the control.

Upperdiff: The upper bound of the 95% confidence interval for the estimated difference.

pValue: The p-value from Dunnett's test, indicating the probability that any observed difference is due to chance, with a lower value suggesting more significant differences.

The rows labeled "ANOVA (Overall)" present the results of an ANOVA test assessing overall differences among all conditions and the control.

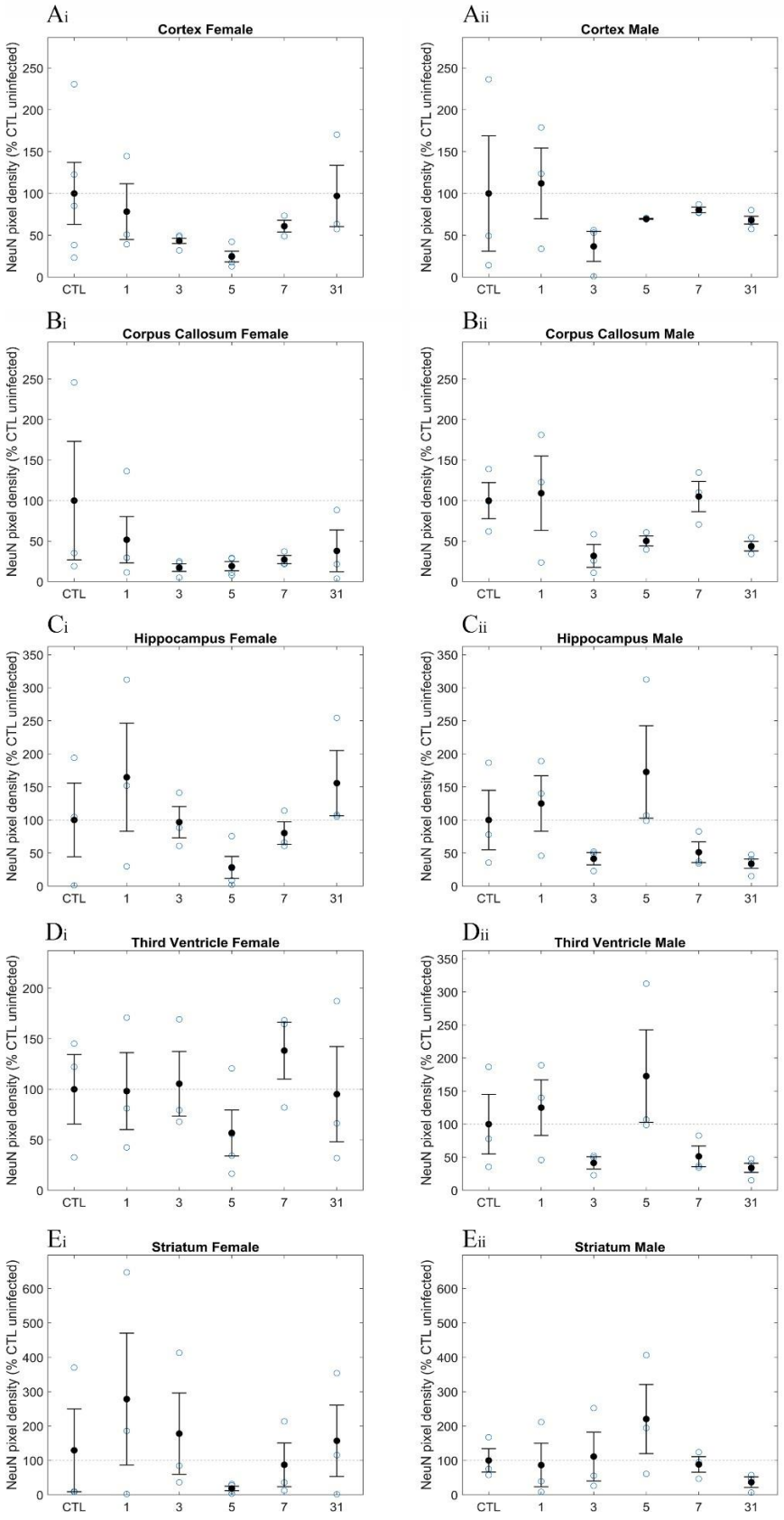
Ai
Cortex Female
Aii
Cortex Male
Bi
Corpus Callosum Female
Bii
Corpus Callosum Male
Ci
Hippocampus Female
Cii
Hippocampus Male
Di
Third Ventricle Female
Dii
Third Ventricle Male
Ei
Striatum Female
Eii
Striatum Male
NeuN pixel density (% CTL uninfected)
CTL
1
3
5
7
31

Figure 11. No changes in NeuN-positive cell density in the context of mild peripheral COVID-19

Scatter plots displaying the relative pixel density of NeuN in male and female Syrian hamsters over several days post-inoculation (CTL, 1 DPI, 3 DPI, 5 DPI, 7 DPI, 31 DPI) in (A) the cortex of (i) females, and (ii) males, (B) the corpus callosum of (i) females, and (ii) males, (C) the hippocampus of (i) females, and (ii) males, (D) the third ventricle of (i) females and (ii) males and (E) the striatum of (i) females and (ii) males expressed as percent control based on CTL values. Each blue point represents one biological replicate, with sample sizes (N) varying from 3 to 5. Black points represent the average values, with horizontal lines indicating the standard error of the mean (SEM). The data indicate no significant changes in NeuN staining (analyzed by one-way ANOVA).

Fig. name	Comparison	Lowerdiff	ESTdiff	Upperdiff	pValue
A_i	1 vs. CTL	-125.086	-21.7318	81.62273	0.969134
	3 vs. CTL	-146.222	-56.7143	32.79335	0.318569
	5 vs. CTL	-170.387	-75.4494	19.48782	0.149679
	7 vs. CTL	-142.427	-39.0726	64.28195	0.760638
	31 vs. CTL	-106.269	-2.9141	100.4405	0.999998
	ANOVA (Overall)	NaN	NaN	NaN	0.251726
A_{ii}	1 vs. CTL	-120.052	12.06455	144.1808	0.998913
	3 vs. CTL	-195.381	-63.2648	68.85145	0.530267
	5 vs. CTL	-162.55	-30.4337	101.6825	0.939903
	7 vs. CTL	-151.778	-19.6617	112.4545	0.989802
	31 vs. CTL	-155.452	-31.8689	91.7145	0.910045
	ANOVA (Overall)	NaN	NaN	NaN	0.655734
B_i	1 vs. CTL	-167.344	-48.2968	70.75061	0.671599
	3 vs. CTL	-201.749	-82.7014	36.34598	0.227157
	5 vs. CTL	-199.901	-80.854	38.19341	0.243412
	7 vs. CTL	-200.089	-72.8219	54.44507	0.381168
	31 vs. CTL	-189.365	-62.0975	65.16946	0.519828
	ANOVA (Overall)	NaN	NaN	NaN	0.446143
B_{ii}	1 vs. CTL	-85.9401	9.156099	104.2523	0.998548
	3 vs. CTL	-163.349	-68.2533	26.84297	0.198539
	5 vs. CTL	-144.903	-49.8072	45.28901	0.447373
	7 vs. CTL	-90.019	5.077247	100.1735	0.999915
	31 vs. CTL	-151.399	-56.3028	38.79342	0.34266
	ANOVA (Overall)	NaN	NaN	NaN	0.111559
C_i	1 vs. CTL	-120.654	64.65941	249.9723	0.771015
	3 vs. CTL	-188.517	-3.20424	182.1087	1
	5 vs. CTL	-244.967	-71.6226	101.7218	0.652152
	7 vs. CTL	-204.999	-19.6858	165.6272	0.99778
	31 vs. CTL	-129.532	55.78049	241.0934	0.85068
	ANOVA (Overall)	NaN	NaN	NaN	0.292034
C_{ii}	1 vs. CTL	-126.563	24.99338	176.5499	0.984085
	3 vs. CTL	-210.118	-58.5615	92.99503	0.70238
	5 vs. CTL	-78.8804	72.67617	224.2327	0.528754
	7 vs. CTL	-200.247	-48.6903	102.8663	0.818357
	31 vs. CTL	-207.76	-65.992	75.77617	0.554219
	ANOVA (Overall)	NaN	NaN	NaN	0.106856
D_i	1 vs. CTL	-141.245	-1.85267	137.54	1
	3 vs. CTL	-133.926	5.467042	144.8597	0.999982
	5 vs. CTL	-173.664	-43.2737	87.11613	0.800687
	7 vs. CTL	-101.104	38.28822	177.6809	0.888601
	31 vs. CTL	-144.269	-4.87622	134.5164	0.99999
	ANOVA (Overall)	NaN	NaN	NaN	0.655631
D_{ii}	1 vs. CTL	-150.373	-29.2464	91.87981	0.926873
	3 vs. CTL	-170.298	-49.1714	71.95478	0.661228
	5 vs. CTL	-99.6427	21.48348	142.6096	0.97785
	7 vs. CTL	-150.7	-29.5733	91.55283	0.923921
	31 vs. CTL	-120.513	0.612687	121.7389	1
	ANOVA (Overall)	NaN	NaN	NaN	0.585596
E_i	1 vs. CTL	-300.591	148.9606	598.5118	0.801596
	3 vs. CTL	-401.108	48.44308	497.9942	0.997629
	5 vs. CTL	-531.568	-111.051	309.4654	0.902349
	7 vs. CTL	-491.738	-42.1865	407.3647	0.998758
	31 vs. CTL	-421.972	27.57921	477.1304	0.99984
	ANOVA (Overall)	NaN	NaN	NaN	0.631558
E_{ii}	1 vs. CTL	-256.624	-13.5781	229.4679	0.999895
	3 vs. CTL	-231.804	11.24199	254.288	0.999958
	5 vs. CTL	-122.602	120.4443	363.4904	0.495563
	7 vs. CTL	-254.619	-11.5728	231.4733	0.999952
	31 vs. CTL	-306.422	-63.3762	179.6698	0.904407
	ANOVA (Overall)	NaN	NaN	NaN	0.426947

Table 7. Statistical analyses for NeuN distribution

This table provides the outcomes of statistical tests comparing each DPI against the control (CTL) for each brain region using ANOVA and the post hoc Dunnett's test. It is organized according to figure labels from Ai to Eii. Each row, except those labeled "ANOVA (Overall)", corresponds to a Dunnett's post hoc test, comparing specific conditions labeled as "1 vs. CTL" and so on, against the control group. The columns in the table are defined as follows:

Figure Name: Identifier for the specific graph in Figure 11.

Comparison: Specifies the experimental condition compared against the control.

Lowerdiff: The lower bound of the 95% confidence interval for the estimated difference between the experimental condition and the control.

ESTdiff: The point estimate of the difference between the experimental condition and the control.

Upperdiff: The upper bound of the 95% confidence interval for the estimated difference.

pValue: The p-value from Dunnett's test, indicating the probability that any observed difference is due to chance, with a lower value suggesting more significant differences.

The rows labeled "ANOVA (Overall)" present the results of an ANOVA test assessing overall differences among all conditions and the control.

2.2.2.Summary

In adult female hamsters, GFAP distribution significantly increased in the cortex three DPI. SOX9 levels stayed consistent across all regions and time points, suggesting that the number of astrocytes did not change. Together this data suggests there is a brief neuroinflammatory response consisting of transient and partial astrogliosis in the early days of peripheral COVID-19 in adult female animals.

Chapter three

Discussion

My study focused on examining the effects of mild COVID-19 on neuroinflammation and astrocyte responses in the brains of Syrian hamsters. I specifically aimed to identify both regional and sex-specific variations in astrocytic markers such as GFAP and SOX9 across various DPI. My study sheds light on the dynamics of mild neuroinflammation triggered by peripheral infection with the SARS-CoV-2 virus.

The main important finding from my research was the transient change in GFAP distribution in female animals at 3 DPI. Astrocytes, in their reactive state, become hypertrophic and extend their processes into affected areas to mitigate the effects of inflammation; this could partially account for the increased GFAP distribution (Azzolini et al. 2022; D. Li et al. 2020; Sticozzi et al. 2013). This transient increase subsequently disappeared at later time points. My observations support my hypothesis that astrogliosis might occur in mild peripheral COVID-19. Our findings are in line with work from others showing that changes in GFAP are associated with central nervous system disorders that share some similarities with COVID-19 (reviewed in Cekanaviciute and Buckwalter 2016; and Colombo and Farina 2016; and Lee et al. 2023; Kanberg et al. 2020). My work also suggests that mild peripheral COVID-19-associated neurological impacts could share some common mechanisms with more severe neurological impairments in COVID-19, which have also been suggested to arise from heightened systemic inflammation and subsequent disruptions in the BBB, rather than direct viral damage to neural cells (Murta, Villarreal, and Ramos 2020; Najjar et al. 2020).

In my study, I noted a significant increase in GFAP coverage in the cortex of female hamsters at 3 DPI. This significant increase indicates heightened astrocytic activation in response to infection. However, this trend was not consistent across all brain regions or between sexes. For example, I observed a notable (not statistically significant) decrease in GFAP coverage in the dorsal striatum. Astrocytes generally expand their coverage in response to injury or inflammation (reviewed in Sofroniew 2015; Sofroniew and Vinters 2010), yet the reduction in GFAP signal in the dorsal striatum suggests a region-specific response to the infection. This decrease may reflect differential regulation of astrocytic activity in the striatum compared to the cortex. Possible explanations for this unique response include the intrinsic properties of the striatum, its neural connectivity, or the specific immune environment it facilitates post-infection (Choi et al. 2009; reviewed in Haber 2016; Hald and Lotharius 2005; Jeong et al. 2022; Kaur et al. 2017; Pott Godoy, Ferrari, and Pitossi 2010; Silvestroni et al. 2009).

Another notable observation was the stability of SOX9 expression across the different time points. SOX9 is a transcription factor crucial for the maintenance and differentiation of astrocytes (Sun et al. 2017). I anticipated that SOX9 expression would follow a similar trend to GFAP; however, stable levels of SOX9 suggest that the total number of astrocytes may not undergo significant fluctuations in response to mild neuroinflammation. This stability in SOX9 expression indicates that the astrocytic response to mild COVID-19-induced neuroinflammation primarily involves changes in astrocyte reactivity—reflected by GFAP levels—and morphology, rather than alterations in their proliferation or overall numbers.

These findings provide insights into the complex and region-specific responses of the brain to COVID-19 infection. While my initial hypotheses were partially supported—such as the expected early peak in astrocytic reactivity—other results, like the region-specific decrease in GFAP coverage in the dorsal striatum, reveal neuroinflammation's intricate and sometimes unpredictable nature. These results suggest that astrocytic reactivity and neuronal changes following mild neuroinflammation are not uniform across different brain regions or between sexes.

3.1. Methodological considerations in quantification

To compare my methodological approach to those existing in the literature, I will provide some studies that used different techniques for quantifying GFAP distribution. For example, Finney, Jones, and Morris (2021) used an automated protocol that emphasized optical density and pixel proportion, while Marques et al. (2023) implemented a semi-automatic method emphasizing the structural analysis of astrocytes. Luijerink, Rodriguez, and Machaalani (2024) introduced a Reactivity score (R-score) for assessing astrocyte activation, which they found to be highly reproducible and sensitive. My study differentiates itself by using MATLAB for image analysis, specifically applying Kapur’s entropy thresholding to enhance the accuracy and objectivity in quantifying GFAP expression (Kapur, Sahoo, and Wong 1985; Kiani, Safabakhsh, and Khadangi

2009). Unlike methods relying on manual or semi-automatic threshold settings, this method dynamically determines the optimal threshold for each image based on its unique histogram. As a result, this approach reduces potential biases and ensures a consistent analysis across samples.

3.2. Sex-specific responses in neuroinflammation

Research into sex differences in the context of long-COVID suggests that women appear to be more susceptible to brain fog (reviewed in Sylvester et al. 2022). Moreover, in a rodent model of ischemic injury, heightened astrocyte activation was noted in female animals compared to males (Cordeau et al. 2008). This is potentially mediated by estrogen signaling pathways, which could affect the degree of GFAP upregulation following injury. My findings align with these observations, as I noted increased GFAP distribution in female hamsters in response to mild COVID-19. The mechanisms behind these differences, however, may extend beyond hormonal influences and include complex interactions within the neuroimmune environment, likely influenced by both the severity of peripheral inflammation and the specific dynamics of mild SARS-CoV-2 infection (Asadi-Pooya et al. 2022; Hanamsagar and Bilbo 2016).

3.3. Implications and broader context of findings

The observed increase in GFAP density suggests that even mild COVID-19 can trigger changes that may negatively impact synaptic functions. GFAP plays a crucial role in cell shape, proliferation, and synaptic plasticity (Kashon et al. 2005; McCall et al. 1996). Elevated GFAP levels in blood correlate with lower memory scores and reduced white matter integrity in older adults, even after controlling for Alzheimer's disease biomarkers (Bettcher et al. 2021). Furthermore, increased plasma GFAP concentrations are linked to postoperative cognitive dysfunction in non-cardiac surgery patients, suggesting brain cellular injury (Rappold et al.

2016). As a result, such inflammation can interfere with normal synaptic activity, impairing memory and learning processes and contributing to symptoms such as brain fog.

3.4. Limitations of the study

One of the primary limitations of my study came from necessary precautions in handling and preparing high biohazard level brain samples. The samples were fixed in formalin for an extended period (>30 days) before the slicing procedure, to ensure complete neutralization of any viral particles. This prolonged fixation can negatively affect tissue integrity and subsequent histological analyses. Additionally, due to safety protocols at the National Microbiology Laboratory, sharp objects were not permitted during tissue collection. Given the animals therefore could not be perfused, and tissue removal was hampered by the lack of allowable tools, the brains I received were of varying quality. This issue was particularly challenging as it hindered our ability to obtain fully intact slices from the desired bregma levels from some samples. The prolonged fixation and suboptimal slicing adversely affected the quality of staining and imaging, impacting the quantifiability of cellular structures in the samples. Specifically, the staining of NeuN in the hippocampus presented challenges. The expression was not very distinct, and cells often appeared clumped together, making it difficult to quantify or analyze these regions compared to other brain areas where cells were more clearly defined. As a result, I increased the number of samples (N) analyzed to mitigate these effects and ensure better results. Additionally, I did not limit my imaging and analysis to traditional brain regions associated with memory and learning, such as the cortex and hippocampus. Instead, I included multiple brain regions to achieve a more comprehensive understanding of the COVID- 19 neuroinflammatory response.

Moreover, using Syrian hamsters as a model organism was both a strength and a limitation. On the positive side, hamsters endogenously express the ACE2 receptor, which SARS-CoV-2 uses to enter cells, making them a relevant model for studying COVID-19 (Castellan et al. 2022, 2023; Fomin et al. 2022; Frere et al. 2022; reviewed in Gruber et al. 2022; Israelow et al. 2020; Knight et al. 2021; Moreau et al. 2020; Oliveira 2020; Patil, Mohandas, and Yadav 2021; Rosenke et al. 2020; Shou et al. 2021; Sia et al. 2020). Hamsters are also commonly used in immunological research and typically exhibit only mild symptoms of the disease, which aligns with the objectives of my study to model mild COVID-19 (Castellan et al. 2022, 2023; Fomin et al. 2022; Frere et al. 2022). However, a significant limitation was the lack of detailed and updated anatomical atlases for Syrian hamsters, unlike the extensive resources available for mice. I partially addressed this challenge by referencing the Allen mouse brain atlas (https://mouse.brain- map.org/experiment/thumbnails/100142143) and Golden hamster atlas (Halsey et al. 1963).

4. References

Abassi, Zaid, Abd Al Roof Higazi, Safa Kinaneh, Zaher Armaly, Karl Skorecki, and Samuel N. Heyman. 2020. "ACE2, COVID-19 Infection, Inflammation, and Coagulopathy: Missing Pieces in the Puzzle." *Frontiers in Physiology* 11: 574753. doi:10.3389/fphys.2020.574753.

Abenza Abildúa, M. J., S. Atienza, G. Carvalho Monteiro, M. E. Erro Aguirre, L. Imaz Aguayo, E. Freire Álvarez, D. García-Azorín, et al. 2021. "Encephalopathy and Encephalitis during Acute SARS-CoV-2 Infection. Spanish Society of Neurology's COVID-19 Registry." *Neurología (English Edition)* 36(2): 127–34. doi:10.1016/j.nrleng.2020.11.003.

Agarwal, Shashank, Kara Melmed, Siddhant Dogra, Rajan Jain, Jenna Conway, Steven Galetta, and Ariane Lewis. 2021. "Increase in Ventricle Size and the Evolution of White Matter Changes on Serial Imaging in Critically Ill Patients with COVID-19." *Neurocritical Care* 35(2): 491–500. doi:10.1007/s12028-021-01207-2.

Ahmad, Sufiyan, Md. Rageeb Md. Usman, Kiran D. Baviskar, and Tushar P. Patil. 2020. "Break the Chain of Coronavirus Disease (Covid-19) Infection: A Review." In *International Journal of Pharmaceutical Sciences Review and Research*, , 187–91. doi:10.47583/ijpsrr.2020.v64i02.030.

Ahmadpour, Noushin, Meher Kantroo, and Jillian L. Stobart. 2021. "Extracellular Calcium Influx Pathways in Astrocyte Calcium Microdomain Physiology." *Biomolecules* 11(10): 1467. doi:10.3390/biom11101467.

Akyuz, Enes, Chiara Villa, Merve Beker, and Birsen Elibol. 2020. "Unraveling the Role of Inwardly Rectifying Potassium Channels in the Hippocampus of an Aβ(1–42)-Infused Rat Model of Alzheimer's Disease." *Biomedicines* 8(3): 58. doi:10.3390/biomedicines8030058.

Alberca, Gabriela Gama Freire, Iara Grigoletto Fernandes, Maria Notomi Sato, and Ricardo Wesley Alberca. 2020. "What Is COVID-19?" In *Frontiers for Young Minds*, , 74. doi:10.3389/frym.2020.00074.

Alberini, Cristina M., Emmanuel Cruz, Giannina Descalzi, Benjamin Bessières, and Virginia Gao. 2018. "Astrocyte Glycogen and Lactate: New Insights into Learning and Memory Mechanisms." *Glia* 66(6): 1244–62. doi:10.1002/glia.23250.

Ali, M., P. Siarry, and M. Pant. 2017. "Multi-Level Image Thresholding Based on Hybrid Differential Evolution Algorithm. Application on Medical Images." In Studies in Computational Intelligence, eds. Amir Nakib and El-Ghazali Talbi. Berlin, Heidelberg: Springer Berlin Heidelberg, 23–36. doi:10.1007/978-3-662-54428-0_2.

Andrews, Madeline G., Tanzila Mukhtar, Ugomma C. Eze, Camille R. Simoneau, Jayden Ross, Neelroop Parikshak, Shaohui Wang, et al. 2022. "Tropism of SARS-CoV-2 for Human Cortical Astrocytes." *Proceedings of the National Academy of Sciences of the United States of America* 119(30). doi:10.1073/pnas.2122236119.

Araújo, Sara Tavares, Clara Tavares Araújo, Rafael Silva E Castro, Lara Machado de Oliveira Brügger, Nathália Gualberto Souza E Silva, Debora Marques de Miranda, and Ana Cristina Simões E Silva. 2023. "Imaging Markers of Neurologic Damage in COVID-19: A Systematic Review." *Current Medicinal Chemistry* 30(9): 1086–1106. doi:10.2174/0929867329666220701124945.

Arıkan, Fatma Akkoyun, Gönül Akdağ, Mustafa Çetiner, Niyazi Uysal, and Sibel Canbaz Kabay. 2022. "Isolated Corpus Callosum Lesion Associated with Cytokine Storm in COVID-19." *Proceedings (Baylor University. Medical Center)* 35(3): 337–38. doi:10.1080/08998280.2022.2044655.

Asadi-Pooya, Ali A., Ali Akbari, Amir Emami, Mehrzad Lotfi, Mahtab Rostamihosseinkhani, Hamid Nemati, Zohreh Barzegar, et al. 2022. "Long COVID Syndrome-Associated Brain Fog." *Journal of Medical Virology* 94(3): 979–84. doi:10.1002/jmv.27404.

Azizan, E., and M. Brown. 2020. "ACE2 Role in SARS-CoV-2 Infectivity and Covid-19 Severity." *The Malaysian Journal of Pathology* 42(3): 363–67.

Azzolini, Elena, Riccardo Levi, Riccardo Sarti, Chiara Pozzi, Maximiliano Mollura, Alberto Mantovani, and Maria Rescigno. 2022. "Association Between BNT162b2 Vaccination and Long COVID After Infections Not Requiring Hospitalization in Health Care Workers." *JAMA* 328(7): 676–78. doi:10.1001/jama.2022.11691.

Baghel, Neha Singh. 2020. "Optimization of Methods for Image Segmentation by Using Thresholding Techniques." *International Journal for Research in Applied Science and Engineering Technology* 8(2): 222–27. doi:10.22214/ijraset.2020.2032.

Balouch, Bailey, Jessica L. Funnell, Alexis M. Ziemba, Devan L. Puhl, Kathy Lin, Manoj K. Gottipati, and Ryan J. Gilbert. 2021. "Conventional Immunomarkers Stain a Fraction of Astrocytes *in Vitro* : A Comparison of Rat Cortical and Spinal Cord Astrocytes in Naïve and Stimulated Cultures." *Journal of Neuroscience Research* 99(3): 806–26. doi:10.1002/jnr.24759.

Bangare, Sunil L., Amruta Dubal, Pallavi S. Bangare, and S.T. Patil. 2015. "Reviewing Otsu's Method For Image Thresholding." In *International Journal of Applied Engineering Research*, , 21777–83. doi:10.37622/IJAER/10.9.2015.21777-21783.

Bauer, Lisa, Brigitta M. Laksono, Femke M. S. de Vrij, Steven A. Kushner, Oliver Harschnitz, and Debby van Riel. 2022. "The Neuroinvasiveness, Neurotropism, and Neurovirulence of SARS-CoV-2." *Trends in Neurosciences* 45(5): 358–68. doi:10.1016/j.tins.2022.02.006.

Bayat, Amir-Hossein, Helia Azimi, Meysam Hassani Moghaddam, Vahid Ebrahimi, Mobina Fathi, Kimia Vakili, Gholam-Reza Mahmoudiasl, et al. 2022. "COVID-19 Causes Neuronal Degeneration and Reduces Neurogenesis in Human Hippocampus." *Apoptosis: An International Journal on Programmed Cell Death* 27(11–12): 852–68. doi:10.1007/s10495- 022-01754-9.

Beard, Elidie, Sylvain Lengacher, Sara Dias, Pierre J. Magistretti, and Charles Finsterwald. 2022. "Astrocytes as Key Regulators of Brain Energy Metabolism: New Therapeutic Perspectives." *Frontiers in Physiology* 12: 825816. doi:10.3389/fphys.2021.825816.

Beckman, Danielle, Alyssa Bonillas, Giovanne B. Diniz, Sean Ott, Jamin W. Roh, Sonny R. Elizaldi, Brian A. Schmidt, et al. 2022. "SARS-CoV-2 Infects Neurons and Induces Neuroinflammation in a Non-Human Primate Model of COVID-19." *Cell Reports* 41(5). doi:10.1016/j.celrep.2022.111573.

Bélanger, Mireille, Igor Allaman, and Pierre J. Magistretti. 2011. "Brain Energy Metabolism: Focus on Astrocyte-Neuron Metabolic Cooperation." *Cell Metabolism* 14(6): 724–38. doi:10.1016/j.cmet.2011.08.016.

Bellot-Saez, Alba, Orsolya Kékesi, John W. Morley, and Yossi Buskila. 2017. "Astrocytic Modulation of Neuronal Excitability through K + Spatial Buffering." *Neuroscience & Biobehavioral Reviews* 77: 87–97. doi:10.1016/j.neubiorev.2017.03.002.

Benedict, Ralph H. B., Bianca Weinstock-Guttman, Inna Fishman, Jitendra Sharma, Christopher W. Tjoa, and Rohit Bakshi. 2004. "Prediction of Neuropsychological Impairment in Multiple Sclerosis: Comparison of Conventional Magnetic Resonance Imaging Measures of Atrophy and Lesion Burden." *Archives of Neurology* 61(2): 226–30. doi:10.1001/archneur.61.2.226.

Benraya, Imane, and Nadjia Benblidia. 2018. "Comparison of Background Subtraction Methods." *2018 International Conference on Applied Smart Systems (ICASS)*: 1–5. doi:10.1109/ICASS.2018.8652040.

Bettcher, Brianne M., Kaitlin E. Olson, Nichole E. Carlson, Brice V. McConnell, Tim Boyd, Vanesa Adame, D. Adriana Solano, et al. 2021. "Astrogliosis and Episodic Memory in Late Life: Higher GFAP Is Related to Worse Memory and White Matter Microstructure in Healthy Aging and Alzheimer's Disease." *Neurobiology of Aging* 103: 68–77. doi:10.1016/j.neurobiolaging.2021.02.012.

Beyerstedt, Stephany, Expedito Barbosa Casaro, and Érika Bevilaqua Rangel. 2021. "COVID-19: Angiotensin-Converting Enzyme 2 (ACE2) Expression and Tissue Susceptibility to SARS-CoV-2 Infection." *European Journal of Clinical Microbiology & Infectious Diseases* 40(5): 905–19. doi:10.1007/s10096-020-04138-6.

Biadsee, Ameen, Ameer Biadsee, Firas Kassem, Or Dagan, Shchada Masarwa, and Zeev Ormianer. 2020. "Olfactory and Oral Manifestations of COVID-19: Sex-Related Symptoms—A Potential Pathway to Early Diagnosis." *Otolaryngology–Head and Neck Surgery* 163(4): 722–28. doi:10.1177/0194599820934380.

Bilinska, Katarzyna, Patrycja Jakubowska, Christopher S. von Bartheld, and Rafal Butowt. 2020. "Expression of the SARS-CoV-2 Entry Proteins, ACE2 and TMPRSS2, in Cells of the Olfactory Epithelium: Identification of Cell Types and Trends with Age." *ACS chemical neuroscience* 11(11): 1555–62. doi:10.1021/acschemneuro.0c00210.

Booz, George W., Raffaele Altara, Ali H. Eid, Zena Wehbe, Souha Fares, Hassan Zaraket, Nada J. Habeichi, and Fouad A. Zouein. 2020. "Macrophage Responses Associated with COVID-19: A Pharmacological Perspective." *European Journal of Pharmacology* 887: 173547. doi:10.1016/j.ejphar.2020.173547.

Braxton, Alicia M, Patrick S Creisher, Camilo A Ruiz-Bedoya, Katie R Mulka, Santosh Dhakal, Alvaro A Ordonez, Sarah E Beck, Sanjay K Jain, and Jason S Villano. 2021. "Hamsters as a Model of Severe Acute Respiratory Syndrome Coronavirus-2." *Comparative Medicine* 71(5): 398–410. doi:10.30802/AALAS-CM-21-000036.

Bridwell, Rachel, Brit Long, and Michael Gottlieb. 2020. "Neurologic Complications of COVID-19." *The American Journal of Emergency Medicine* 38(7): 1549.e3-1549.e7. doi:10.1016/j.ajem.2020.05.024.

Calculli, Alessandra, Tommaso Bocci, Mattia Porcino, Micol Avenali, Chiara Casellato, Sebastiano Arceri, Simone Regalbuto, Alberto Priori, and Antonio Pisani. 2023. "Parkinson Disease Following COVID-19: Report of Six Cases." *European Journal of Neurology* 30(5): 1272–80. doi:10.1111/ene.15732.

Callan, Caitriona, Emma Ladds, Laiba Husain, Kyle Pattinson, and Trisha Greenhalgh. 2022. "'I Can't Cope with Multiple Inputs': A Qualitative Study of the Lived Experience of 'Brain Fog' after COVID-19." *BMJ Open* 12(2): e056366. doi:10.1136/bmjopen-2021- 056366.

Cares-Marambio, Kevin, Yessenia Montenegro-Jiménez, Rodrigo Torres-Castro, Roberto Vera-Uribe, Yolanda Torralba, Xavier Alsina-Restoy, Luis Vasconcello-Castillo, and Jordi Vilaró. 2021. "Prevalence of Potential Respiratory Symptoms in Survivors of Hospital

Admission after Coronavirus Disease 2019 (COVID-19): A Systematic Review and Meta- Analysis." *Chronic Respiratory Disease* 18: 147997312110022. doi:10.1177/14799731211002240.

Castellan, Martina, Gianpiero Zamperin, Giulia Franzoni, Greta Foiani, Maira Zorzan, Petra Drzewnioková, Marzia Mancin, et al. 2022. "In-Depth Characterization of the Syrian Hamster as Translational Model for COVID-19 in Humans." : 2022.11.22.517339. doi:10.1101/2022.11.22.517339.

Castellan, Martina, Gianpiero Zamperin, Giulia Franzoni, Greta Foiani, Maira Zorzan, Petra Drzewnioková, Marzia Mancin, et al. 2023. "Host Response of Syrian Hamster to SARS- CoV-2 Infection Including Differences with Humans and between Sexes." *Viruses* 15(2): 428. doi:10.3390/v15020428.

Cekanaviciute, Egle, and Marion S. Buckwalter. 2016. "Astrocytes: Integrative Regulators of Neuroinflammation in Stroke and Other Neurological Diseases." *Neurotherapeutics: The Journal of the American Society for Experimental NeuroTherapeutics* 13(4): 685–701. doi:10.1007/s13311-016-0477-8.

Chakrabarti, Swarup K. 2022. "Brain Fog: A Post-COVID-19 Sequelae? A Perspective." *Journal of Clinical Case Reports Medical Images and Health Sciences* 2(2). doi:10.55920/JCRMHS.2022.02.001062.

Chatton, Jean-Yves, Pierre J. Magistretti, and L. Felipe Barros. 2016. "Sodium Signaling and Astrocyte Energy Metabolism." *Glia* 64(10): 1667–76. doi:10.1002/glia.22971.

Chen, Zhuangzhuang, and Guozhong Li. 2021. "Immune Response and Blood-Brain Barrier Dysfunction during Viral Neuroinvasion." *Innate Immunity* 27(2): 109–17. doi:10.1177/1753425920954281.

Choi, Dong-Young, Mei Liu, Randy L. Hunter, Wayne A. Cass, Jignesh D. Pandya, Patrick G. Sullivan, Eun-Joo Shin, et al. 2009. "Striatal Neuroinflammation Promotes Parkinsonism in Rats." *PloS One* 4(5): e5482. doi:10.1371/journal.pone.0005482.

Chudzik, Michał, Mateusz Babicki, Joanna Kapusta, Żaneta Kałuzińska-Kołat, Damian Kołat, Piotr Jankowski, and Agnieszka Mastalerz-Migas. 2022. "Long-COVID Clinical Features and Risk Factors: A Retrospective Analysis of Patients from the STOP-COVID Registry of the PoLoCOV Study." *Viruses* 14(8): 1755. doi:10.3390/v14081755.

Colombo, Emanuela, and Cinthia Farina. 2016. "Astrocytes: Key Regulators of Neuroinflammation." *Trends in Immunology* 37(9): 608–20. doi:10.1016/j.it.2016.06.006.

Cordeau, Pierre, Mélanie Lalancette-Hébert, Yuan Cheng Weng, and Jasna Kriz. 2008. "Live Imaging of Neuroinflammation Reveals Sex and Estrogen Effects on Astrocyte Response to Ischemic Injury." *Stroke* 39(3): 935–42. doi:10.1161/STROKEAHA.107.501460.

Correa-Cerro, Lina S., and James W. Mandell. 2007. "Molecular Mechanisms of Astrogliosis: New Approaches With Mouse Genetics." *Journal of Neuropathology and Experimental Neurology* 66(3): 169–76. doi:10.1097/01.jnen.0000248555.53079.d5.

"COVID-19 Cases | WHO COVID-19 Dashboard." *datadot*. https://data.who.int/dashboards/covid19/cases (September 11, 2024).

Cristillo, Viviana, Andrea Pilotto, Stefano Cotti Piccinelli, Stefano Gipponi, Matilde Leonardi, Michela Bezzi, and Alessandro Padovani. 2022. "Predictors of 'Brain Fog' 1 Year after COVID-19 Disease." *Neurological Sciences* 43(10): 5795–97. doi:10.1007/s10072- 022-06285-4.

Crook, Harry, Sanara Raza, Joseph Nowell, Megan Young, and Paul Edison. 2021. "Long Covid—Mechanisms, Risk Factors, and Management." *BMJ*: n1648. doi:10.1136/bmj.n1648.

Davalos, Dimitrios, Jaime Grutzendler, Guang Yang, Jiyun V. Kim, Yi Zuo, Steffen Jung, Dan R. Littman, Michael L. Dustin, and Wen-Biao Gan. 2005. "ATP Mediates Rapid Microglial Response to Local Brain Injury in Vivo." *Nature Neuroscience* 8(6): 752–58. doi:10.1038/nn1472.

Dey, Rajen. 2024. "Covid-19 Induced Neuroinflammation." *Journal of Advanced Zoology*. doi:10.53555/jaz.v45i2.4447.

Dibaj, Payam, Melanie Kaiser, Johannes Hirrlinger, Frank Kirchhoff, and Clemens Neusch. 2007. "Kir4.1 Channels Regulate Swelling of Astroglial Processes in Experimental Spinal Cord Edema." *Journal of Neurochemistry* 103(6): 2620–28. doi:10.1111/j.1471- 4159.2007.04979.x.

Dietzel, I., U. Heinemann, G. Hofmeier, and H. D. Lux. 1982. "Stimulus-Induced Changes in Extracellular Na+ and Cl- Concentration in Relation to Changes in the Size of the Extracellular Space." *Experimental Brain Research* 46(1): 73–84. doi:10.1007/BF00238100.

DiSabato, Damon J., Ning Quan, and Jonathan P. Godbout. 2016. "Neuroinflammation: The Devil Is in the Details." *Journal of Neurochemistry* 139(S2): 136–53. doi:10.1111/jnc.13607.

Donoghue, M., F. Hsieh, E. Baronas, K. Godbout, M. Gosselin, N. Stagliano, M. Donovan, et al. 2000. "A Novel Angiotensin-Converting Enzyme-Related Carboxypeptidase (ACE2)

Converts Angiotensin I to Angiotensin 1-9." *Circulation Research* 87(5): E1-9. doi:10.1161/01.res.87.5.e1.

Doobay, Marc F., Lauren S. Talman, Teresa D. Obr, Xin Tian, Robin L. Davisson, and Eric Lazartigues. 2007. "Differential Expression of Neuronal ACE2 in Transgenic Mice with Overexpression of the Brain Renin-Angiotensin System." *American Journal of Physiology. Regulatory, Integrative and Comparative Physiology* 292(1): R373-381. doi:10.1152/ajpregu.00292.2006.

Ellul, Mark A., Laura Benjamin, Bhagteshwar Singh, Suzannah Lant, Benedict Daniel Michael, Ava Easton, Rachel Kneen, et al. 2020. "Neurological Associations of COVID-19." *The Lancet. Neurology* 19(9): 767–83. doi:10.1016/S1474-4422(20)30221-0.

Elorza-Vidal, Xabier, Héctor Gaitán-Peñas, and Raúl Estévez. 2019. "Chloride Channels in Astrocytes: Structure, Roles in Brain Homeostasis and Implications in Disease." *International Journal of Molecular Sciences* 20(5): 1034. doi:10.3390/ijms20051034.

Emmi, Aron, Aleksandar Tushevski, Alessandro Sinigaglia, Silvia Barbon, Michele Sandre, Elena Stocco, Veronica Macchi, et al. 2023. "ACE2 Receptor and TMPRSS2 Protein Expression Patterns in the Human Brainstem Reveal Anatomical Regions Potentially Vulnerable to SARS-CoV-2 Infection." *ACS Chemical Neuroscience* 14(11): 2089–97. doi:10.1021/acschemneuro.3c00101.

Enkvist, M. O., and K. D. McCarthy. 1994. "Astroglial Gap Junction Communication Is Increased by Treatment with Either Glutamate or High K+ Concentration." *Journal of Neurochemistry* 62(2): 489–95. doi:10.1046/j.1471-4159.1994.62020489.x.

Escalada, Paula, Amaia Ezkurdia, María Javier Ramírez, and Maite Solas. 2024. "Essential Role of Astrocytes in Learning and Memory." *International Journal of Molecular Sciences* 25(3): 1899. doi:10.3390/ijms25031899.

Fang, Xiao-Xia, Heng Wang, Hao-Lin Song, Juan Wang, and Zhi-Jun Zhang. 2022. "Neuroinflammation Involved in Diabetes-Related Pain and Itch." *Frontiers in Pharmacology* 13: 921612. doi:10.3389/fphar.2022.921612.

Fekete, Rebeka, Alba Simats, Eduárd Bíró, Csaba Cserép, Anett D Schwarcz, Balázs Pósfai, Eszter Szabadits, et al. 2023. "Infection-Induced Vascular Inflammation in COVID- 19 Links Focal Microglial Dysfunction with Neuropathologies through IL-1/IL-6-Related Systemic Inflammatory States." doi:10.1101/2023.06.23.546214.

Felix, Lisa, Andrea Delekate, Gabor C. Petzold, and Christine R. Rose. 2020. “Sodium Fluctuations in Astroglia and Their Potential Impact on Astrocyte Function.” *Frontiers in Physiology* 11: 871. doi:10.3389/fphys.2020.00871.

Finney, Caitlin A., Nicole M. Jones, and Margaret J. Morris. 2021. “A Scalable, Fully Automated Approach for Regional Quantification of Immunohistochemical Staining of Astrocytes in the Rat Brain.” *Journal of Neuroscience Methods* 348: 108994. doi:10.1016/j.jneumeth.2020.108994.

Fomin, Gleb, Kairat Tabynov, Nurkeldy Turebekov, Dinara Turegeldiyeva, and Rinat Islamov. 2022. *EXPERIMENTAL MODEL OF SARS COV-2 IN YOUNG SYRIAN HAMSTERS FOR PRECLINICAL STUDIES*. doi:10.5593/sgem2022/6.1/s25.10.

Francis, Magen Ellen, Una Goncin, Andrea Kroeker, Cynthia Swan, Robyn Ralph, Yao Lu, Athema Louise Etzioni, et al. 2021. “SARS-CoV-2 Infection in the Syrian Hamster Model Causes Inflammation as Well as Type I Interferon Dysregulation in Both Respiratory and Non-Respiratory Tissues Including the Heart and Kidney.” *PLOS Pathogens* 17(7): e1009705. doi:10.1371/journal.ppat.1009705.

Frank-Cannon, Tamy C., Laura T. Alto, Fiona E. McAlpine, and Malú G. Tansey. 2009. “Does Neuroinflammation Fan the Flame in Neurodegenerative Diseases?” *Molecular Neurodegeneration* 4(1): 47. doi:10.1186/1750-1326-4-47.

Frere, Justin J., Randal A. Serafini, Kerri D. Pryce, Marianna Zazhytska, Kohei Oishi, Ilona Golynker, Maryline Panis, et al. 2022. “SARS-CoV-2 Infection in Hamsters and Humans Results in Lasting and Unique Systemic Perturbations after Recovery.” *Science Translational Medicine* 14(664). doi:10.1126/scitranslmed.abq3059.

Gao, Xiang, Wei Li, Fahim Syed, Fang Yuan, Ping Li, and Qigui Yu. 2022. “PD-L1 Signaling in Reactive Astrocytes Counteracts Neuroinflammation and Ameliorates Neuronal Damage after Traumatic Brain Injury.” *Journal of Neuroinflammation* 19(1): 43. doi:10.1186/s12974- 022-02398-x.

Garcia Castro, Jesús, Cristina Utrilla Contreras, and Ángel Martín Montes. 2022. “Reversible Cytotoxic Lesion of the Corpus Callosum and COVID-19.” *The Neurohospitalist* 12(3): 585–86. doi:10.1177/19418744211039374.

Garcia, Maria A., Paula V. Barreras, Allie Lewis, Gabriel Pinilla, Lori J. Sokoll, Thomas Kickler, Heba Mostafa, et al. 2021. “Cerebrospinal Fluid in COVID-19 Neurological Complications: Neuroaxonal Damage, Anti-SARS-Cov2 Antibodies but No Evidence of Cytokine Storm.” *Journal of the Neurological Sciences* 427: 117517. doi:10.1016/j.jns.2021.117517.

Gasmi, Amin, Torsak Tippairote, Pavan Kumar Mujawdiya, Asma Gasmi Benahmed, Alain Menzel, Maryam Dadar, and Geir Bjørklund. 2021. "Neurological Involvements of SARS- CoV2 Infection." *Molecular neurobiology* 58(3): 944–49. doi:10.1007/s12035-020-02070-6.

Goenaga, Julianna, Alfonso Araque, Paulo Kofuji, and Daniela Herrera Moro Chao. 2023. "Calcium Signaling in Astrocytes and Gliotransmitter Release." *Frontiers in Synaptic Neuroscience* 15: 1138577. doi:10.3389/fnsyn.2023.1138577.

Gruber, Achim D., Theresa C. Firsching, Jakob Trimpert, and Kristina Dietert. 2022. "Hamster Models of COVID-19 Pneumonia Reviewed: How Human Can They Be?" *Veterinary Pathology* 59(4): 528–45. doi:10.1177/03009858211057197.

Haber, Suzanne N. 2016. "Corticostriatal Circuitry." *Dialogues in Clinical Neuroscience* 18(1): 7–21. doi:10.31887/DCNS.2016.18.1/shaber.

Halassa, Michael M., Tommaso Fellin, Hajime Takano, Jing-Hui Dong, and Philip G. Haydon. 2007. "Synaptic Islands Defined by the Territory of a Single Astrocyte." *The Journal of Neuroscience: The Official Journal of the Society for Neuroscience* 27(24): 6473–77. doi:10.1523/JNEUROSCI.1419-07.2007.

Hald, Andreas, and Julie Lotharius. 2005. "Oxidative Stress and Inflammation in Parkinson's Disease: Is There a Causal Link?" *Experimental Neurology* 193(2): 279–90. doi:10.1016/j.expneurol.2005.01.013.

Hamad, Arin H., Hozheen O. Muhamad, and Sardar P. Yaba. 2015. "De-Noising of Medical Images by Using Some Filters." https://www.semanticscholar.org/paper/De-noising-of- medical-images-by-using-some-filters-Hamad-Muhamad/b4a3094306065739868e23aff22bde9915b1ad01 (August 14, 2024).

Hamming, I., W. Timens, M. L. C. Bulthuis, A. T. Lely, G. J. Navis, and H. van Goor. 2004. "Tissue Distribution of ACE2 Protein, the Functional Receptor for SARS Coronavirus. A First Step in Understanding SARS Pathogenesis." *The Journal of Pathology* 203(2): 631–37. doi:10.1002/path.1570.

Hanamsagar, Richa, and Staci D. Bilbo. 2016. "Sex Differences in Neurodevelopmental and Neurodegenerative Disorders: Focus on Microglial Function and Neuroinflammation during Development." *The Journal of Steroid Biochemistry and Molecular Biology* 160: 127–33. doi:10.1016/j.jsbmb.2015.09.039.

Haverty, Ruth, Janet McCormack, Christopher Evans, Kevin Purves, Sophie O'Reilly, Virginie Gautier, Keith Rochfort, Aurelie Fabre, and Nicola F. Fletcher. 2024. "SARS-CoV-2 Infects Neurons, Astrocytes, Choroid Plexus Epithelial Cells and Pericytes of the Human

Central Nervous System in Vitro." *The Journal of General Virology* 105(7): 002009. doi:10.1099/jgv.0.002009.

Healey, Quin, Aziz Sheikh, Luke Daines, and Eleftheria Vasileiou. 2022. "Symptoms and Signs of Long COVID: A Rapid Review and Meta-Analysis." *Journal of Global Health* 12: 05014. doi:10.7189/jogh.12.05014.

Hosseini, Shirin, Esther Wilk, Kristin Michaelsen-Preusse, Ingo Gerhauser, Wolfgang Baumgärtner, Robert Geffers, Klaus Schughart, and Martin Korte. 2018. "Long-Term Neuroinflammation Induced by Influenza A Virus Infection and the Impact on Hippocampal Neuron Morphology and Function." *The Journal of Neuroscience: The Official Journal of the Society for Neuroscience* 38(12): 3060–80. doi:10.1523/JNEUROSCI.1740-17.2018.

Huang, Jianhan, Meijun Zheng, Xin Tang, Yaxing Chen, Aiping Tong, and Liangxue Zhou. 2020. "Potential of SARS-CoV-2 to Cause CNS Infection: Biologic Fundamental and Clinical Experience." *Frontiers in Neurology* 11: 659. doi:10.3389/fneur.2020.00659.

Israelow, Benjamin, Eric Song, Tianyang Mao, Peiwen Lu, Amit Meir, Feimei Liu, Mia Madel Alfajaro, et al. 2020. "Mouse Model of SARS-CoV-2 Reveals Inflammatory Role of Type i Interferon Signaling." *Journal of Experimental Medicine* 217(12). doi:10.1084/JEM.20201241.

Jackson, Cody B., Michael Farzan, Bing Chen, and Hyeryun Choe. 2022. "Mechanisms of SARS-CoV-2 Entry into Cells." *Nature Reviews Molecular Cell Biology* 23(1): 3–20. doi:10.1038/s41580-021-00418-x.

Jafarzadeh, Abdollah, Prashant Chauhan, Bhaskar Saha, Sara Jafarzadeh, and Maryam Nemati. 2020. "Contribution of Monocytes and Macrophages to the Local Tissue Inflammation and Cytokine Storm in COVID-19: Lessons from SARS and MERS, and Potential Therapeutic Interventions." *Life Sciences* 257: 118102. doi:10.1016/j.lfs.2020.118102.

Jain, Neelesh, Animesh Choudhury, Jayesh Sharma, Venkata Kumar, Divyendu De, and Richa Tiwari. 2020. "A Review of Novel Coronavirus Infection (Coronavirus Disease-19)." *Global Journal of Transfusion Medicine* 5(1): 22. doi:10.4103/GJTM.GJTM_24_20.

Jang, Haeman, David Boltz, Katharine Sturm-Ramirez, Kennie R. Shepherd, Yun Jiao, Robert Webster, and Richard J. Smeyne. 2009. "Highly Pathogenic H5N1 Influenza Virus Can Enter the Central Nervous System and Induce Neuroinflammation and Neurodegeneration." *Proceedings of the National Academy of Sciences of the United States of America* 106(33): 14063–68. doi:10.1073/pnas.0900096106.

Jaraíz-Rodríguez, Myriam, Lucia del Prado, and Eduardo Balsa. 2023. "Metabolic Remodeling in Astrocytes: Paving the Path to Brain Tumor Development." *Neurobiology of Disease* 188: 106327. doi:10.1016/j.nbd.2023.106327.

Jeong, Haengdueng, Youn Woo Lee, In Ho Park, Hyuna Noh, Sung-Hee Kim, Jiseon Kim, Donghun Jeon, et al. 2022. "Comparison of the Pathogenesis of SARS-CoV-2 Infection in K18-hACE2 Mouse and Syrian Golden Hamster Models." *Disease Models & Mechanisms* 15(11): dmm049632. doi:10.1242/dmm.049632.

Jurgens, Heidi A., Kaushik Amancherla, and Rodney W. Johnson. 2012. "Influenza Infection Induces Neuroinflammation, Alters Hippocampal Neuron Morphology, and Impairs Cognition in Adult Mice." *The Journal of Neuroscience: The Official Journal of the Society for Neuroscience* 32(12): 3958–68. doi:10.1523/JNEUROSCI.6389-11.2012.

Kadala, Aklesso, Dorly Verdier, Philippe Morquette, and Arlette Kolta. 2015. "Ion Homeostasis in Rhythmogenesis: The Interplay Between Neurons and Astroglia." *Physiology (Bethesda, Md.)* 30(5): 371–88. doi:10.1152/physiol.00023.2014.

Kanberg, Nelly, Nicholas J. Ashton, Lars-Magnus Andersson, Aylin Yilmaz, Magnus Lindh, Staffan Nilsson, Richard W. Price, et al. 2020. "Neurochemical Evidence of Astrocytic and Neuronal Injury Commonly Found in COVID-19." *Neurology* 95(12): e1754–59. doi:10.1212/WNL.0000000000010111.

Kapur, J. N., P. K. Sahoo, and A. K. C. Wong. 1985. "A New Method for Gray-Level Picture Thresholding Using the Entropy of the Histogram." *Computer Vision, Graphics, and Image Processing* 29(3): 273–85. doi:10.1016/0734-189X(85)90125-2.

Kashon, Michael L., G. Webster Ross, James P. O'Callaghan, Diane B. Miller, Helen Petrovitch, Cecil M. Burchfiel, Dan S. Sharp, et al. 2005. "Associations of Cortical Astrogliosis with Cognitive Performance and Dementia Status." *Journal of Alzheimer's Disease* 6(6): 595–604. doi:10.3233/JAD-2004-6604.

Käufer, Christopher, Cara S. Schreiber, Anna-Sophia Hartke, Ivo Denden, Stephanie Stanelle-Bertram, Sebastian Beck, Nancy Mounogou Kouassi, et al. 2022. "Microgliosis and Neuronal Proteinopathy in Brain Persist beyond Viral Clearance in SARS-CoV-2 Hamster Model." *EBioMedicine* 79: 103999. doi:10.1016/j.ebiom.2022.103999.

Kaur, Karamjeet, Jaskamal Singh Gill, Puneet Kumar Bansal, and Rahul Deshmukh. 2017. "Neuroinflammation - A Major Cause for Striatal Dopaminergic Degeneration in Parkinson's Disease." *Journal of the Neurological Sciences* 381: 308–14. doi:10.1016/j.jns.2017.08.3251.

Khurana, Saloni. 2015. “Comparative Study on Threshold Techniques for Image Analysis.” *International Journal of Engineering Research & Technology* 4(6). doi:10.17577/IJERTV4IS060563.

Kiani, Hamed, Reza Safabakhsh, and Ehsan Khadangi. 2009. “Fast Recursive Segmentation Algorithm Based on Kapur’s Entropy.” *200S 2nd International Conference on Computer, Control and Communication*: 1–6. doi:10.1109/IC4.2009.4909269.

Kim, Jooyoung, Yongmin Sung, HyoJin Park, Dong Il Choi, Ji-il Kim, Hoonwon Lee, Min Kyo Jung, et al. 2023. “Astrocytic Connection to Engram Neurons Increased after Learning.” doi:10.1101/2023.01.25.525617.

Kishor, Rahate Snehal, and Bombale Mayur Ramhari. 2020. “Introduction to Covid-19.” *Research Journal of Science and Technology* 12(4): 338–45. doi:10.5958/2349- 2988.2020.00051.0.

Klein, Robyn S. 2022. “Mechanisms of Coronavirus Infectious Disease 2019-Related Neurologic Diseases.” *Current Opinion in Neurology* 35(3): 392–98. doi:10.1097/WCO.0000000000001049.

Knight, Audrey C, Stephanie A Montgomery, Craig A Fletcher, and Victoria K Baxter. 2021. “Mouse Models for the Study of SARS-CoV-2 Infection.” *Comparative Medicine* 71(5): 383–97. doi:10.30802/AALAS-CM-21-000031.

Knoll, Rainer, Joachim L. Schultze, and Jonas Schulte-Schrepping. 2021. “Monocytes and Macrophages in COVID-19.” *Frontiers in Immunology* 12: 720109. doi:10.3389/fimmu.2021.720109.

Kong, Weili, Mauricio Montano, Michael J. Corley, Ekram Helmy, Hirofumi Kobayashi, Martin Kinisu, Rahul Suryawanshi, et al. 2022. “Neuropilin-1 Mediates SARS-CoV-2 Infection of Astrocytes in Brain Organoids, Inducing Inflammation Leading to Dysfunction and Death of Neurons.” *mBio* 13(6): e0230822. doi:10.1128/mbio.02308-22.

Kosyreva, Anna, Dzhuliia Dzhalilova, Anastasia Lokhonina, Polina Vishnyakova, and Timur Fatkhudinov. 2021. “The Role of Macrophages in the Pathogenesis of SARS-CoV-2- Associated Acute Respiratory Distress Syndrome.” *Frontiers in Immunology* 12: 682871. doi:10.3389/fimmu.2021.682871.

Krause, Daniela L., and Norbert Müller. 2010. “Neuroinflammation, Microglia and Implications for Anti-Inflammatory Treatment in Alzheimer’s Disease.” *International Journal of Alzheimer’s Disease* 2010: 1–9. doi:10.4061/2010/732806.

Krishnan, Kamini, YuFang Lin, Kia-Rai M. Prewitt, and Dawn A. Potter. 2022. "Multidisciplinary Approach to Brain Fog and Related Persisting Symptoms Post COVID-19." *Journal of Health Service Psychology* 48(1): 31–38. doi:10.1007/s42843-022-00056-7.

Kwon, Hyuk Sung, and Seong-Ho Koh. 2020. "Neuroinflammation in Neurodegenerative Disorders: The Roles of Microglia and Astrocytes." *Translational Neurodegeneration* 9(1): 42. doi:10.1186/s40035-020-00221-2.

Lawrence, Jill M., Kayla Schardien, Brian Wigdahl, and Michael R. Nonnemacher. 2023. "Roles of Neuropathology-Associated Reactive Astrocytes: A Systematic Review." *Acta Neuropathologica Communications* 11(1): 42. doi:10.1186/s40478-023-01526-9.

Lee, Hong-Gyun, Joon-Hyuk Lee, Lucas E. Flausino, and Francisco J. Quintana. 2023. "Neuroinflammation: An Astrocyte Perspective." *Science Translational Medicine* 15(721): eadi7828. doi:10.1126/scitranslmed.adi7828.

Li, Dongyang, Xiaoyu Liu, Tianming Liu, Haitao Liu, Li Tong, Shuwei Jia, and Yu-Feng Wang. 2020. "Neurochemical Regulation of the Expression and Function of Glial Fibrillary Acidic Protein in Astrocytes." *Glia* 68(5): 878–97. doi:10.1002/glia.23734.

Li, Juan, Yiyong Wei, Junli Zhou, Helin Zou, Lulin Ma, Chengxi Liu, Zhi Xiao, et al. 2022. "Activation of Locus Coeruleus-Spinal Cord Noradrenergic Neurons Alleviates Neuropathic Pain in Mice via Reducing Neuroinflammation from Astrocytes and Microglia in Spinal Dorsal Horn." *Journal of Neuroinflammation* 19(1): 123. doi:10.1186/s12974-022- 02489-9.

Li, Meng-Yuan, Lin Li, Yue Zhang, and Xiao-Sheng Wang. 2020. "Expression of the SARS- CoV-2 Cell Receptor Gene ACE2 in a Wide Variety of Human Tissues." *Infectious Diseases of Poverty* 9(1): 45. doi:10.1186/s40249-020-00662-x.

Liu, Jia-Mei, Bai-Hong Tan, Shuang Wu, Yue Gui, Jia-Le Suo, and Yan-Chao Li. 2021. "Evidence of Central Nervous System Infection and Neuroinvasive Routes, as Well as Neurological Involvement, in the Lethality of SARS-CoV-2 Infection." *Journal of Medical Virology* 93(3): 1304–13. doi:10.1002/jmv.26570.

Liu, Min, Zhipeng Xu, Long Wang, Lixia Zhang, Yi Liu, Jiangbei Cao, Qiang Fu, et al. 2020. "Cottonseed Oil Alleviates Ischemic Stroke Injury by Inhibiting the Inflammatory Activation of Microglia and Astrocyte." *Journal of Neuroinflammation* 17(1): 270. doi:10.1186/s12974- 020-01946-7.

Liyanagamage, Donisha Shani Niharika Keembiya, and Ryan D. Martinus. 2020. "Role of Mitochondrial Stress Protein HSP60 in Diabetes-Induced Neuroinflammation." *Mediators of Inflammation* 2020: 8073516. doi:10.1155/2020/8073516.

Long, Jian-Wu, Xuan-Jing Shen, and Hai-Peng Chen. 2012. "Adaptive Minimum Error Thresholding Algorithm." *Acta Automatica Sinica* 38(7): 1134. doi:10.3724/SP.J.1004.2012.01134.

Luijerink, Lauren, Michael Rodriguez, and Rita Machaalani. 2024. "Quantifying GFAP Immunohistochemistry in the Brain – Introduction of the Reactivity Score (R-Score) and How It Compares to Other Methodologies." *Journal of Neuroscience Methods* 402: 110025. doi:10.1016/j.jneumeth.2023.110025.

Lukiw, Walter J., Aileen Pogue, and James M. Hill. 2022. "SARS-CoV-2 Infectivity and Neurological Targets in the Brain." *Cellular and Molecular Neurobiology* 42(1): 217–24. doi:10.1007/s10571-020-00947-7.

Mao, Ling, Mengdie Wang, Shengcai Chen, Quanwei He, Jiang Chang, Candong Hong, Yifan Zhou, et al. 2020. "Neurological Manifestations of Hospitalized Patients with COVID-19 in Wuhan, China: A Retrospective Case Series Study." : 2020.02.22.20026500. doi:10.1101/2020.02.22.20026500.

Martinez, Taylor E., Karthick Mayilsamy, Shyam S. Mohapatra, and Subhra Mohapatra. 2024. "Modulation of Paracellular Permeability in SARS-CoV-2 Blood-to-Brain Transcytosis." *Viruses* 16(5): 785. doi:10.3390/v16050785.

Matschke, Jakob, Henri Lahann, Susanne Krasemann, Hermann Altmeppen, Susanne Pfefferle, Giovanna Galliciotti, Antonia Fitzek, et al. 2022. "Young COVID-19 Patients Show a Higher Degree of Microglial Activation When Compared to Controls." *Frontiers in Neurology* 13: 908081. doi:10.3389/fneur.2022.908081.

McCall, M A, R G Gregg, R R Behringer, M Brenner, C L Delaney, E J Galbreath, C L Zhang, et al. 1996. "Targeted Deletion in Astrocyte Intermediate Filament (Gfap) Alters Neuronal Physiology." *Proceedings of the National Academy of Sciences* 93(13): 6361–66. doi:10.1073/pnas.93.13.6361.

Mehta, Om Prakash, Parshal Bhandari, Akshay Raut, Salah Eddine Oussama Kacimi, and Nguyen Tien Huy. 2020. "Coronavirus Disease (COVID-19): Comprehensive Review of Clinical Presentation." *Frontiers in Public Health* 8: 582932. doi:10.3389/fpubh.2020.582932.

Miao, Jinxin, Louisa S. Chard, Zhimin Wang, and Yaohe Wang. 2019. “Syrian Hamster as an Animal Model for the Study on Infectious Diseases.” *Frontiers in Immunology* 10: 2329. doi:10.3389/fimmu.2019.02329.

Minghetti, Luisa. 2005. “Role of Inflammation in Neurodegenerative Diseases.” *Current Opinion in Neurology* 18(3): 315–21. doi:10.1097/01.wco.0000169752.54191.97.

Mishra, Sanskriti, Murray Choueka, Qiang Wang, Chloe Hu, Stephanie Visone, Michael Silver, Evan G. Stein, Steven R. Levine, and Qingliang T. Wang. 2021. “Intracranial Hemorrhage in COVID-19 Patients.” *Journal of Stroke and Cerebrovascular Diseases* 30(4): 105603. doi:10.1016/j.jstrokecerebrovasdis.2021.105603.

Moreau, Gregory Brett, Stacey L. Burgess, Jeffrey M. Sturek, Alexandra N. Donlan, William A. Petri, and Barbara J. Mann. 2020. “Evaluation of K18-hACE2 Mice as a Model of SARS- CoV-2 Infection.” *The American Journal of Tropical Medicine and Hygiene* 103(3): 1215–19. doi:10.4269/ajtmh.20-0762.

Morita, Mitsuhiro, Hiroko Ikeshima-Kataoka, Marko Kreft, Nina Vardjan, Robert Zorec, and Mami Noda. 2019. “Metabolic Plasticity of Astrocytes and Aging of the Brain.” *International Journal of Molecular Sciences* 20(4): 941. doi:10.3390/ijms20040941.

Moyse, Emmanuel, Slavica Krantic, Nesrine Djellouli, Sébastien Roger, Denis Angoulvant, Camille Debacq, Victoire Leroy, Bertrand Fougere, and Amal Aidoud. 2022. “Neuroinflammation: A Possible Link Between Chronic Vascular Disorders and Neurodegenerative Diseases.” *Frontiers in Aging Neuroscience* 14. doi:10.3389/fnagi.2022.827263.

Murta, Veronica, Alejandro Villarreal, and Alberto J. Ramos. 2020. “Severe Acute Respiratory Syndrome Coronavirus 2 Impact on the Central Nervous System: Are Astrocytes and Microglia Main Players or Merely Bystanders?” *ASN NEURO* 12: 1759091420954960. doi:10.1177/1759091420954960.

N, Senthilkumaran, and Vaithegi S. 2016. “Image Segmentation By Using Thresholding Techniques For Medical Images.” In *Computer Science & Engineering: An International Journal*, , 1–13. doi:10.5121/cseij.2016.6101.

Nagu, Priyanka, Arun Parashar, Tapan Behl, and Vineet Mehta. 2021. “CNS Implications of COVID-19: A Comprehensive Review.” *Reviews in the neurosciences* 32(2): 219–34. doi:10.1515/revneuro-2020-0070.

Najjar, Souhel, Amanda Najjar, Derek J. Chong, Bidyut K. Pramanik, Claudia Kirsch, Ruben I. Kuzniecky, Steven V. Pacia, and Salman Azhar. 2020. “Central Nervous System

Complications Associated with SARS-CoV-2 Infection: Integrative Concepts of Pathophysiology and Case Reports." *Journal of Neuroinflammation* 17(1): 231. doi:10.1186/s12974-020-01896-0.

Neprasova, Helena, Miroslava Anderova, David Petrik, Lydia Vargova, Sarka Kubinova, Alexandr Chvatal, and Eva Sykova. 2007. "High Extracellular K(+) Evokes Changes in Voltage-Dependent K(+) and Na (+) Currents and Volume Regulation in Astrocytes." *Pflugers Archiv: European Journal of Physiology* 453(6): 839–49. doi:10.1007/s00424-006- 0151-9.

Nguyen, Nhu Ngoc, Van Thuan Hoang, Thi Loi Dao, Pierre Dudouet, Carole Eldin, and Philippe Gautret. 2022. "Clinical Patterns of Somatic Symptoms in Patients Suffering from Post-Acute Long COVID: A Systematic Review." *European Journal of Clinical Microbiology & Infectious Diseases* 41(4): 515–45. doi:10.1007/s10096-022-04417-4.

Nie, Fangyan, Pingfeng Zhang, Jianqi Li, and Dehong Ding. 2017. "A Novel Generalized Entropy and Its Application in Image Thresholding." *Signal Processing* 134: 23–34. doi:10.1016/j.sigpro.2016.11.004.

Nikbakht, Farnaz, Ali Mohammadkhanizadeh, and Ekram Mohammadi. 2020. "How Does the COVID-19 Cause Seizure and Epilepsy in Patients? The Potential Mechanisms." *Multiple Sclerosis and Related Disorders* 46: 102535. doi:10.1016/j.msard.2020.102535.

Nimmerjahn, Axel, Frank Kirchhoff, and Fritjof Helmchen. 2005. "Resting Microglial Cells Are Highly Dynamic Surveillants of Brain Parenchyma in Vivo." *Science (New York, N.Y.)* 308(5726): 1314–18. doi:10.1126/science.1110647.

Nittas, Vasileios, Manqi Gao, Erin A. West, Tala Ballouz, Dominik Menges, Sarah Wulf Hanson, and Milo Alan Puhan. 2022. "Long COVID Through a Public Health Lens: An Umbrella Review." *Public Health Reviews* 43: 1604501. doi:10.3389/phrs.2022.1604501.

Nouraeinejad, Ali. 2023. "The Functional and Structural Changes in the Hippocampus of COVID-19 Patients." *Acta Neurologica Belgica* 123(4): 1247–56. doi:10.1007/s13760-023- 02291-1.

Nourbakhsh, Fahimeh, Morgayn I. Read, George E. Barreto, and Amirhossein Sahebkar. 2021. "Astrocytes and Inflammasome: A Possible Crosstalk in Neurological Diseases." *Current medicinal chemistry* 28(24): 4972–94. doi:10.2174/0929867328666210301105422.

Nurprilinda, Marliana, and Erica Gilda Misnawati Simanjuntak. 2023. "Description of Leukocytes in Patients Who Are Positive for COVID-19 Infection." *Journal of Drug Delivery and Therapeutics* 13(11): 127–35. doi:10.22270/jddt.v13i11.6026.

Oliveira, Gabriel. 2020. “Laboratory Mouse C COVID-19 Research.” *Open Access Journal of Biomedical Science* 2(2). doi:10.38125/OAJBS.000176.

Orkand, R. K., J. G. Nicholls, and S. W. Kuffler. 1966. “Effect of Nerve Impulses on the Membrane Potential of Glial Cells in the Central Nervous System of Amphibia.” *Journal of Neurophysiology* 29(4): 788–806. doi:10.1152/jn.1966.29.4.788.

Osborn, Lana M., Willem Kamphuis, Wytse J. Wadman, and Elly M. Hol. 2016. “Astrogliosis: An Integral Player in the Pathogenesis of Alzheimer’s Disease.” *Progress in Neurobiology* 144: 121–41. doi:10.1016/j.pneurobio.2016.01.001.

Oxley, Thomas J., J. Mocco, Shahram Majidi, Christopher P. Kellner, Hazem Shoirah, I. Paul Singh, Reade A. De Leacy, et al. 2020. “Large-Vessel Stroke as a Presenting Feature of Covid-19 in the Young.” *The New England Journal of Medicine* 382(20): e60. doi:10.1056/NEJMc2009787.

Pang, Qi-Ming, Si-Yu Chen, Qi-Jing Xu, Meng Zhang, Da-Fei Liang, Sheng-Ping Fu, Jiang Yu, et al. 2022. “Effects of Astrocytes and Microglia on Neuroinflammation after Spinal Cord Injury and Related Immunomodulatory Strategies.” *International Immunopharmacology* 108: 108754. doi:10.1016/j.intimp.2022.108754.

Patel, Smit D., Ryan Kollar, Patrick Troy, Xianyuan Song, Mohammad Khaled, Augusto Parra, and Mubashir Pervez. 2020. “Malignant Cerebral Ischemia in A COVID-19 Infected Patient: Case Review and Histopathological Findings.” *Journal of Stroke and Cerebrovascular Diseases: The Official Journal of National Stroke Association* 29(11): 105231. doi:10.1016/j.jstrokecerebrovasdis.2020.105231.

Patil, Deepak Y., Sreelekshmy Mohandas, and Pragya D. Yadav. 2021. “Role of Syrian Hamsters and Nonhuman Primates in Covid-19 Research.” *Indian Journal of Comparative Microbiology, Immunology and Infectious Diseases* 42(1): 17–29. doi:10.5958/0974- 0147.2021.00002.7.

Pekny, Milos, and Marcela Pekna. 2016. “Reactive Gliosis in the Pathogenesis of CNS Diseases.” *Biochimica et Biophysica Acta (BBA) - Molecular Basis of Disease* 1862(3): 483–91. doi:10.1016/j.bbadis.2015.11.014.

Pott Godoy, María Clara, Carina Cintia Ferrari, and Fernando Juan Pitossi. 2010. “Nigral Neurodegeneration Triggered by Striatal AdIL-1 Administration Can Be Exacerbated by Systemic IL-1 Expression.” *Journal of Neuroimmunology* 222(1–2): 29–39. doi:10.1016/j.jneuroim.2010.02.018.

Pranata, Raymond, Ian Huang, Michael Anthonius Lim, Emir Yonas, Rachel Vania, and Raden Ayu Tuty Kuswardhani. 2021. "Delirium and Mortality in Coronavirus Disease 2019 (COVID-19) - A Systematic Review and Meta-Analysis." *Archives of Gerontology and Geriatrics* 95: 104388. doi:10.1016/j.archger.2021.104388.

Prebil, Mateja, Jørgen Jensen, Robert Zorec, and Marko Kreft. 2011. "Astrocytes and Energy Metabolism." *Archives of Physiology and Biochemistry* 117(2): 64–69. doi:10.3109/13813455.2010.539616.

Proust, Alizé, Christophe J. Queval, Ruth Harvey, Lorin Adams, Michael Bennett, and Robert J. Wilkinson. 2023. "Differential Effects of SARS-CoV-2 Variants on Central Nervous System Cells and Blood-Brain Barrier Functions." *Journal of Neuroinflammation* 20(1): 184. doi:10.1186/s12974-023-02861-3.

Qin, Shuang, Yujie Jiang, Xin Wei, Xiaoyuan Liu, Jingjing Guan, Yingxiao Chen, Hong Lu, et al. 2021. "Dynamic Changes in Monocytes Subsets in COVID-19 Patients." *Human Immunology* 82(3): 170–76. doi:10.1016/j.humimm.2020.12.010.

Rappold, T., A. Laflam, D. Hori, C. Brown, J. Brandt, C. D. Mintz, F. Sieber, et al. 2016. "Evidence of an Association between Brain Cellular Injury and Cognitive Decline after Non- Cardiac Surgery." *BJA: British Journal of Anaesthesia* 116(1): 83–89. doi:10.1093/bja/aev415.

Rasmussen, C., I. Niculescu, S. Patel, and A. Krishnan. 2020. "COVID-19 and Involvement of the Corpus Callosum: Potential Effect of the Cytokine Storm?" *AJNR: American Journal of Neuroradiology* 41(9): 1625–28. doi:10.3174/ajnr.A6680.

Rom, Slava, Viviana Zuluaga-Ramirez, Sachin Gajghate, Alecia Seliga, Malika Winfield, Nathan A. Heldt, Mikhail A. Kolpakov, et al. 2019. "Hyperglycemia-Driven Neuroinflammation Compromises BBB Leading to Memory Loss in Both Diabetes Mellitus (DM) Type 1 and Type 2 Mouse Models." *Molecular Neurobiology* 56(3): 1883–96. doi:10.1007/s12035-018-1195-5.

Rose, C. R., and J.-Y. Chatton. 2016. "Astrocyte Sodium Signaling and Neuro-Metabolic Coupling in the Brain." *Neuroscience* 323: 121–34. doi:10.1016/j.neuroscience.2015.03.002.

Rose, Christine R., and Alexej Verkhratsky. 2024. "Sodium Homeostasis and Signalling: The Core and the Hub of Astrocyte Function." *Cell Calcium* 117: 102817. doi:10.1016/j.ceca.2023.102817.

Rosenke, Kyle, Kimberly Meade-White, Michael Letko, Chad Clancy, Frederick Hansen, Yanan Liu, Atsushi Okumura, et al. 2020. "Defining the Syrian Hamster as a Highly Susceptible Preclinical Model for SARS-CoV-2 Infection." : 2020.09.25.314070. doi:10.1101/2020.09.25.314070.

Roy, A., A. Gupta, A. Nayyar, S. Bhargava, V. Dawar, V. Verma, T. Mishra, et al. 2023. "RWD82 To Study the Impact of Long COVID-19 in the US - A 9-Month Retrospective Study." *Value in Health* 26(6): S376. doi:10.1016/j.jval.2023.03.2111.

Sadasivan, Shankar, Mark Zanin, Kevin O'Brien, Stacey Schultz-Cherry, and Richard J. Smeyne. 2015. "Induction of Microglia Activation after Infection with the Non-Neurotropic A/CA/04/2009 H1N1 Influenza Virus." *PloS One* 10(4): e0124047. doi:10.1371/journal.pone.0124047.

Sahoo, P.K, S Soltani, and A.K.C Wong. 1988. "A Survey of Thresholding Techniques." *Computer Vision, Graphics, and Image Processing* 41(2): 233–60. doi:10.1016/0734-189X(88)90022-9.

Saikarthik, Jayakumar, Ilango Saraswathi, Abdulaziz Alarifi, Abdulrahman A. Al-Atram, Suresh Mickeymaray, Anand Paramasivam, Saleem Shaikh, Mathew Jeraud, and Abdulaziz S. Alothaim. 2022. "Role of Neuroinflammation Mediated Potential Alterations in Adult Neurogenesis as a Factor for Neuropsychiatric Symptoms in Post-Acute COVID-19 Syndrome-A Narrative Review." *PeerJ* 10: e14227. doi:10.7717/peerj.14227.

Salamanna, Francesca, Francesca Veronesi, Lucia Martini, Maria Paola Landini, and Milena Fini. 2021. "Post-COVID-19 Syndrome: The Persistent Symptoms at the Post-Viral Stage of the Disease. A Systematic Review of the Current Data." *Frontiers in Medicine* 8. doi:10.3389/fmed.2021.653516.

Sanabria-Diaz, Gretel, Manina Maja Etter, Lester Melie-Garcia, Johanna M. Lieb, Marios- Nikos Psychogios, Gregor Hutter, and Cristina Granziera. 2022. "Brain Cortical Alterations in COVID-19 Patients with Neurological Symptoms." *Frontiers in Neuroscience* 16: 992165. doi:10.3389/fnins.2022.992165.

Sarubbo, Fiorella, Khaoulah El Haji, Aina Vidal-Balle, and Joan Bargay Lleonart. 2022. "Neurological Consequences of COVID-19 and Brain Related Pathogenic Mechanisms: A New Challenge for Neuroscience." *Brain, behavior, & immunity - health* 19: 100399. doi:10.1016/j.bbih.2021.100399.

Shah, Waqaar, Toby Hillman, E Diane Playford, and Lyth Hishmeh. 2021. "Managing the Long Term Effects of Covid-19: Summary of NICE, SIGN, and RCGP Rapid Guideline." *BMJ*: n136. doi:10.1136/bmj.n136.

Shou, Shuyu, Menghui Liu, Yang Yang, Ning Kang, Yingying Song, Dan Tan, Nannan Liu, et al. 2021. "Animal Models for COVID-19: Hamsters, Mouse, Ferret, Mink, Tree Shrew, and Non-Human Primates." *Frontiers in Microbiology* 12: 626553. doi:10.3389/fmicb.2021.626553.

Sia, Sin Fun, Li-Meng Yan, Alex W. H. Chin, Kevin Fung, Ka-Tim Choy, Alvina Y. L. Wong, Prathanporn Kaewpreedee, et al. 2020. "Pathogenesis and Transmission of SARS-CoV-2 in Golden Hamsters." *Nature* 583(7818): 834–38. doi:10.1038/s41586-020-2342-5.

Silvestroni, Aurelio, Richard L. M. Faull, Andrew D. Strand, and Thomas Möller. 2009. "Distinct Neuroinflammatory Profile in Post-Mortem Human Huntington's Disease." *Neuroreport* 20(12): 1098–1103. doi:10.1097/WNR.0b013e32832e34ee.

Smith Jr., Orville A., Charles N. Bodemer, and Helen N. Halsey. 1963. "A Stereotaxic Atlas of the Brain of the Golden Hamster (Mesocricetus Auratus)." *Journal of Comparative Neurology* 120(1): 53–63. doi:10.1002/cne.901200106.

Sofroniew, Michael V. 2015. "Astrogliosis." *Cold Spring Harbor Perspectives in Biology* 7(2): a020420. doi:10.1101/cshperspect.a020420.

Sofroniew, Michael V., and Harry V. Vinters. 2010. "Astrocytes: Biology and Pathology." *Acta Neuropathologica* 119(1): 7–35. doi:10.1007/s00401-009-0619-8.

Somjen, George G. 2002. "Ion Regulation in the Brain: Implications for Pathophysiology." *The Neuroscientist* 8(3): 254–67. doi:10.1177/1073858402008003011.

Soriano, Joan B., Srinivas Murthy, John C. Marshall, Pryanka Relan, Janet V. Diaz, and WHO Clinical Case Definition Working Group on Post-COVID-19 Condition. 2022. "A Clinical Case Definition of Post-COVID-19 Condition by a Delphi Consensus." *The Lancet. Infectious Diseases* 22(4): e102–7. doi:10.1016/S1473-3099(21)00703-9.

Soung, Allison L., Abigail Vanderheiden, Anna S. Nordvig, Cheick A. Sissoko, Peter Canoll, Madeline B. Mariani, Xiaoping Jiang, et al. 2022. "COVID-19 Induces CNS Cytokine Expression and Loss of Hippocampal Neurogenesis." *Brain* 145(12): 4193–4201. doi:10.1093/brain/awac270.

Spindler, Katherine R., and Tien-Huei Hsu. 2012. "Viral Disruption of the Blood-Brain Barrier." *Trends in Microbiology* 20(6): 282–90. doi:10.1016/j.tim.2012.03.009.

Sriwastava, Shitiz, Medha Tandon, Sanjiti Podury, Apoorv Prasad, Sijin Wen, Garret Guthrie, Mihir Kakara, et al. 2021. "COVID-19 and Neuroinflammation: A Literature Review of Relevant Neuroimaging and CSF Markers in Central Nervous System Inflammatory

Disorders from SARS-COV2." *Journal of Neurology* 268(12): 4448–78. doi:10.1007/s00415- 021-10611-9.

Stefano, George B. 2021. "Historical Insight into Infections and Disorders Associated with Neurological and Psychiatric Sequelae Similar to Long COVID." *Medical Science Monitor: International Medical Journal of Experimental and Clinical Research* 27: e931447. doi:10.12659/MSM.931447.

Sticozzi, C., G. Belmonte, A. Meini, P. Carbotti, G. Grasso, and M. Palmi. 2013. "IL-1β Induces GFAP Expression in Vitro and in Vivo and Protects Neurons from Traumatic Injury- Associated Apoptosis in Rat Brain Striatum via NFκB/Ca2+–Calmodulin/ERK Mitogen- Activated Protein Kinase Signaling Pathway." *Neuroscience* 252: 367–83. doi:10.1016/j.neuroscience.2013.07.061.

Subhramanyam, Charannya Sozheesvari, Cheng Wang, Qidong Hu, and S Thameem Dheen. 2019. "Microglia-Mediated Neuroinflammation in Neurodegenerative Diseases." *Seminars in Cell & Developmental Biology* 94: 112–20. doi:10.1016/j.semcdb.2019.05.004.

Sun, Wei, Adam Cornwell, Jiashu Li, Sisi Peng, M. Joana Osorio, Nadia Aalling, Su Wang, et al. 2017. "SOX9 Is an Astrocyte-Specific Nuclear Marker in the Adult Brain Outside the Neurogenic Regions." *Journal of Neuroscience* 37(17): 4493–4507. doi:10.1523/JNEUROSCI.3199-16.2017.

Sun, Yuanjie, Yoshihisa Koyama, and Shoichi Shimada. 2022. "Inflammation From Peripheral Organs to the Brain: How Does Systemic Inflammation Cause Neuroinflammation?" *Frontiers in Aging Neuroscience* 14: 903455. doi:10.3389/fnagi.2022.903455.

Süß, Patrick, Tobias Rothe, Alana Hoffmann, Johannes C. M. Schlachetzki, and Jürgen Winkler. 2020. "The Joint-Brain Axis: Insights From Rheumatoid Arthritis on the Crosstalk Between Chronic Peripheral Inflammation and the Brain." *Frontiers in Immunology* 11: 612104. doi:10.3389/fimmu.2020.612104.

Sylvester, Shirley V., Rada Rusu, Biankha Chan, Martha Bellows, Carly O'Keefe, and Susan Nicholson. 2022. "Sex Differences in Sequelae from COVID-19 Infection and in Long COVID Syndrome: A Review." *Current Medical Research and Opinion* 38(8): 1391–99. doi:10.1080/03007995.2022.2081454.

Takagi, Tomohisa, Yuji Naito, Ryo Inoue, Saori Kashiwagi, Kazuhiko Uchiyama, Katsura Mizushima, Saeko Tsuchiya, et al. 2019. "Differences in Gut Microbiota Associated with Age, Sex, and Stool Consistency in Healthy Japanese Subjects." *Journal of Gastroenterology* 54(1): 53–63. doi:10.1007/s00535-018-1488-5.

Takahashi, Takehiro, Mallory K. Ellingson, Patrick Wong, Benjamin Israelow, Carolina Lucas, Jon Klein, Julio Silva, et al. 2020. "Sex Differences in Immune Responses That Underlie COVID-19 Disease Outcomes." *Nature* 588(7837): 315–20. doi:10.1038/s41586- 020-2700-3.

Taquet, Maxime, John R. Geddes, Masud Husain, Sierra Luciano, and Paul J. Harrison. 2021. "6-Month Neurological and Psychiatric Outcomes in 236 379 Survivors of COVID-19: A Retrospective Cohort Study Using Electronic Health Records." *The Lancet Psychiatry* 8(5): 416–27. doi:10.1016/S2215-0366(21)00084-5.

Tipnis, S. R., N. M. Hooper, R. Hyde, E. Karran, G. Christie, and A. J. Turner. 2000. "A Human Homolog of Angiotensin-Converting Enzyme. Cloning and Functional Expression as a Captopril-Insensitive Carboxypeptidase." *The Journal of Biological Chemistry* 275(43): 33238–43. doi:10.1074/jbc.M002615200.

Tremblay, Marie Eve, Charlotte Madore, Maude Bordeleau, Li Tian, and Alexei Verkhratsky. 2020. "Neuropathobiology of COVID-19: The Role for Glia." *Frontiers in Cellular Neuroscience* 14. doi:10.3389/fncel.2020.592214.

Untiet, Verena, Felix R. M. Beinlich, Peter Kusk, Ning Kang, Antonio Ladrón-de-Guevara, Wei Song, Celia Kjaerby, et al. 2023. "Astrocytic Chloride Is Brain State Dependent and Modulates Inhibitory Neurotransmission in Mice." *Nature Communications* 14(1): 1871. doi:10.1038/s41467-023-37433-9.

Vezzoli, E, C Calì, M De Roo, L Ponzoni, E Sogne, N Gagnon, M Francolini, et al. 2020. "Ultrastructural Evidence for a Role of Astrocytes and Glycogen-Derived Lactate in Learning-Dependent Synaptic Stabilization." *Cerebral Cortex* 30(4): 2114–27. doi:10.1093/cercor/bhz226.

Vints, Wouter A. J., Kristina Valatkevičienė, Oron Levin, Akila Weerasekera, Simonas Jesmanas, Simona Kušleikienė, Vida J. Česnaitienė, et al. 2024. "Hippocampal Neurometabolic and Structural Changes from Pre-to Post-COVID-19: A Case-Series Study." *Magnetic Resonance Imaging* 109: 249–55. doi:10.1016/j.mri.2024.03.032.

Volk, Parker, Mohammadreza Rahmani Manesh, Mary E. Warren, Katie Besko, Elisa Gonçalves de Andrade, Leigh E. Wicki-Stordeur, and Leigh Anne Swayne. 2023. "Long- Term Neurological Dysfunction Associated with COVID-19: Lessons from Influenza and Inflammatory Diseases?" *Journal of neurochemistry*. doi:10.1111/jnc.16016.

Webb, Cerian Ruth, Mirela Domijan, Cerian Ruth Webb, and Mirela Domijan. 2019. "Exploring Built-In Functions." : 69–84. doi:10.1007/978-3-030-21337-4_6.

Weber, Bruno, and L. Felipe Barros. 2015. “The Astrocyte: Powerhouse and Recycling Center.” *Cold Spring Harbor Perspectives in Biology*: a020396. doi:10.1101/cshperspect.a020396.

Wesselingh, Robb. 2023. “Prevalence, Pathogenesis and Spectrum of Neurological Symptoms in COVID-19 and Post-COVID-19 Syndrome: A Narrative Review.” *The Medical Journal of Australia* 219(5): 230–36. doi:10.5694/mja2.52063.

Xu, Evan, Yan Xie, and Ziyad Al-Aly. 2022. “Long-Term Neurologic Outcomes of COVID-19.” *Nature Medicine* 28(11): 2406–15. doi:10.1038/s41591-022-02001-z.

Yong, Shin Jie. 2021. “Long COVID or Post-COVID-19 Syndrome: Putative Pathophysiology, Risk Factors, and Treatments.” *Infectious Diseases* 53(10): 737–54. doi:10.1080/23744235.2021.1924397.

Zarate, Sara M., Annet Kirabo, Antentor O. Hinton Jr., and Monica M. Santisteban. 2024. “Neuroimmunology of Cardiovascular Disease.” *Current Hypertension Reports* 26(7): 339–47. doi:10.1007/s11906-024-01301-8.

Zhang, Xiaoqing, Shuren Li, and Shaoqian Niu. 2020. “ACE2 and COVID-19 and the Resulting ARDS.” *Postgraduate Medical Journal* 96(1137): 403–7. doi:10.1136/postgradmedj-2020-137935.

Zhao, Kaochang, Ruiyun Li, Xiaojun Wu, Yang Zhao, Tao Wang, Zhishui Zheng, Shaolin Zeng, Xuhong Ding, and Hanxiang Nie. 2020. “Clinical Features in 52 Patients with COVID- 19 Who Have Increased Leukocyte Count: A Retrospective Analysis.” *European Journal of Clinical Microbiology & Infectious Diseases* 39(12): 2279–87. doi:10.1007/s10096-020- 03976-8.

Zorzo, Candela, Lucía Solares, Marta Mendez, and Magdalena Mendez-Lopez. 2023. “Hippocampal Alterations after SARS-CoV-2 Infection: A Systematic Review.” *Behavioural Brain Research* 455: 114662. doi:10.1016/j.bbr.2023.114662.